AD-A171 498 MECHANICAL PROPERTIES OF REID-BEDFORD MODEL SAND(U) 1/1
ARMY ENGINEER WATERWAYS EXPERIMENT STATION VICKSBURG MS
STRUCTURES LAB B R PHILLIPS SEP 86 WES/TR/SL-86-29
UNCLASSIFIED F/G 8/13 NL

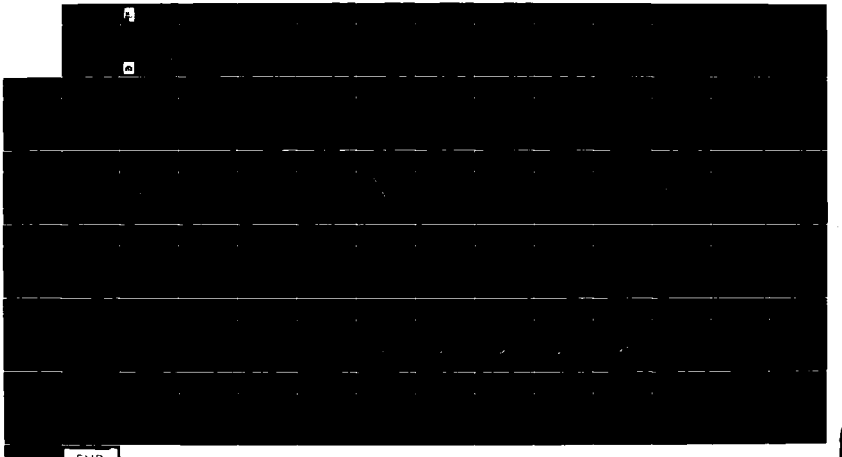

END
DATE FILMED
10-86
DTIC

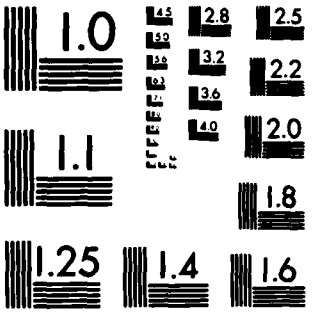

US Army Corps of Engineers

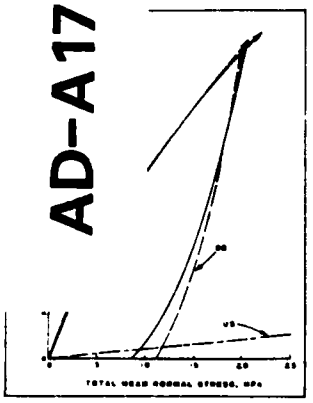

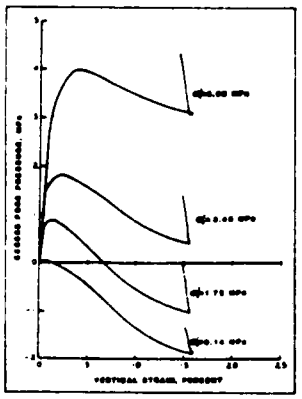

STRUCTURES LABORATORY

TECHNICAL REPORT SL-86-29

MECHANICAL PROPERTIES OF REID-BEDFORD MODEL SAND

by

Bruce R. Phillips

Structures Laboratory

DEPARTMENT OF THE ARMY
Waterways Experiment Station, Corps of Engineers
PO Box 631, Vicksburg, Mississippi 39180-0631

September 1986
Final Report

Prepared for Air Force Office of Scientific Research
Bolling Air Force Base
Washington, DC 20332

Under AFOSR-MIPR-82-00003,
Project 2307/C1 FY 82

Destroy this report when no longer needed. Do not return it to the originator.

The findings in this report are not to be construed as an official Department of the Army position unless so designated by other authorized documents.

The contents of this report are not to be used for advertising, publication, or promotional purposes. Citation of trade names does not constitute an official endorsement or approval of the use of such commercial products.

Unclassified
SECURITY CLASSIFICATION OF THIS PAGE

ADA 171498

REPORT DOCUMENTATION PAGE

Form Approved
OMB No 0704-0188
Exp Date Jun 30 1986

1a REPORT SECURITY CLASSIFICATION Unclassified	1b RESTRICTIVE MARKINGS
2a SECURITY CLASSIFICATION AUTHORITY	3 DISTRIBUTION/AVAILABILITY OF REPORT Approved for public release; distribution unlimited.
2b DECLASSIFICATION/DOWNGRADING SCHEDULE	
4 PERFORMING ORGANIZATION REPORT NUMBER(S) Technical Report SL-86-29	5 MONITORING ORGANIZATION REPORT NUMBER(S)
6a NAME OF PERFORMING ORGANIZATION USAEWES Structures Laboratory 6b OFFICE SYMBOL (If applicable) WESSD	7a NAME OF MONITORING ORGANIZATION
6c ADDRESS (City, State, and ZIP Code) PO Box 631 Vicksburg, MS 39180-0631	7b ADDRESS (City, State, and ZIP Code)
8a NAME OF FUNDING/SPONSORING ORGANIZATION Air Force Office of Scientific Research 8b OFFICE SYMBOL (If applicable)	9 PROCUREMENT INSTRUMENT IDENTIFICATION NUMBER
8c ADDRESS (City, State, and ZIP Code) Bolling Air Force Base Washington, DC 20332	10 SOURCE OF FUNDING NUMBERS See reverse. PROGRAM ELEMENT NO. / PROJECT NO. / TASK NO. / WORK UNIT ACCESSION NO

11 TITLE (Include Security Classification)
Mechanical Properties of Reid-Bedford Model Sand

12 PERSONAL AUTHOR(S)
Phillips, Bruce R.

13a TYPE OF REPORT	13b TIME COVERED	14 DATE OF REPORT (Year, Month, Day)	15 PAGE COUNT
Final report	FROM _____ TO _____	September 1986	83

16 SUPPLEMENTARY NOTATION
This report was originally published as a draft report to the sponsor in February 1983.

17 COSATI CODES			18 SUBJECT TERMS (Continue on reverse if necessary and identify by block number)
FIELD	GROUP	SUB-GROUP	See reverse.

19 ABSTRACT (Continue on reverse if necessary and identify by block number)

This report documents (a) the results of laboratory tests performed to supplement data previously reported on Reid-Bedford Model (RB) sand and (b) the results of an analysis of all of the RB laboratory data to develop representative laboratory material properties. The laboratory tests and analysis were conducted for use in evaluating the ability of mathematical constitutive models to simulate the behavior of soils subjected to complex dynamic loadings produced by both explosive- and earthquake-induced ground shock.

RB sand is a fine-grained, uniform sand obtained along the Big Black River in Mississippi. The laboratory tests reported consist of consolidated-drained tests and consolidated-undrained tests on saturated sand. The analysis considered the response of the sand under three different test conditions, i.e., unconsolidated-undrained tests on dry sand, consolidated-drained tests on saturated sand, and consolidated-undrained tests on saturated sand. Representative responses of RB sand in terms of uniaxial strain (UX) compressibility;

(Continued)

20 DISTRIBUTION/AVAILABILITY OF ABSTRACT	21 ABSTRACT SECURITY CLASSIFICATION	
☒ UNCLASSIFIED/UNLIMITED ☐ SAME AS RPT ☐ DTIC USERS	Unclassified	
22a NAME OF RESPONSIBLE INDIVIDUAL	22b TELEPHONE (Include Area Code)	22c OFFICE SYMBOL

DD FORM 1473, 84 MAR — 83 APR edition may be used until exhausted. All other editions are obsolete.

SECURITY CLASSIFICATION OF THIS PAGE
Unclassified

10. SOURCE OF FUNDING NUMBERS (Continued).

AFOSR-MIPR-82-00003, Project 2307/C1 FY 82

18. SUBJECT TERMS (Continued).

Consolidated-drained	Triaxial compression
Consolidated-undrained	Unconsolidated-undrained
Laboratory tests	Uniaxial strain compression
Reid-Bedford sand	

19. ABSTRACT (Continued).

—UX stress path; and triaxial compression stress-strain, stress path, and failure are presented for each of the test conditions.—

PREFACE

The U.S. Army Engineer Waterways Experiment Station (WES) was requested by the Air Force Office of Scientific Research (AFOSR) to provide a complete and consistent set of laboratory mechanical properties for two soils for use in support of AFOSR contract number F49620-80-C-008, "Fundamental Properties of Soils for Complex Dynamic Loading," with Applied Research Associates, Inc., Albuquerque, New Mexico. The work reported herein was funded under AFOSR-MIPR-82-00003, Project 2307/C1 FY 82; the technical contact was LTC John J. Allen, AFOSR/NA.

The WES project engineer for this study was Mr. B. R. Phillips of the Geomechanics Division (GD), Structures Laboratory (SL), working under the general direction of Mr. J. Q. Ehrgott, Chief, Operations Group, GD, and Dr. J. G. Jackson, Jr., Chief, GD. The laboratory composition and mechanical property tests were conducted by personnel of GD and the Instrumentation Services Division. The laboratory classification and index tests were conducted by personnel of the Soils Testing Facility, Soil Mechanics Division, Geotechnical Laboratory. This report was prepared by Mr. Phillips and transmitted to the sponsor in February 1983.

COL Tilford C. Creel, CE, and COL Robert C. Lee, CE, were the Commanders and Directors of WES during this investigation. COL Allen F. Grum, USA, was the previous Director and COL Dwayne G. Lee, CE, is the present Commander and Director. Mr. F. R. Brown and Dr. Robert W. Whalin were the WES Technical Directors. Mr. Bryant Mather was Chief, SL.

A-1

CONTENTS

CONVERSION FACTORS, NON-SI TO SI (METRIC)
UNITS OF MEASUREMENT

Non-SI units of measurement used in this report can be converted to SI (metric) units as follows:

Multiply	By	To Obtain
degrees (angle)	0.01745329	radians
feet	0.3048	metres
gallons (US liquid)	3.785412	cubic decimetres (litres)
inches	2.54	centimetres
kips (force)	4.448222	kilonewtons
kips (force) per square inch	6.894757	megapascals
megatons (nuclear equivalent of TNT)	4.184	petajoules
pounds (force) per square inch	6.894757	kilopascals
pounds (mass)	0.4535924	kilograms
pounds (mass) per cubic foot	16.01846	kilograms per cubic metre

CHAPTER 1

INTRODUCTION

1.1 BACKGROUND

Applied Research Associates, Inc. (ARA), was funded by the Air Force Office of Scientific Research (AFOSR) to evaluate the ability of different mathematical constitutive models to simulate the behavior of soils subjected to complex dynamic loadings produced by both explosive- and earthquake-induced ground shock. To accomplish this study, ARA required a complete set of laboratory data for two sands. A complete set of properties included static and dynamic uniaxial strain and triaxial shear data on both dry and fully-saturated specimens. The U. S. Army Engineer Waterways Experiment Station (WES) was requested by AFOSR to assemble data from WES files on two sands and to supplement the information with additional laboratory tests as required. In January 1982, the available laboratory data on dry Reid-Bedford Model (RB) sand and back-pressure saturated Misers Bluff (MB) sand were reported in convenient formats for constitutive property analyses (Reference 1). Additional data obtained for MB sand and an analysis of the complete set of MB sand data were reported in Reference 2. Additional laboratory tests were also conducted on RB sand to complete that data set. All of the available RB sand data were then analyzed to develop a complete and consistent set of material properties for use in numerical calculations.

1.2 PURPOSE AND SCOPE

The purposes of this report are to (a) present the results of the additional laboratory tests conducted on saturated specimens of RB sand remolded to an air-dried density of approximately 1.65 g/cc and (b) document an analysis of all the RB sand laboratory data. Results of laboratory classification, index, and composition property tests and the mechanical property data on saturated RB sand are presented in Chapter 2. Chapter 3 documents the analysis of all the laboratory data on RB sand and presents

representative responses. Comparisons of the representative relations for this material undet three different test conditions are contained in Chapter 4.

CHAPTER 2

LABORATORY TESTS

2.1 CONVENTIONAL SOIL TESTS

Samples of RB sand were split from the available supply of material and tested to determine grain size distribution, Atterberg limits, and specific gravity (Reference 3). Results of these tests indicated that the RB sand used in this study was nonplastic and had a specific gravity of 2.65. The results of grain size distribution tests are shown in Figure 2.1. Using these data, the RB sand was classified according to the Unified Soil Classification System (Reference 4) as an SP sand.

The grain size distribution and specific gravity reported in Reference 1 for RB sand are almost identical to the data in Figure 2.1. A comparison of the gradation data is shown in Figure 2.2. The material tested previously is essentially the same as the material used for tests reported in this chapter.

2.2 COMPOSITION PROPERTY TESTS

Prior to performing each mechanical property test, the height and diameter of each remolded specimen were obtained. These measurements, along with the known weight of material and the sand's specific gravity, were used to calculate air-dried density γ_d and void ratio e (the ratio of void volume to solid volume). Using measurements taken during the test and assuming that the specimen was completely saturated, the wet density γ and water content w at the end of the back-pressure saturation phase were calculated. These data are given for each test in Table 2.1.

2.3 MECHANICAL PROPERTY TESTS

A total of 24 consolidated-undrained and consolidated-drained mechanical property tests were performed on fully saturated specimens of remolded RB sand to complete the laboratory data base for this material.

2.3.1 Description of Tests and Test Program

A brief description of each type of test conducted to augment the RB sand data in Reference 1 follows:

a. The isotropic compression (IC) test subjects a cylindrically shaped specimen to an equal all-around confining stress (after initial effective stresses are applied) while measurements of the specimen's height and diameter changes are made. The data are normally plotted as pressure versus volumetric strain, the slope of which is the bulk modulus K.

b. The triaxial compression (TX) test is conducted after a desired initial effective stress is applied during the IC test. During a drained test, the cell pressure and the pore pressure (and therefore the effective stress) are held constant while vertical load is increased and measurements of the specimen's height and diameter changes are made. As vertical stress is applied during an undrained TX test, the cell pressure is held constant while pore pressure (and the resulting effective stress) is allowed to change. The data can be plotted as principal stress difference versus axial strain, the slope of which is Young's modulus E, or as principal stress difference versus principal strain difference, the slope of which is twice the shear modulus G. The maximum principal stress difference the specimen can support or the principal stress difference at 15 percent axial strain during shear loading (whichever occurs first) is defined as failure and describes one point on a failure surface. The failure surface is depicted as a plot of principal stress difference versus mean normal stress.

c. Two types of uniaxial strain (UX) tests were conducted:

(1) The first (designated UX) is conducted by applying a vertical pressure to a wafer-shaped specimen that is physically constrained from deflecting radially by a steel ring. Measurements are made of the applied vertical stress and the specimen's height change. The data are plotted as vertical stress versus vertical strain, the slope of which is the constrained modulus M.

(2) The second type of UX test (designated UX/K_o) is conducted by applying radial pressure to a specimen until a slight inward movement of the diameter is detected. Vertical load is then applied until the specimen returns to its original radial position (zero radial strain). This process is repeated throughout the test. As in the UX test, the data are plotted as vertical stress versus vertical strain, the slope of which is the constrained modulus M. When the data are plotted as principal stress difference versus mean normal stress, the slope (assuming elastic theory) is $2G/K$, or in terms of Poisson's ratio ν, $3(1-2\nu)/1+\nu)$.

The test program consisted of 3 static and 2 dynamic undrained UX tests, 1 static drained UX test, 7 static consolidated-undrained IC-TX tests, 3 static consolidated-drained IC-TX tests, 2 undrained and 1 drained IC tests, 3 static consolidated-undrained UX/K_o tests and 2 static consolidated-drained UX/K_o tests. All IC-TX and UX/K_o tests were performed at one of four initial

effective stresses, i.e., nominally 0.14, 1.72, 3.45, or 6.90 MPa. Each specimen was back-pressure saturated prior to the application of the effective stress.

2.3.2 Test Procedures

2.3.2.1 UX Tests. Procedures to prepare static and dynamic UX test specimens of saturated RB sand were identical. The weight of air-dried material required to obtain a density of 1.65 g/cc was split from the supply of RB sand. The material was then "spooned" directly into the 9.1-centimeter-diameter and 2.3-centimeter-high specimen chamber which was three-fourths filled with tap water. As the sand was placed into the chamber, the water was displaced, and the resulting specimen was "almost" saturated. The test device was assembled by placing a rubber membrane containing a footing over the specimen and securing the top of the chamber. The footing rode directly on the center of the specimen and was connected to a linear variable differential transducer (LVDT) which measured vertical deflection during the test. After assembling the test device, the specimen was fully saturated by increasing both the external vertical stress and the internal back pressure (maintaining an effective vertical stress of 0.69 MPa) until the vertical stress was approximately 3.45 MPa. Once the specimen was saturated, the static effective vertical stress was further increased to the desired level by increasing the applied vertical stress while holding the pore pressure constant. The drainage line was then closed for an undrained test or left open for a drained test. Vertical stress was then increased statically or dynamically to the desired total stress level while measurements of vertical stress and vertical deflection were made. During an undrained test, pore pressure measurements were also made using a hypodermic needle which extended into the center of the specimen. Both drained and undrained tests were conducted; dynamic tests were performed only under undrained conditions. Test measurements were stored on both magnetic tape and light beam oscillograph for later processing and plotting.

2.3.2.2 IC-TX and UX/K_o Tests. The preparation of specimens for IC-TX and UX/K_o testing was identical, and the tests were performed in the same test device. The required amount of air-dried material was split from the supply of RB sand and placed into a steel remolding jacket containing a 0.06-centimeter-thick rubber membrane. A vacuum was applied through the jacket to

pull the membrane against the jacket's sides. The sand was spooned into the device until a density of approximately 1.65 g/cc was obtained. Each specimen was remolded to about 5.1 centimeters in diameter by 11.4 centimeters in height. The membrane was then released from the jacket, attached to a top cap and base with rubber bands, and coated with a layer of liquid synthetic rubber to inhibit breakdown of the membrane due to the hydraulic oil confining fluid.

The vertical measurement system consisted of two vertically-mounted LVDT's positioned 180 degrees apart on top of the specimen. The radial measurement system for the IC-TX tests was a lateral deformeter consisting of four strain-gaged steel arms positioned equidistant around the specimen's midheight. The radial measurement system for the UX/K_o tests was a single lateral deformeter consisting of four horizontally-mounted LVDT's positioned at quarter points around the specimen's midheight.

After the specimen and its instrumentation were in place, the test device was assembled, the specimen was back-pressure saturated, and one of four initial isotropic effective stresses (0.14, 1.72, 3.45, and 6.90 MPa) was applied to the specimen with the drainage line open. If the specimen was to be tested in a drained condition, the test was performed immediately after application of the effective stress. For undrained tests the drainage line was closed prior to continuing the test.

After back-pressure saturation and application of the effective stress, the IC-TX tests were loaded vertically until failure (see Section 2.3.1) occurred. Measurements were made of vertical load, confining pressure, movement of the piston, and vertical and radial deflection of the specimen. During undrained IC-TX tests, pore pressure measurements were also made. Data were recorded by a digital data acquisition system which sampled the data channels at designated time intervals and recorded the data on a minicassette tape for later processing and plotting.

Zero radial deflection for UX/K_o tests was maintained after the isotropic effective stress was applied to the specimen. Hence, some radial deflection occurred prior to UX loading. As vertical load was applied to the specimen during the UX/K_o test, the radial deflections were constantly monitored and adjusted back to zero by changing the confining pressure. The data

obtained for these tests were the same as those obtained for IC-TX tests and were recorded by the digital data acquisition system.

2.3.3 Test Data

The recorded data were related to the pretest calibration steps of the corresponding measurement unit to calculate pressure, load, or deformation. Using these raw data along with the specimen's height and diameter, calculations were made of appropriate stresses and strains and computer plots were generated. For RB sand, the specimens deformed predominately as right circular cylinders during the IC tests; hence the equations used to calculate volumetric strain were based on this assumed shape (Reference 5). The results of the mechanical property tests conducted on saturated RB sand specimens are presented in Plates 1-24 and are summarized in Table 2.1 with the composition property data.

Results of the static and dynamic UX tests are shown as plots of vertical stress versus vertical strain in Plates 1-6. The dynamic tests are shown with both a static and a dynamic portion. The static portion includes the back-pressure saturation phase and application of the initial effective stress; the dynamic portion is the remainder of the test.

The UX/K_o tests are shown in Plates 7-11. Each plate includes plots of (a) total mean normal stress versus volumetric strain, (b) principal stress difference versus total mean normal stress, (c) total axial (vertical) stress versus axial (vertical) strain, (d) principal stress difference versus effective mean normal stress, and (e) pore pressure versus axial strain. Each plot shows the results of the entire back-pressure saturation phase, application of the isotropic effective stress, and UX/K_o loading.

Plates 12-14 and 15-24 show the results of the IC and IC-TX tests, respectively. The IC data plates contain the same plots as those described for the UX/K_o tests. For the IC-TX tests, each plate contains plots of (a) total mean normal stress versus volumetric strain, (b) principal stress difference versus total mean normal stress, (c) principal stress difference versus both principal strain difference and axial strain, (d) principal stress difference versus effective mean normal stress, and (e) pore pressure versus axial strain.

Table 2.1 Summary of mechanical property tests on saturated Reid-Bedford model sand.

Plate No.	Test Number	Air Dried Density γ_d, g/cc	After Back-Pressure Saturation: Wet Density γ, g/cc	After Back-Pressure Saturation: Water Content w, %	Specific Gravity G_s	Void Ratio e	Test Type*	Test Conditions	Initial Effective Stress σ'_c, MPa	UX and UX/K_o Tests: Peak Vertical Stress σ_a, MPa	UX and UX/K_o Tests: Vertical Strain at Peak Vertical Stress %	IC Tests: Peak Total Mean Normal Stress p, MPa	IC Tests: Volumetric Strain at Peak Stress $\Delta V/V$, %	TX Tests: Vertical Strain at Failure ϵ_z, %	TX Tests: Principal Stress Difference at Failure $\sigma_z - \sigma_r$, MPa	TX Tests: Total Mean Normal Stress at Failure p, MPa
1	RBUX.1	1.650	2.038	22.3	2.65	0.61	S-UX	Drained	0.69	40.7	5.3	---	---	---	---	---
2	RBUX.2	1.650	2.034	23.3	2.65	0.61	S-UX	Undrained	0.69	41.9	1.4	---	---	---	---	---
3	RBUX.2A	1.650	2.026	22.8	2.65	0.61	S-UX	Undrained	0.69	41.6	1.2	---	---	---	---	---
4	RBUX.3	1.650	2.038	23.5	2.65	0.61	D-UX	Undrained	0.69	43.0	1.3	---	---	---	---	---
5	RBUX.4	1.650	2.030	23.0	2.65	0.61	S-UX	Undrained	3.45	41.7	1.7	---	---	---	---	---
6	RBUX.5	1.650	2.033	23.2	2.65	0.61	D-UX	Undrained	3.45	43.1	1.8	---	---	---	---	---
7	RBDK.1	1.637	2.025	23.0	2.65	0.61	UX/K_o	Undrained	0.16	35.3	0.7	---	---	---	---	---
8	RBDK.2	1.643	2.027	22.9	2.65	0.61	UX/K_o	Undrained	1.73	37.2	0.9	---	---	---	---	---
9	RBDK.3	1.637	2.019	23.4	2.65	0.62	UX/K_o	Drained	1.73	21.5	3.2	---	---	---	---	---
10	RBDK.4	1.631	2.020	23.3	2.65	0.62	UX/K_o	Drained	3.48	21.9	2.9	---	---	---	---	---
11	RBDK.5	1.637	2.025	23.0	2.65	0.61	UX/K_o	Undrained	3.49	38.0	1.0	---	---	---	---	---
12	RBIC.1	1.637	2.021	22.9	2.65	0.61	IC	Undrained	0.14	---	---	34.5	1.0	---	---	---
13	RBIC.2	1.658	2.034	22.2	2.65	0.59	IC	Undrained	3.46	---	---	34.5	2.2	---	---	---
14	RBIC.3	1.634	2.020	23.0	2.65	0.61	IC	Drained	0.24	---	---	34.0	8.3	---	---	---
15	RBTX.1	1.647	2.033	22.3	2.65	0.59	IC-TX	Undrained	1.69	---	---	3.8	1.7	13.0	5.8	5.7
16	RBTX.2	1.634	2.024	22.8	2.65	0.60	IC-TX	Undrained	1.67	---	---	3.8	1.6	15.0	6.0	5.8
17	RBTX.3	1.632	2.022	23.2	2.65	0.62	IC-TX	Drained	1.76	---	---	4.0	1.3	11.5	4.6	5.3
18	RBTX.4	1.655	2.036	22.1	2.65	0.58	IC-TX	Undrained	0.12	---	---	2.2	0.8	15.0	4.5	3.7
19	RBTX.5	1.626	2.019	23.4	2.65	0.62	IC-TX	Undrained	0.10	---	---	2.2	0.7	15.0	4.1	3.6
20	RBTX.6	1.645	2.030	22.7	2.65	0.60	IC-TX	Drained	0.16	---	---	2.2	0.6	8.7	0.8	2.5
21	RBTX.7	1.634	2.024	23.1	2.65	0.61	IC-TX	Undrained	3.47	---	---	5.6	2.1	15.0	6.6	7.7
22	RBTX.8	1.626	2.021	23.2	2.65	0.62	IC-TX	Undrained	3.44	---	---	5.5	2.5	15.0	6.7	7.7
23	RBTX.9	1.637	2.023	22.9	2.65	0.60	IC-TX	Drained	3.46	---	---	5.6	2.3	12.5	7.8	8.1
24	RBTX.10	1.666	2.045	21.8	2.65	0.58	IC-TX	Undrained	7.26	---	---	8.8	3.0	15.0	8.1	12.2

* For UX tests, "S" refers to static and "D" refers to dynamic.

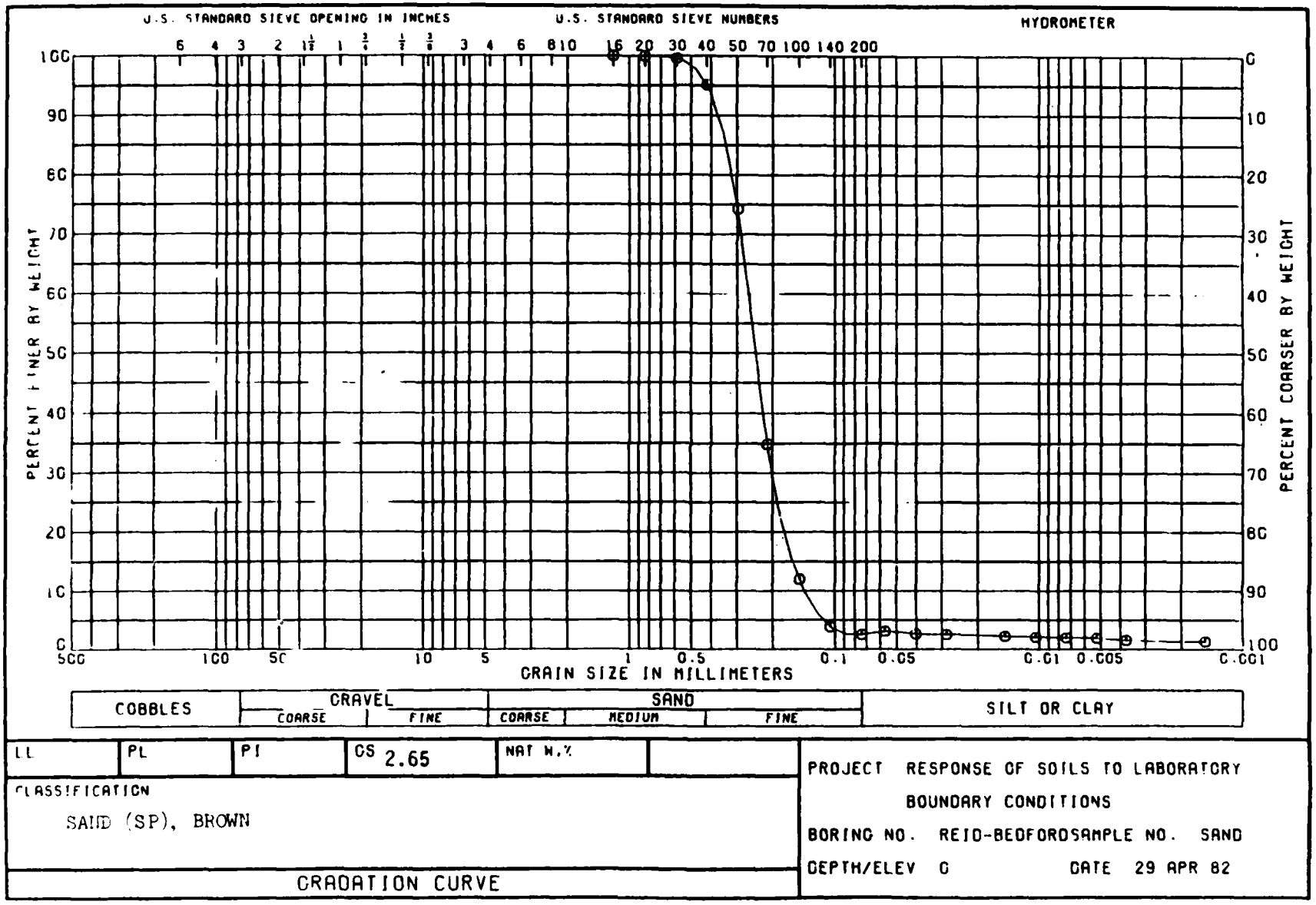

Figure 2.1 Gradation of RB Model sand.

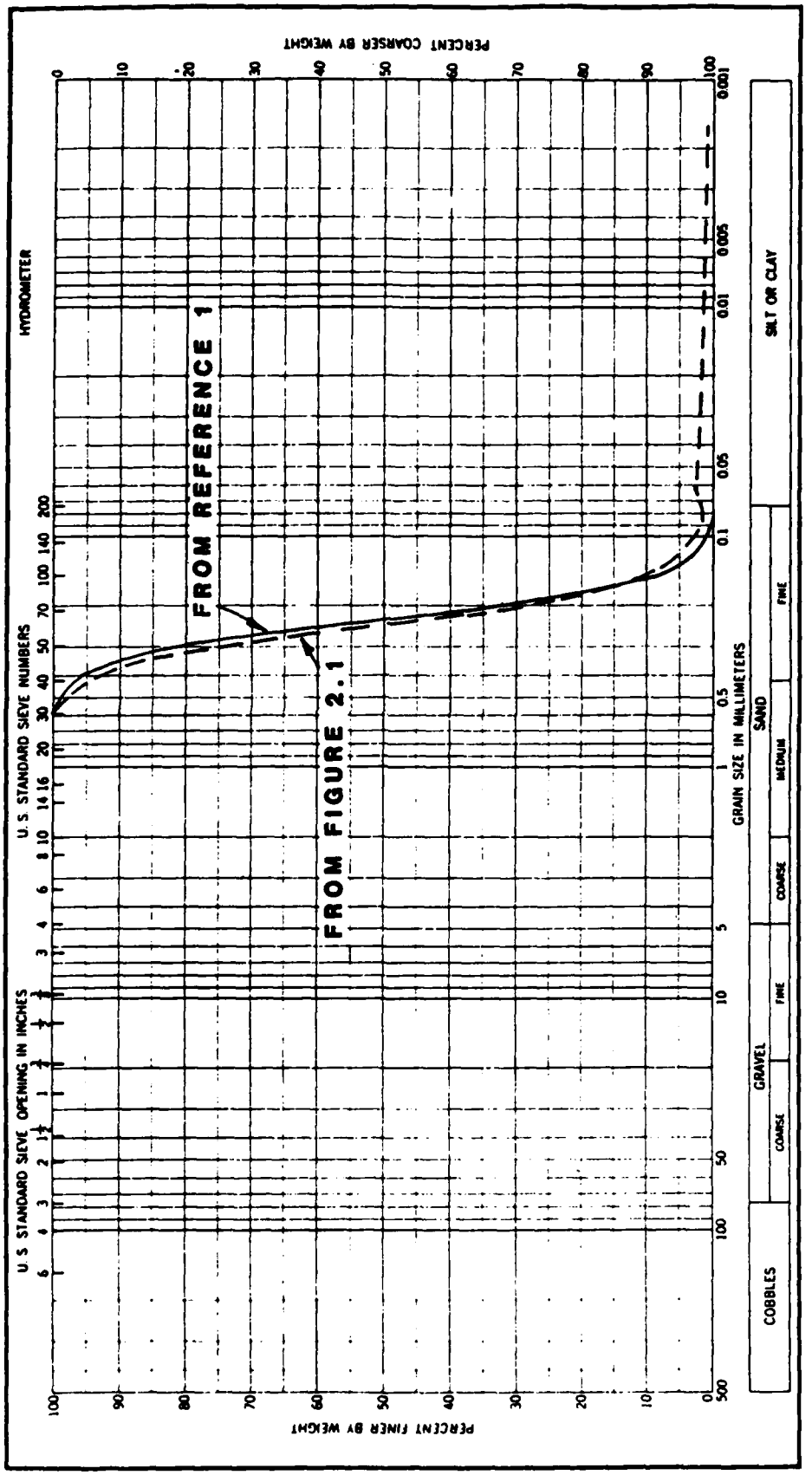

Figure 2.2 Comparison of gradation data for RB sand from two test programs.

CHAPTER 3

DATA ANALYSIS AND REPRESENTATIVE PROPERTY RECOMMENDATIONS

The laboratory test results on RB sand, reported in Reference 1 and in Chapter 2 of this report, were used to develop a consistent set of representative laboratory properties that could subsequently be used to develop mathematical constitutive models.

Representative property recommendations include a uniaxial strain (UX) compressibility relation, a UX stress path, a total-stress TX failure relation, and a total-stress TX stress path under three different conditions, i.e., unconsolidated-undrained (UU) tests on dry material, consolidated-drained (CD) tests on saturated material, and consolidated-undrained (CU) tests on saturated material. In addition, an effective TX stress path relation and pore pressure versus axial strain relation are given to represent the CU response of the saturated sand. All representative curves for the saturated RB sand are shown referenced to the point at the end of back-pressure saturation and after application of a given effective stress.

To develop these representative responses, all of the valid test data of a given type were plotted on a single page and a representative curve was selected based on an initial air-dried density of 1.65 g/cc and, for the saturated specimens, initial effective stresses of 0.14, 1.72, 3.45, and 6.90 MPa. When all representative curves were available for each type of test and condition, the curves were re-examined and adjusted (if required) so that the complete set of representative properties was internally consistent. The analysis results presented in this chapter constitute only one approach to the development of representative calculational properties; other approaches and analysis results are possible.

3.1 UX COMPRESSIBILITY

3.1.1 UU Tests on Dry Sand

The results from the static UX tests, the static UX/K_o tests and the static UX/Null test (described in Reference 1) on dry RB sand are shown in Figure 3.1. The two UX/K_o tests (TK.1 and TK.2) are slightly less compressible than the remaining tests because the densities of both these specimens were greater than those of the other test specimens. A representative

loading relation was drawn through the center of the data. Representative unloading relations from vertical stress levels of 17.7 and 35.4 MPa are also shown in Figure 3.1.

3.1.2 CD Tests on Saturated Sand

The uniaxial strain portions of the static CD UX tests and the static CD UX/K_o tests are shown in Figure 3.2. The UX tests were rezeroed at the end of the back-pressure saturation phase and the UX/K_o tests were rezeroed at the end of application of the effective stress. The UX/K_o test results are slightly more compressible than results of the UX tests. This is thought to be caused by the procedure used to conduct the tests. During the UX/K_o test, only the specimen's midheight is monitored and maintained at zero radial deflection; it is assumed that the entire length of the specimen responds similarly. During the UX test, the radial deflection is physically restricted by a steel ring and, therefore, uniaxial strain response along the entire height of the specimen is insured. For this reason, the results of the UX tests were more heavily weighted in the selection of a representative relation than the UX/K_o tests.

3.1.3 CU Tests on Saturated Sand

Linear approximations of the static and dynamic CU UX tests and the static CU UX/K_o tests are shown in Figure 3.3 rezeroed to the point after back-pressure saturation and application of the effective stress. The static and dynamic UX tests group together indicating that no significant rate effect occurs when times to peak stress are greater than 70 msec. The UX/K_o test results show more variability and are more compressible than the UX tests. This is believed to be due to the UX/K_o tests not being under as strict a uniaxial strain condition as the UX tests (see Section 3.1.2). Mixture theory (Reference 6) assumes that the compressibility of individual minerals and water can be mathematically combined to calculate the compressibility of the mixture. If it is assumed that the only mineral in RB is quartz, a quartz/water mixture with a back-pressure saturated density of 2.020 g/cc would yield a bulk modulus of 7840 MPa. Since a saturated specimen should have a constrained modulus approximately equal to the bulk modulus (based on elastic theory), the calculated modulus is slightly more

compressible than the UX test results. The representative relation was drawn through the center of the UX tests and represents a constrained modulus of 8700 MPa.

3.2 UX STRESS PATH

3.2.1 UU Tests on Dry Sand

The results of two static UX/K_o tests and one static UX/Null test are shown in Figure 3.4 as plots of principal stress difference versus mean normal stress. The two UX/K_o tests have the same characteristic shape; the initial behavior of the UX/Null test is slightly different from these. A representative loading relation was selected that is initially through the center of the data and, at higher stress levels, is more like the lower density UX/K_o specimen (TK.1). This representative relation implies an initial loading Poisson's ratio of 0.29 and a loading Poisson's ratio of 0.37 at a principal stress difference of 10 MPa.

3.2.2 CD Tests on Saturated Sand

A summary of the static CD UX/K_o test results are shown as plots of principal stress difference versus total mean normal stress in Figure 3.5. The data were rezeroed to the point after application of the isotropic effective stress. Although the two tests were performed at different initial effective stresses, the estimated dry densities at the beginning of uniaxial strain loading were the same. The curves exhibit the same characteristic shape. The dashed line indicates that the initial portion of test RBDK.4 was not in a state of uniaxial strain; for this reason, the results from test RBKD.3 were more closely followed at lower stress levels. A representative curve was selected which goes through the center of the data.

3.2.3 CU Tests on Saturated Sand

The results from the static CU Tests on saturated RB sand are shown in Figure 3.6. The test data were rezeroed to the point after application of effective stress. Each of the tests show an initially steep UX stress path followed by a flat portion, which implies a loading Poisson's ratio of about 0.49. A thorough examination of the test results indicated that immediately after the effective stress was applied, the drain closed, and loading begun, the specimens behaved as though they were not completely saturated. During

the stiff portion of the curves, no radial strain resulted from the applied load (so no offsetting confining pressure was needed), very little increase in pore pressure occurred, and a large increase in vertical strain resulted from a very small increase in vertical stress. At the "break point," the specimen began to strain radially, the pore pressure began to increase rapidly, and a large increase in vertical stress resulted in a small increase in vertical strain, i.e., the specimen began to respond as though it was saturated. Experience has shown that the air should be in solution with water when pore pressures equal or exceed 2 MPa (the pore pressure to which the RB specimens were saturated). In addition, B-factors (values used to determine the degree to which a specimen is saturated; Reference 7) for each of the tests were calculated to be greater than 0.99. Therefore, for the purposes of this investigation, the initial portions of the UX stress path data were ignored and a representative UX stress path was constructed with an implied value of Poisson's ratio of 0.49.

3.3 TX FAILURE

The TX failure and TX stress-strain data were analyzed together to develop representative TX responses of the RB sand. The TX failure data provided an overall look at TX response and aided in identifying possible anomalous tests. The TX stress-strain data provided information for a further, more detailed screening. This section of the report addresses TX failure relations for RB sand; TX stress-strain responses are discussed in Section 3.4.

3.3.1 UU Tests on Dry Sand

The failure points from the static TX tests on dry RB sand are shown as circles in Figure 3.7. As discussed in Section 2.3.1, failure is defined as the maximum principal stress difference which the specimen can support or the principal stress difference at 15 percent vertical strain during the application of the shearing load (whichever occurs first). For confining pressures (σ_r) $\leq$ 4 MPa, failure actually occurred at vertical strains of less than 15 percent. For σ_r > 4 MPa, failure was assumed to occur at 15 percent vertical strain. A linear approximation to the failure points was selected as the representative failure relation. This line has a slope of 1.10 which implies a Coulomb friction angle of about 28 degrees.

3.3.2 CD Tests on Saturated Sand

Failure points from the three static CD TX tests on saturated RB sand specimens are shown as circles in Figure 3.8. These data were rezeroed at the end of the back-pressure saturation phase. Failure points represent the results of tests at three levels of effective stress, i.e. 0.14, 1.72, and 3.45 MPa. Examination of the TX stress-strain data indicated that failure in each test occurred at less than 15 percent vertical strain. The failure data implied a gradually softening representative failure relation which is shown in Figure 3.8 with the representative TX stress path for each level of effective stress.

3.3.3 CU Tests on Saturated Sand

TX data from the CU tests on saturated RB sand are plotted as principal stress difference versus effective mean normal stress in Figure 3.9. The representative failure relation was constructed through zero and along the apparent failure portions of the test results. The representative TX stress path relations were selected by beginning at the target levels of effective stress and following parallel to the closest stress path until the representative failure relation was encountered. The stress paths continued along the representative failure relation until the maximum principal stress difference (as defined by the representative TX stress-strain relations) was encountered. Unloading relations for the tests at each effective stress were very similar. The representative unloading TX stress path relations were drawn parallel to the unloading test results starting at the maximum principal stress difference achievable at each level of effective stress.

The CU failure data were also plotted as principal stress difference versus total mean normal stress (Figure 3.10). This plot shows the maximum (von Mises) strengths which the saturated RB sand can achieve at each initial effective stress level. For initial effective stresses of 0.14, 1.72, 3.45, and 6.90 MPa, the limiting principal stress differences are 4.40, 6.00, 6.70, and 7.60 MPa, respectively. The Coulomb portion of the representative total stress failure relations in Figure 3.10 is the same as the CD TX failure relation shown in Figure 3.8.

3.4 TX STRESS-STRAIN

3.4.1 UU Tests on Dry Sand

Figure 3.11 shows the results of dry RB TX tests conducted at constant confining pressures of 0.4 and 4.0 MPa. Representative TX stress-strain relations were developed for the three target confining stresses (0.14, 1.72, and 3.45 MPa) based on maximum principal stress differences determined from the representative failure relation in Figure 3.7 and the shapes of the TX test results.

3.4.2 CD Tests on Saturated Sands

The test results from CD tests on saturated sands are shown in Figure 3.12 plotted as principal stress difference versus both vertical strain and principal strain difference. These data were rezeroed to the beginning of application of the TX load. Representative TX stress-strain relations were developed for each target effective stress by adjusting the test results to agree with the maximum principal stress differences determined from the representative failure relation shown in Figure 3.8.

3.4.3 CU Tests on Saturated Sands

Figure 3.13 shows the results of the static CU tests on saturated sand at four initial effective stresses, i.e., 0.14, 1.72, 3.45, and 6.90 MPa. These curves were rezeroed to the beginning of the application of the TX load. Each of the curves has a characteristic shape that ties with the TX stress paths in Figure 3.9. For the 0.14-MPa effective stress, the stress-strain curve is initially stiff while its corresponding TX stress path approaches the failure relation. The stress-strain curve then flattens exhibiting a plastic response while its TX stress path rides on the failure relation. As the maximum principal stress difference is approached, the stress-strain curve begins to flatten more and then unloads. For the higher levels of effective stress, the deviation from the initial stiff portion of the stress-strain curve occurs at the point where the TX stress path changes curvature near the failure relation. Representative TX stress-strain relations were developed from the test data by adjusting for the target density and level of effective stress. The representative TX stress-strain relations are shown as heavy lines in Figure 3.13.

3.5 PORE PRESSURE RESPONSE DURING TX LOADING

Figure 3.14 shows the results of the CU TX tests plotted as pore pressure versus vertical strain. Each curve in Figure 3.14 was initialized so that the pore pressure at the beginning of TX loading equaled zero. Representative pore pressure versus axial strain relations (heavy lines in Figure 3.14) were based on the target effective stresses.

3.6 SUMMARY

The analyses discussed in this chapter represent one approach to the development of representative relations for calculational properties. Each representative relation was compared and correlated with the others to insure internal consistency of all the properties. Individual plots of these representative relations for dry RB sand are shown in Figures 3.15-3.18. Plots of the representative drained and undrained responses of saturated RB sand are shown in Figures 3.19-3.22 and Figures 3.23-3.28, respectively.

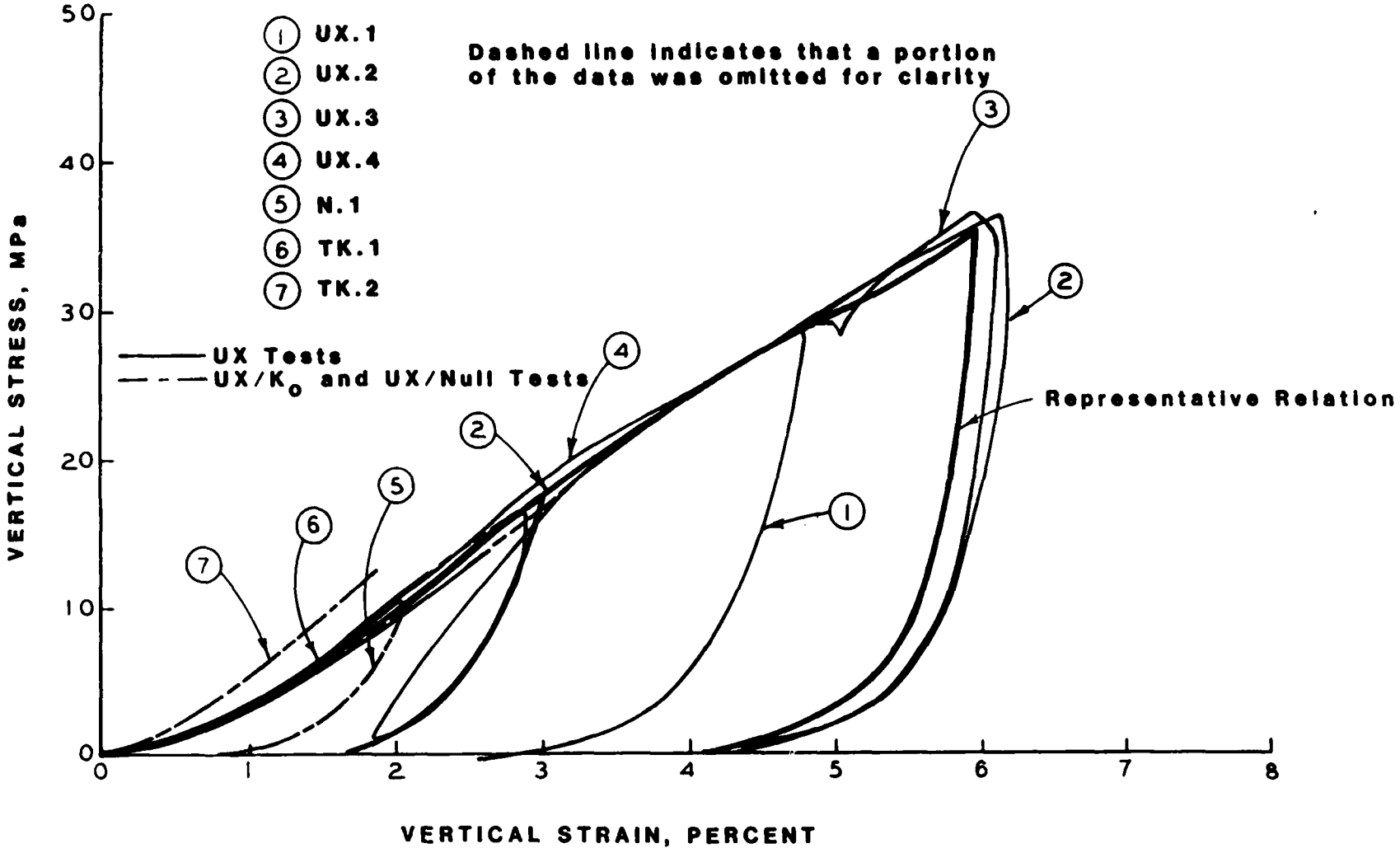

Figure 3.1 Static UX, UX/K_o, UX/Null test results and representative undrained UX compressibility relation for dry RB sand.

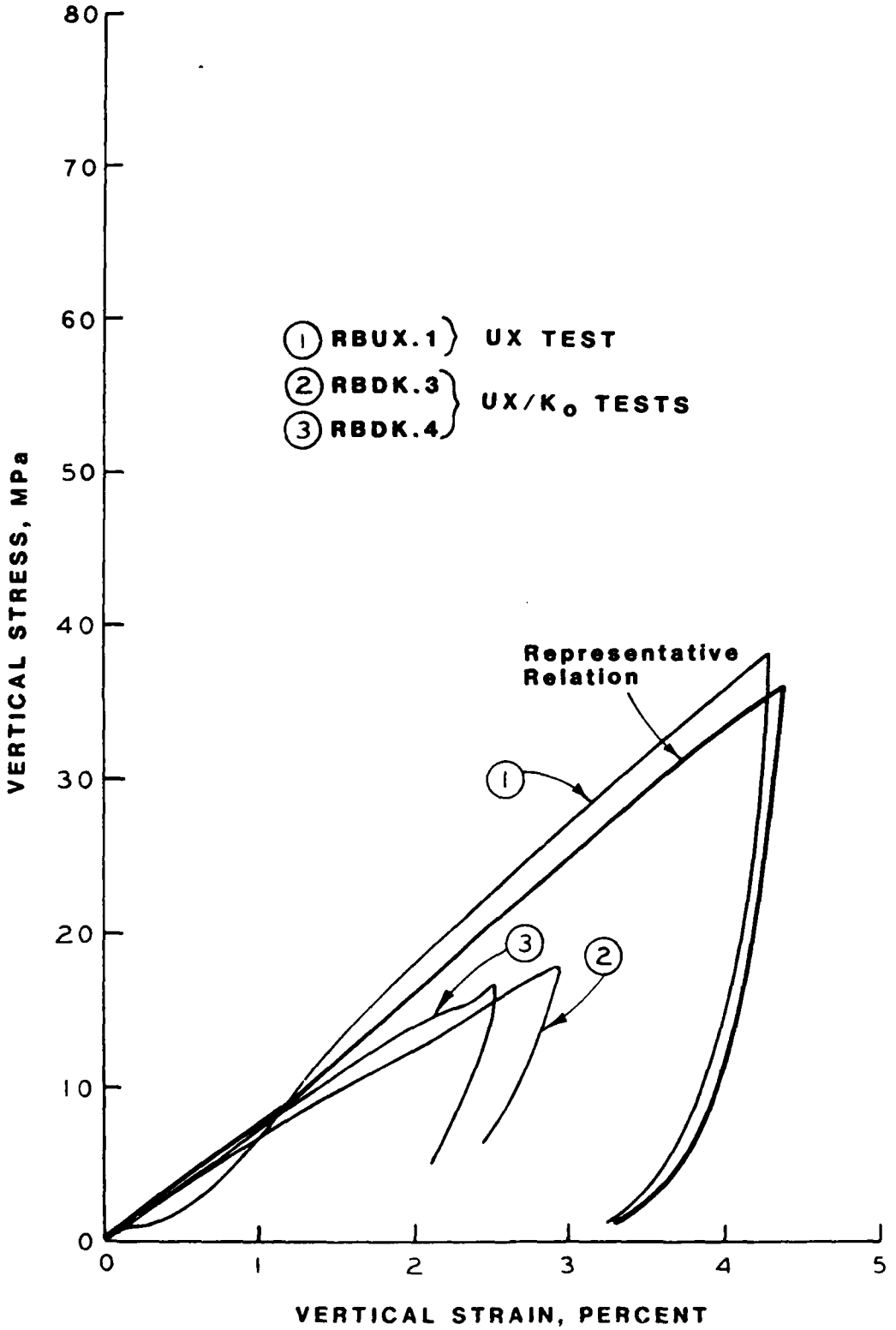

Figure 3.2 Static UX and UX/K_o test results and representative drained UX compressibility relation for saturated RB sand.

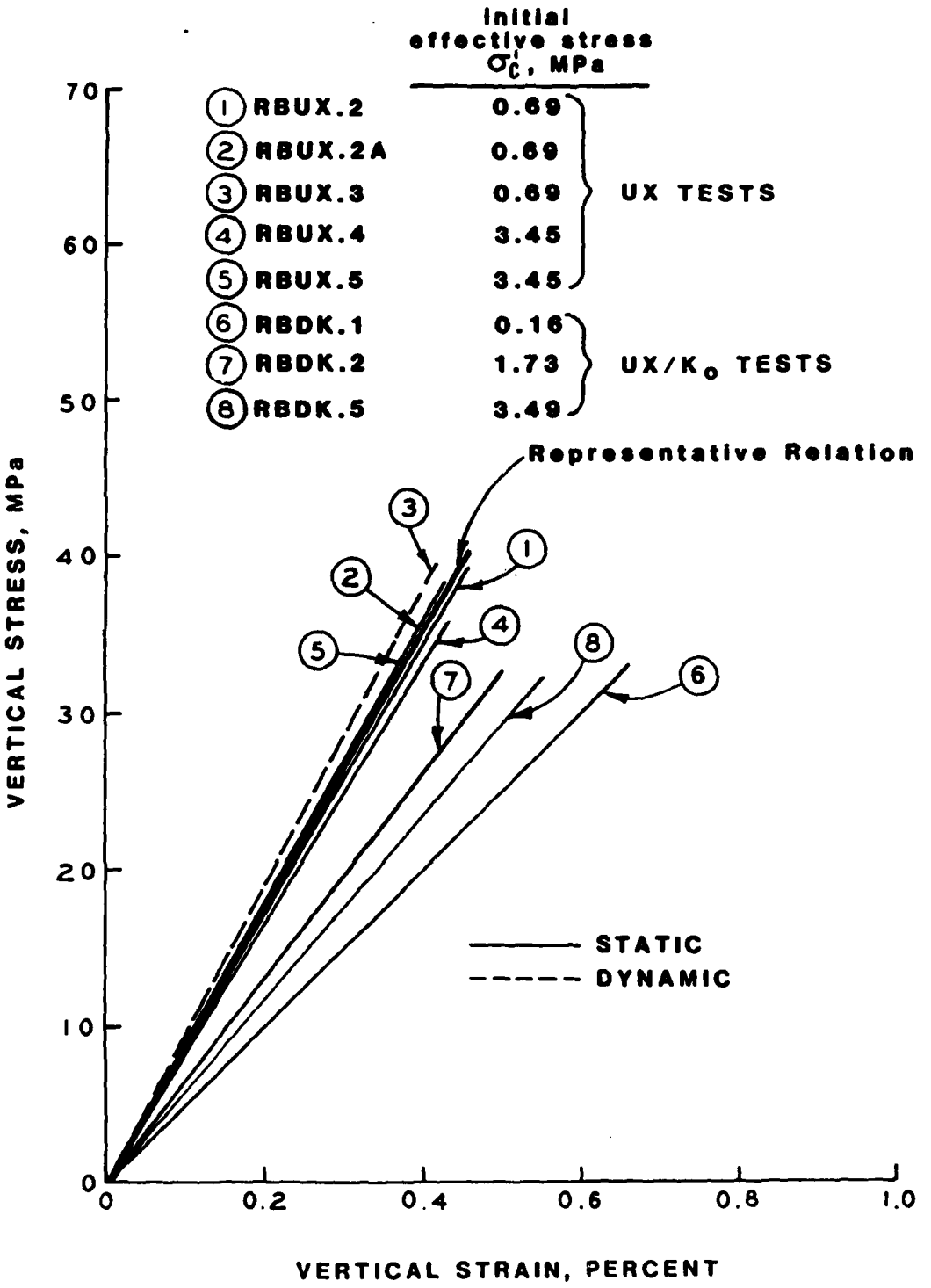

Figure 3.3 Static and dynamic UX and static UX/K_o test results and representative undrained UX compressibility relation for saturated RB sand.

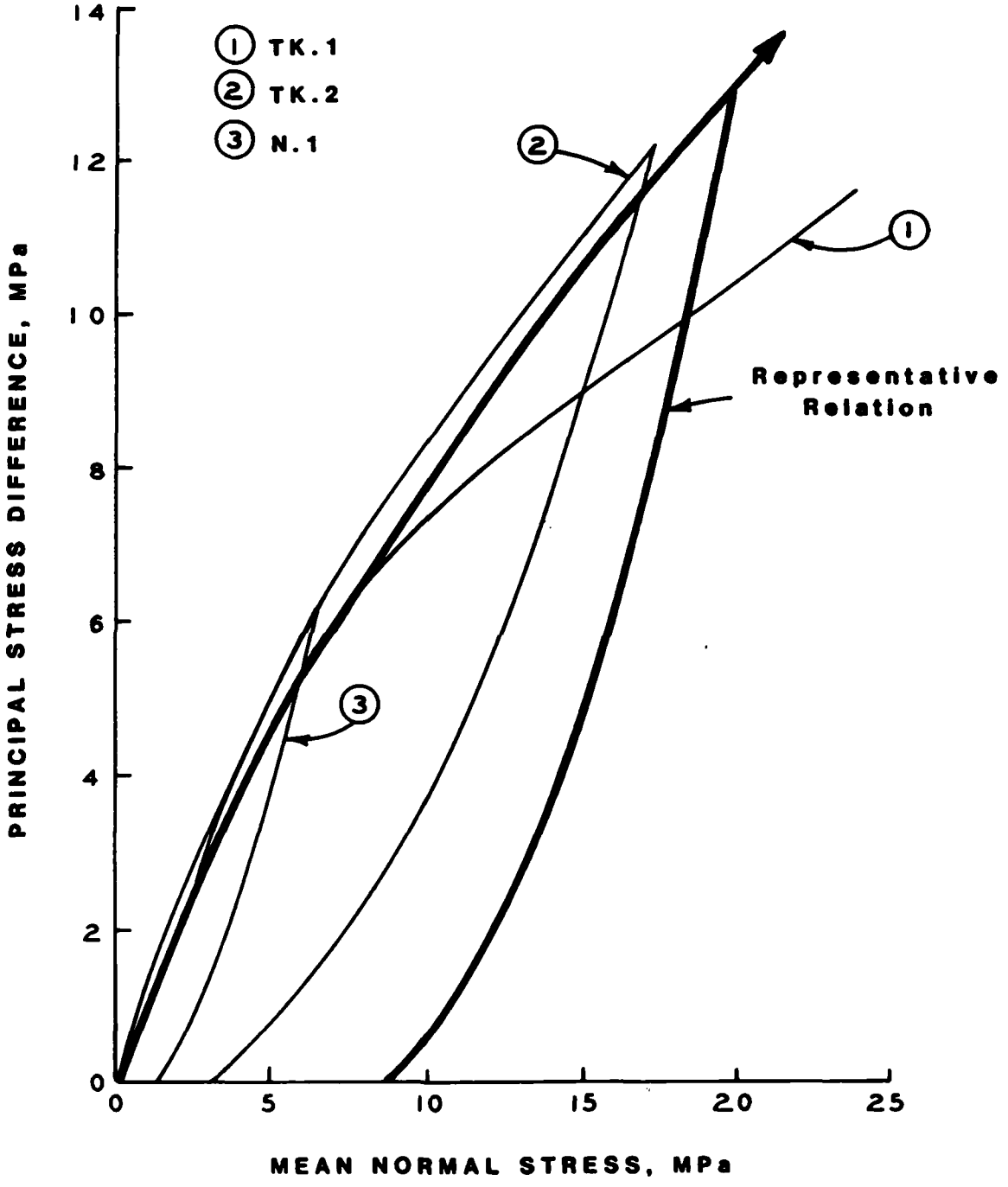

Figure 3.4 Static UX/K_o test results and representative undrained UX stress path relation for dry RB sand.

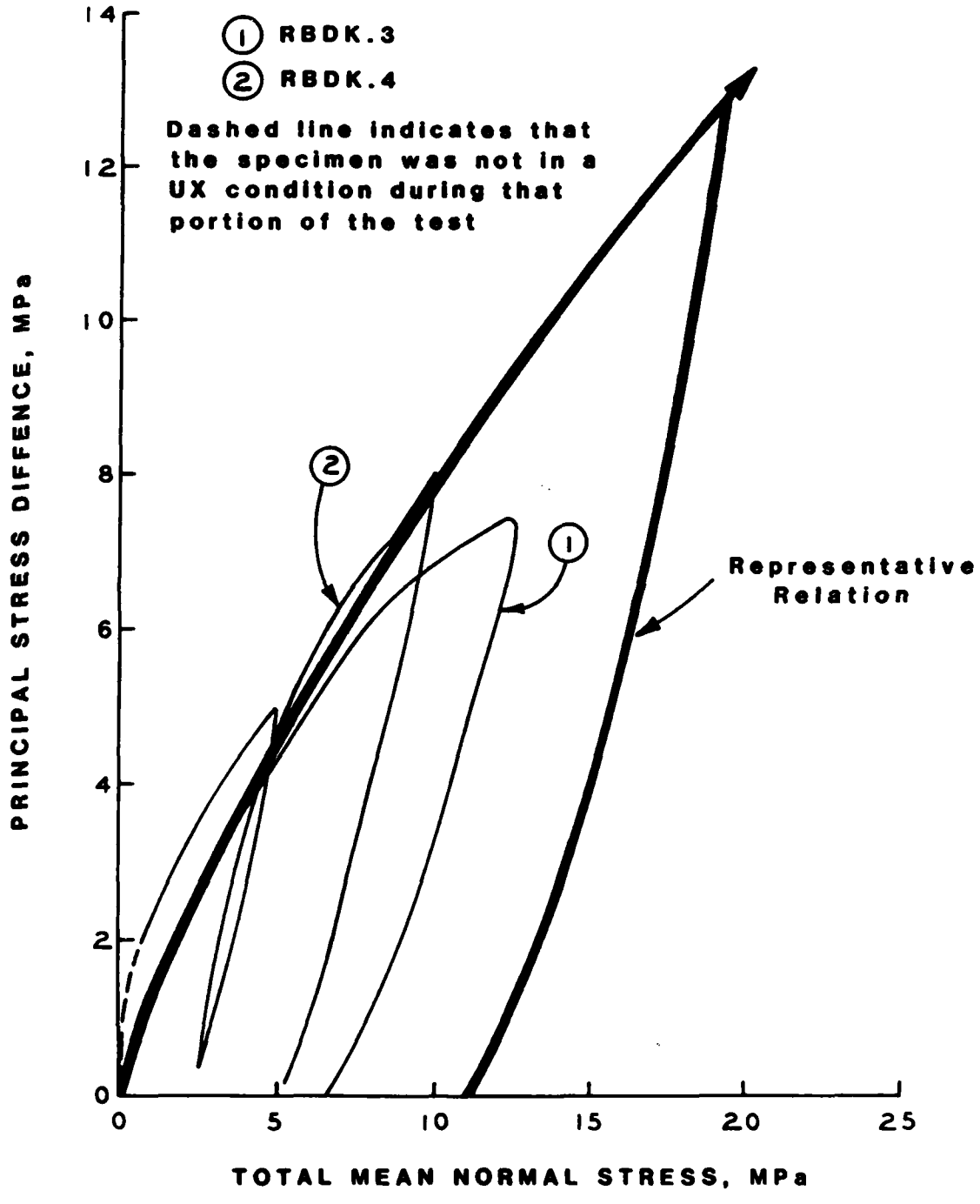

Figure 3.5 Static UX/K_o test results and representative drained UX stress path relation for saturated RB sand.

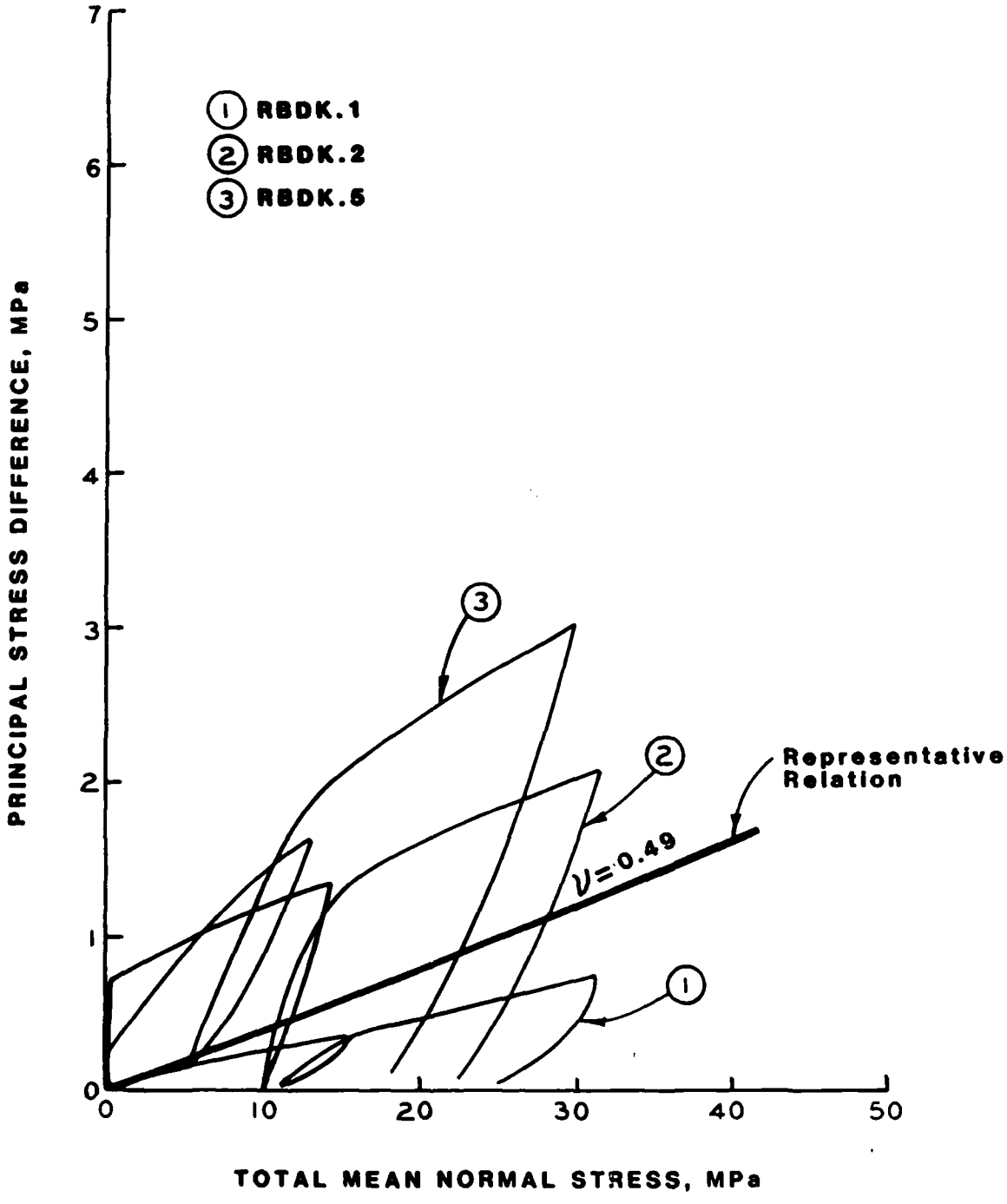

Figure 3.6 Static UX/K_o test results and representative undrained UX stress path relation for saturated RB sand.

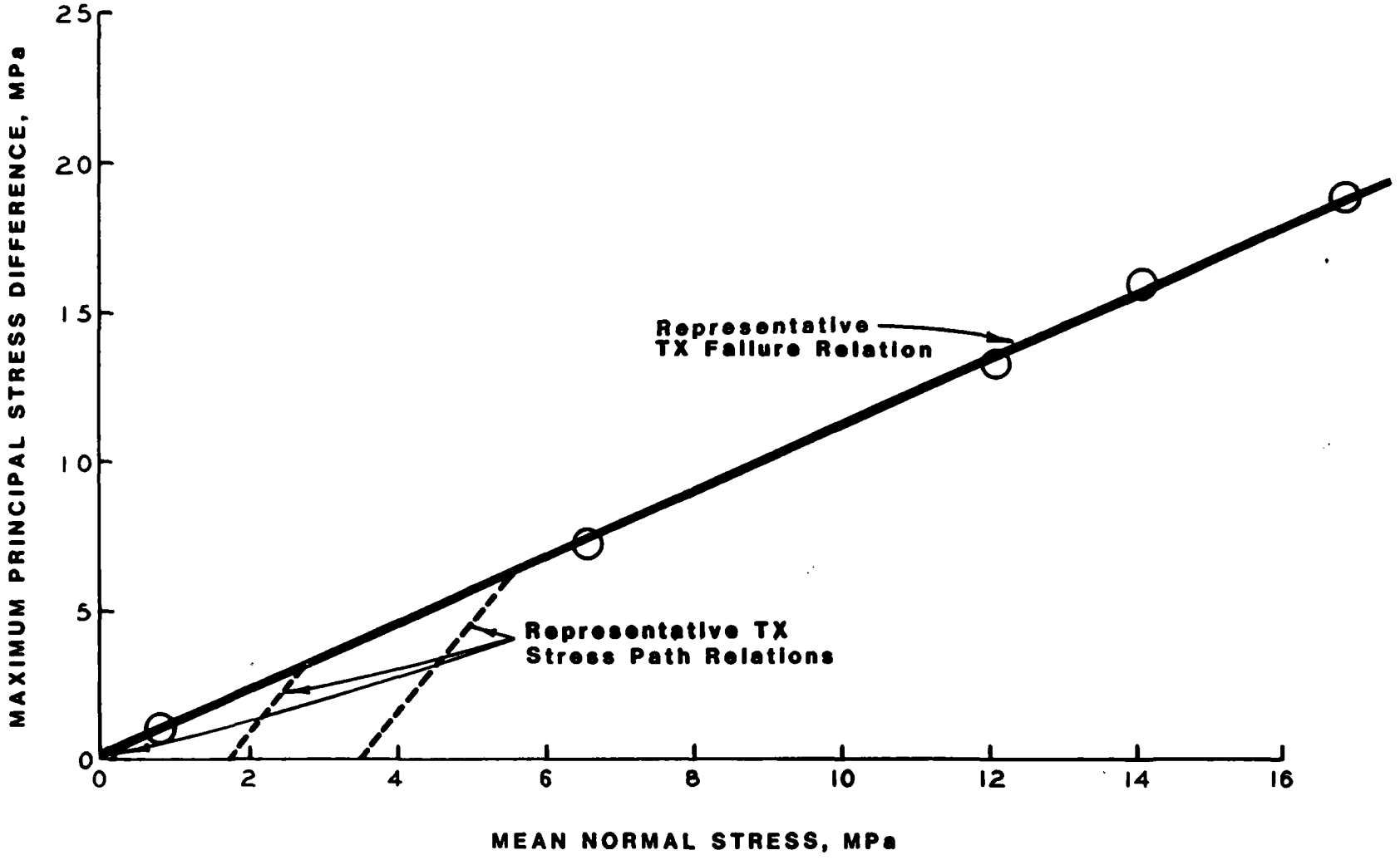

Figure 3.7 Static TX failure points and representative undrained TX failure relation and undrained TX stress path relations for dry RB sand.

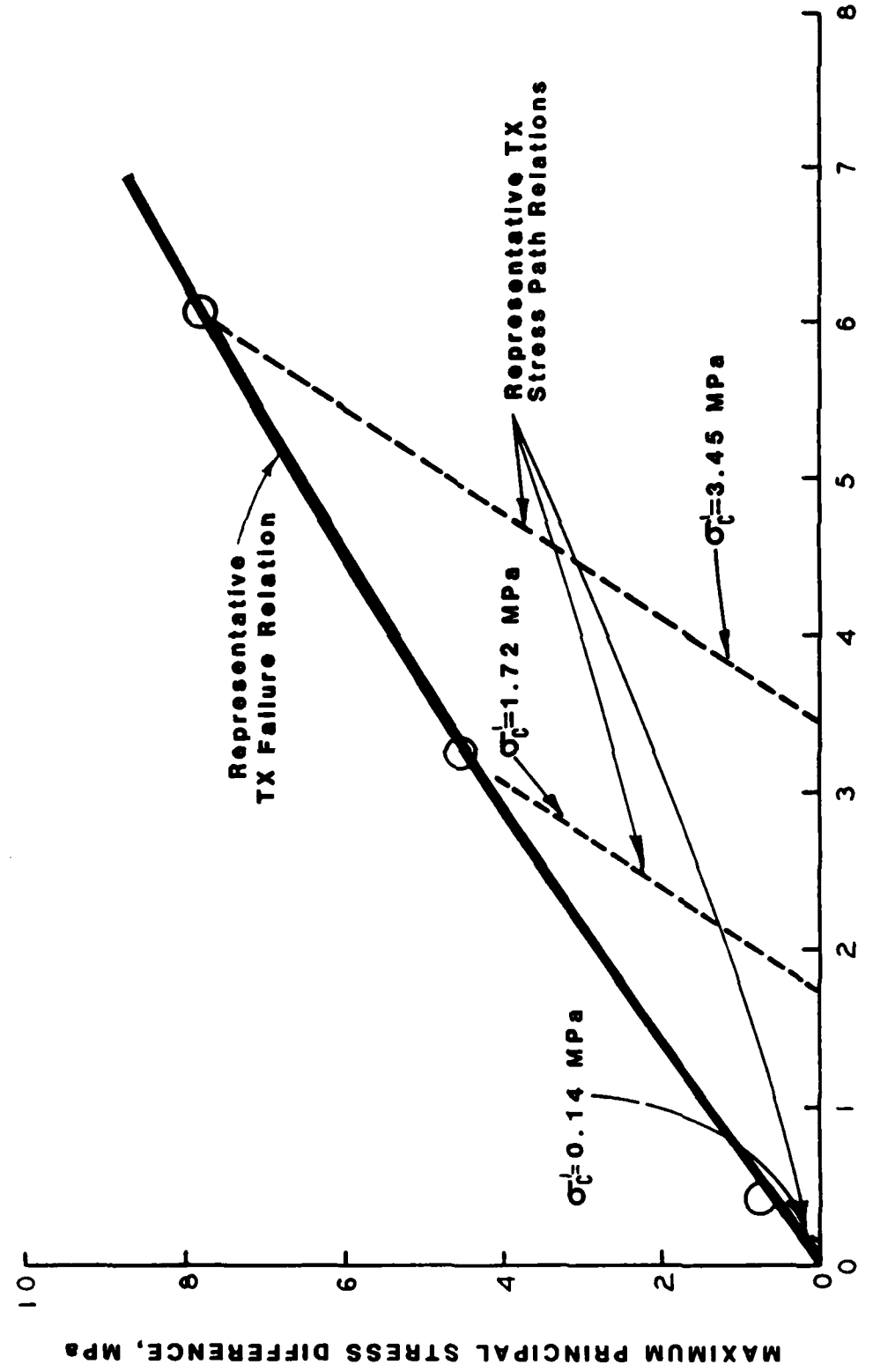

Figure 3.8 Static TX failure points and representative drained TX failure relation and drained TX stress path relations for saturated RB sand.

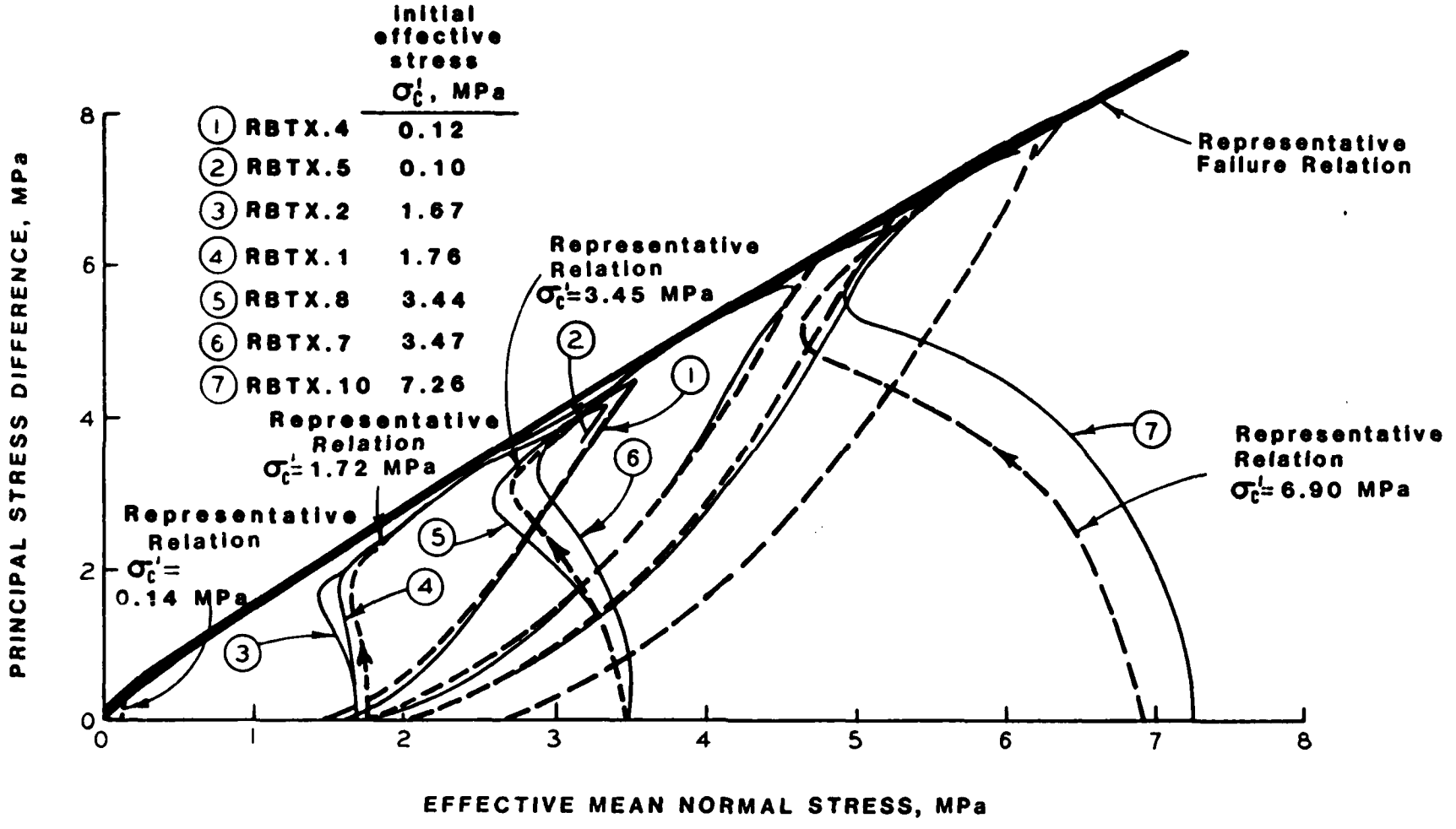

Figure 3.9 Static TX test results and representative undrained TX failure relation and undrained TX stress path relations for saturated RB sand at initial effective stresses of 0.14, 1.72, 3.45, and 6.90 MPa.

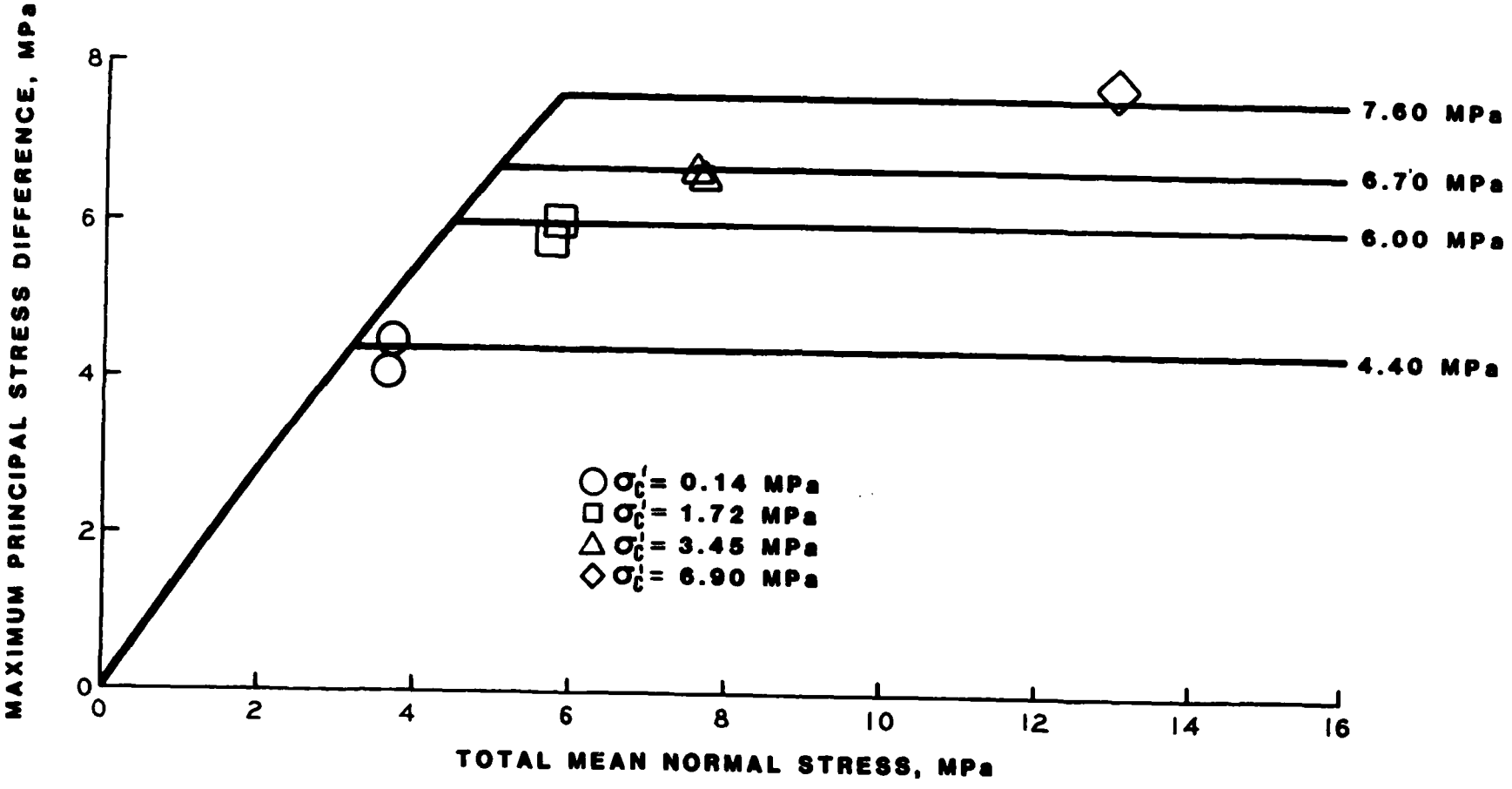

Figure 3.10 Static TX failure points and representative undrained TX total stress failure relation for saturated RB sand at initial effective stresses of 0.14, 1.72, 3.45, and 6.90 MPa.

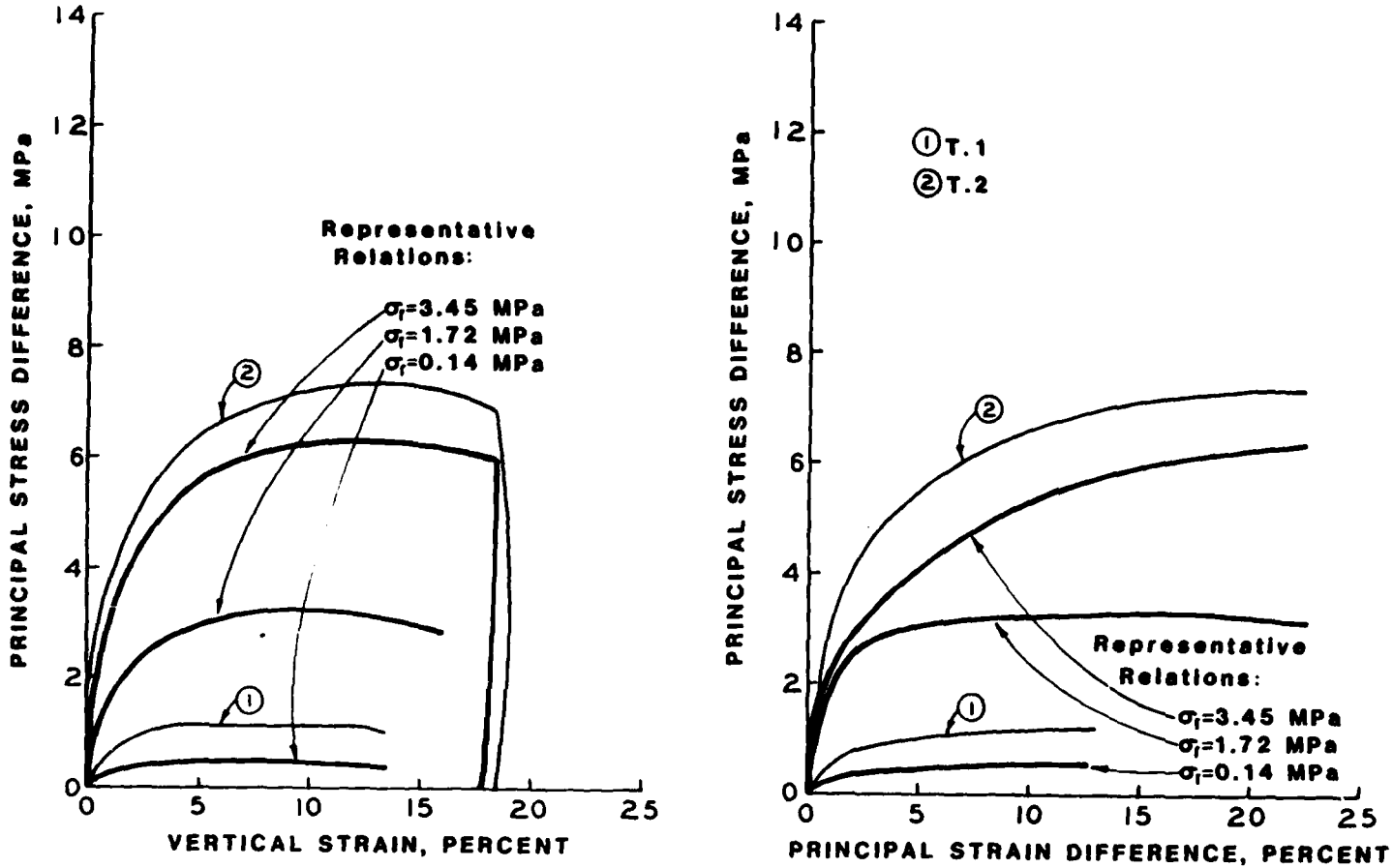

Figure 3.11 Static TX test results and representative undrained TX stress-strain relations for dry RB sand at confining pressures of 0.14, 1.72, and 3.45 MPa.

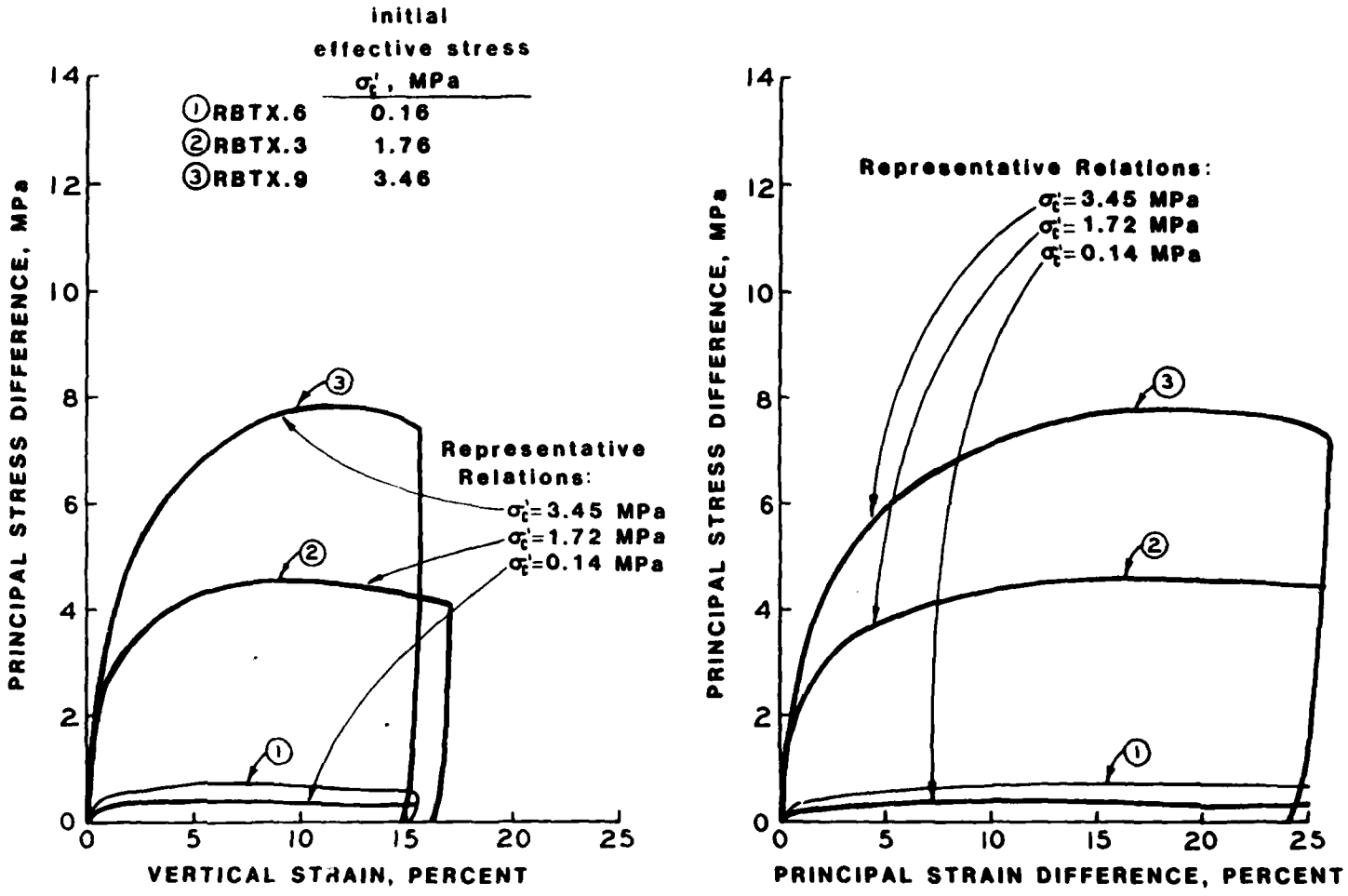

Figure 3.12 Static TX test results and representative drained TX stress-strain relations for saturated RB sand at effective stresses of 0.14, 1.72, and 3.45 MPa.

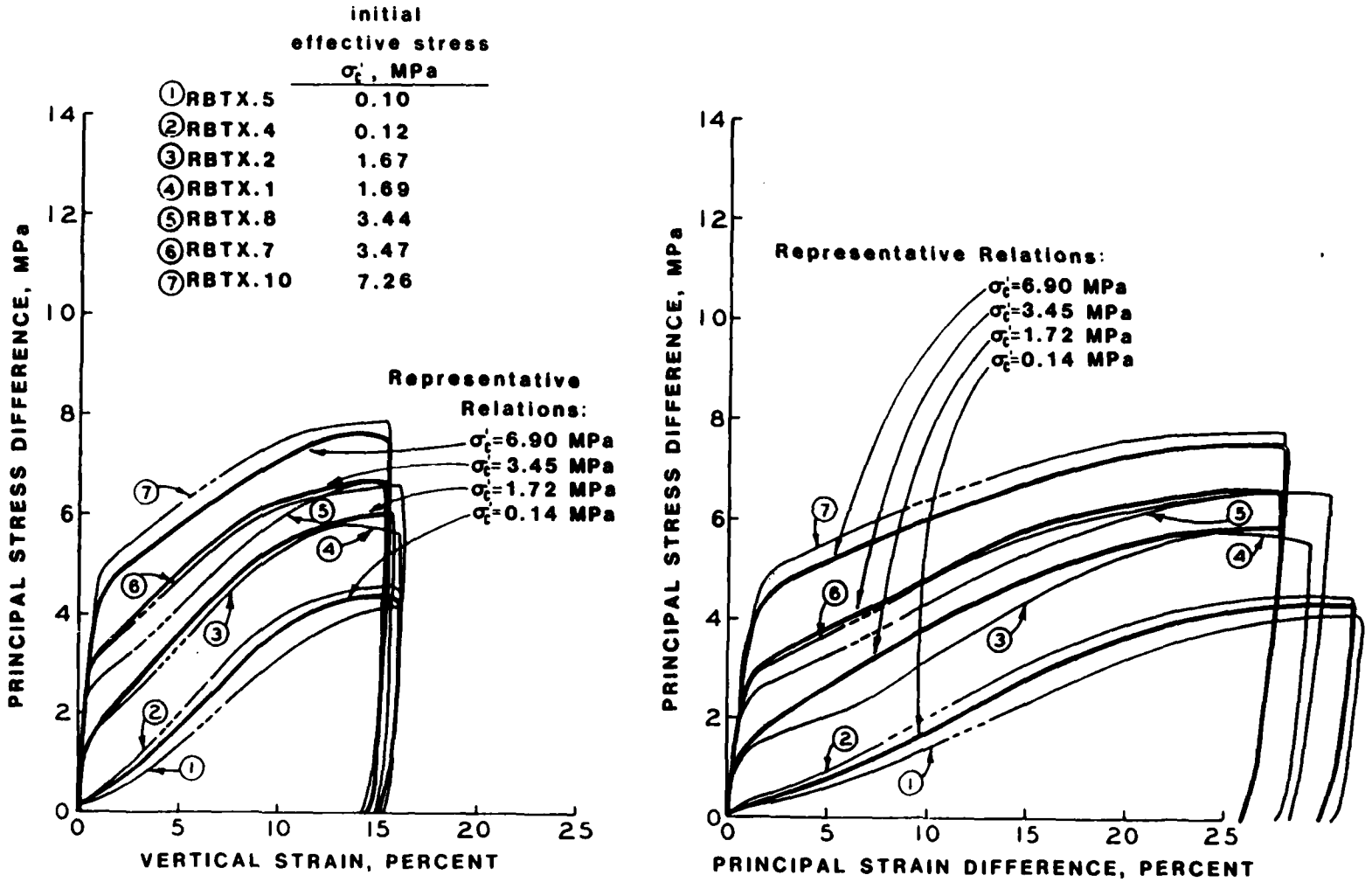

Figure 3.13 Static TX test results and representative undrained TX stress-strain relations for saturated RB sand at initial effective stresses of 0.14, 1.72, 3.45, and 6.90 MPa.

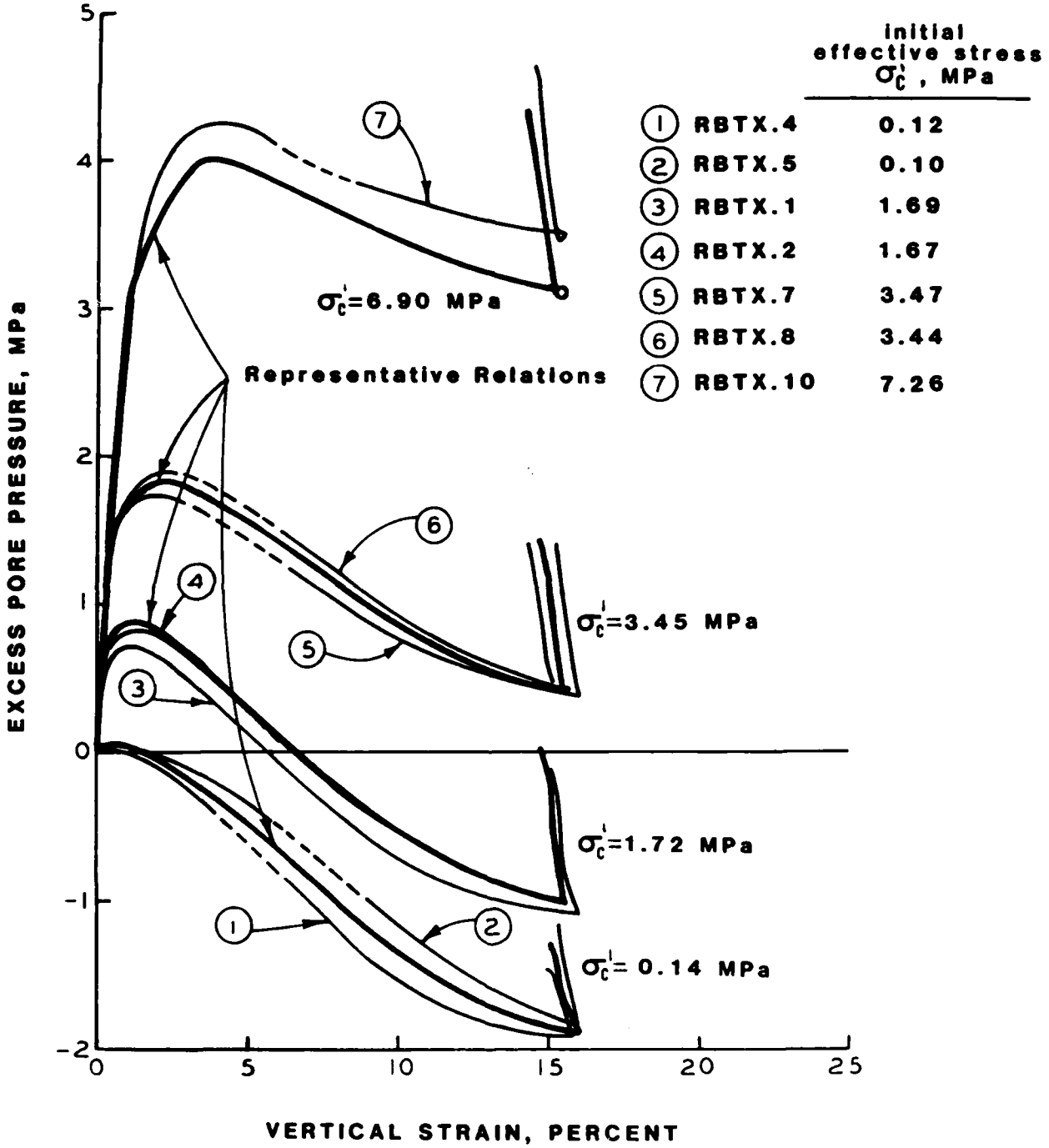

Figure 3.14 Static undrained TX test results and representative pore pressure versus vertical strain relations for saturated RB sand at initial effective stresses of 0.14, 1.72, 3.45, and 6.90 MPa.

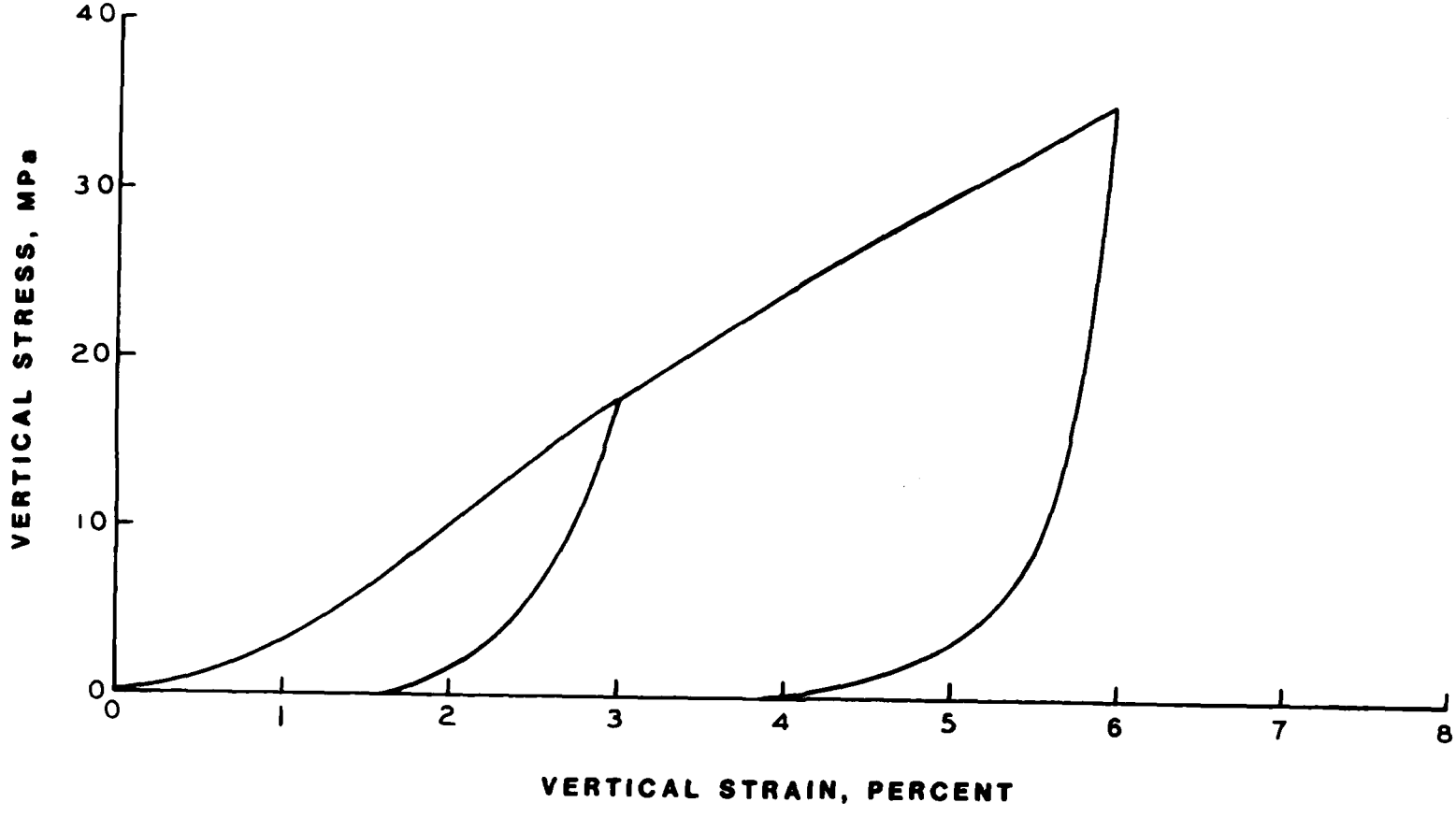

Figure 3.15 Representative UX compressibility for dry RB sand.

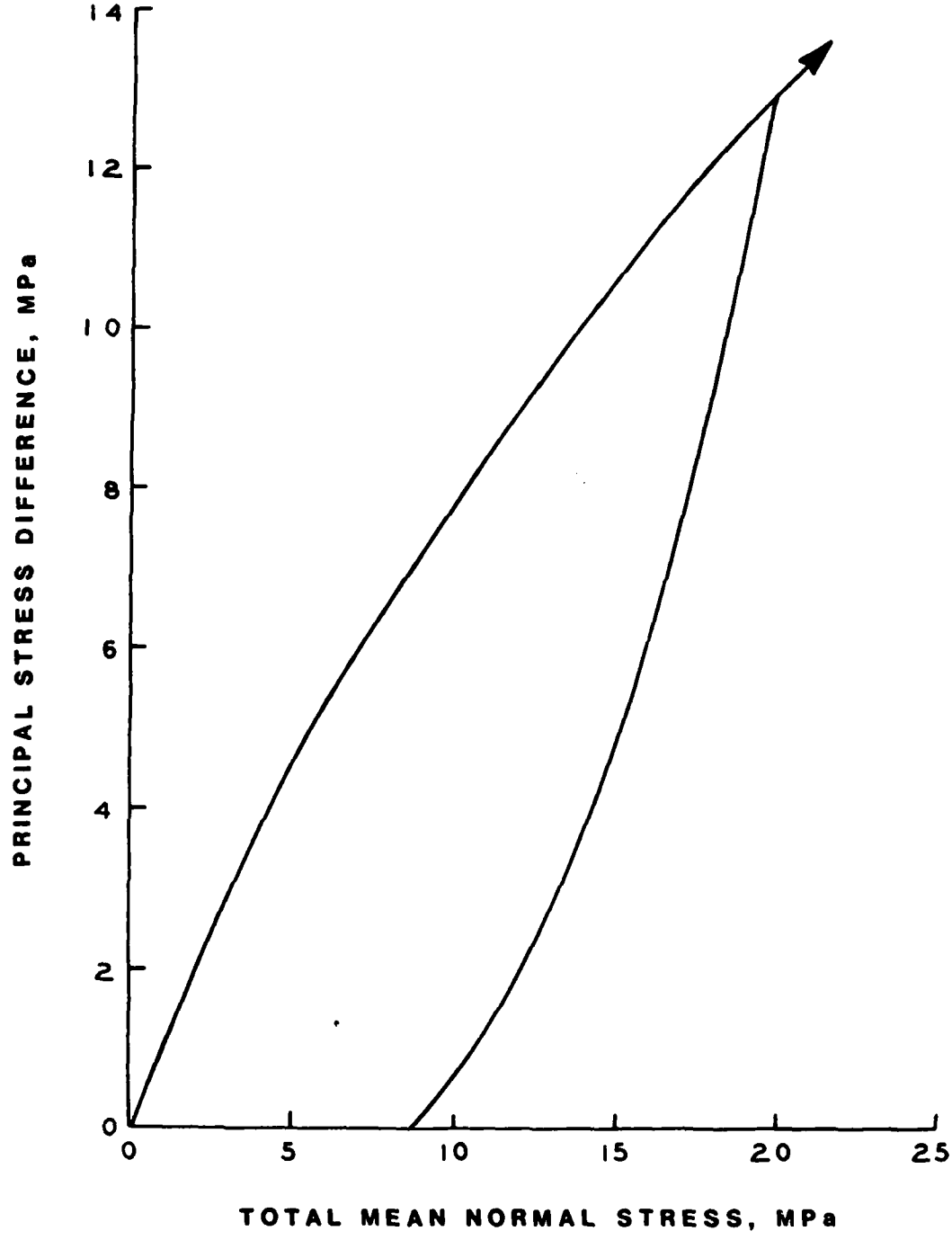

Figure 3.16 Representative UX stress path for dry RB sand.

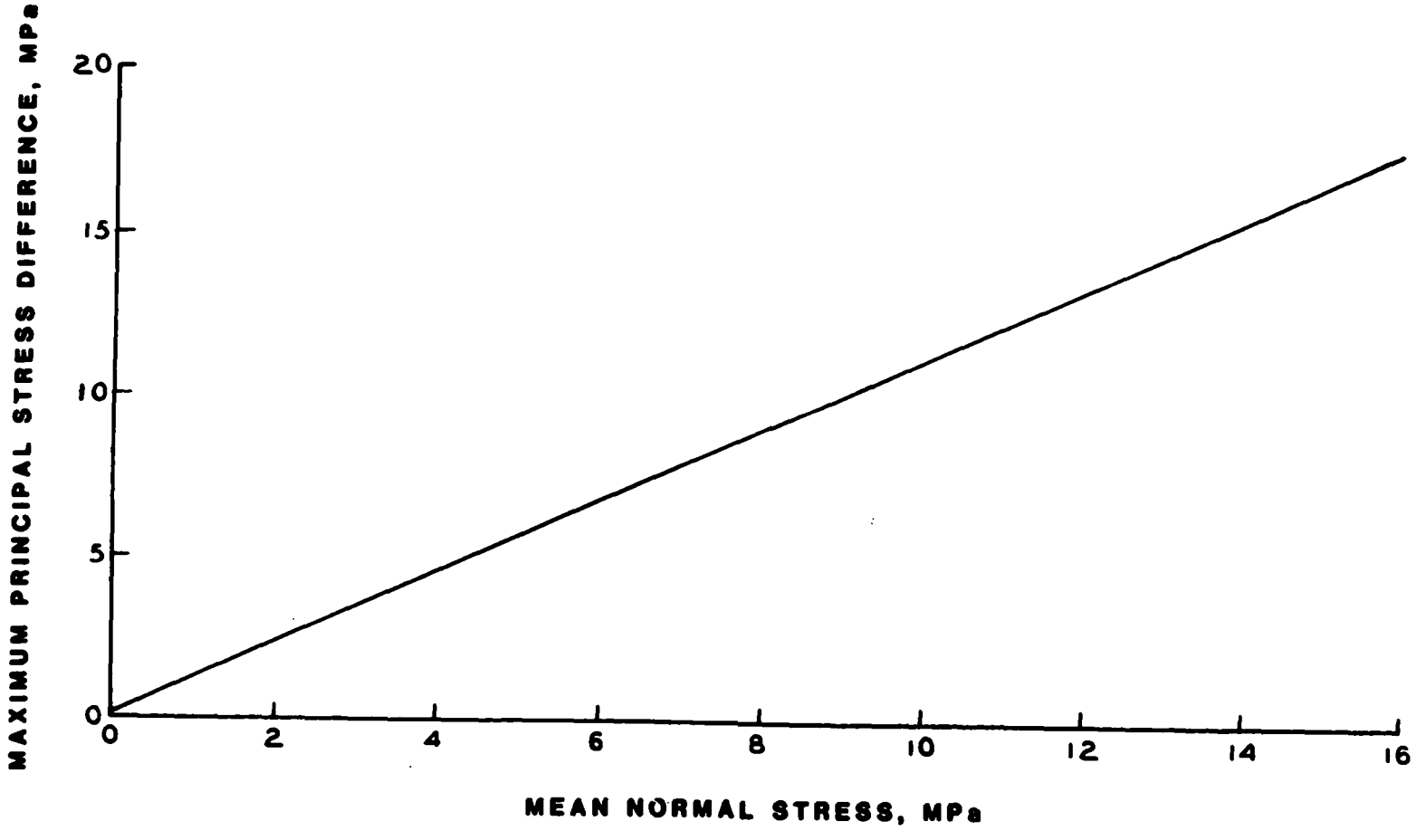

Figure 3.17 Representative TX failure relation for dry RB sand.

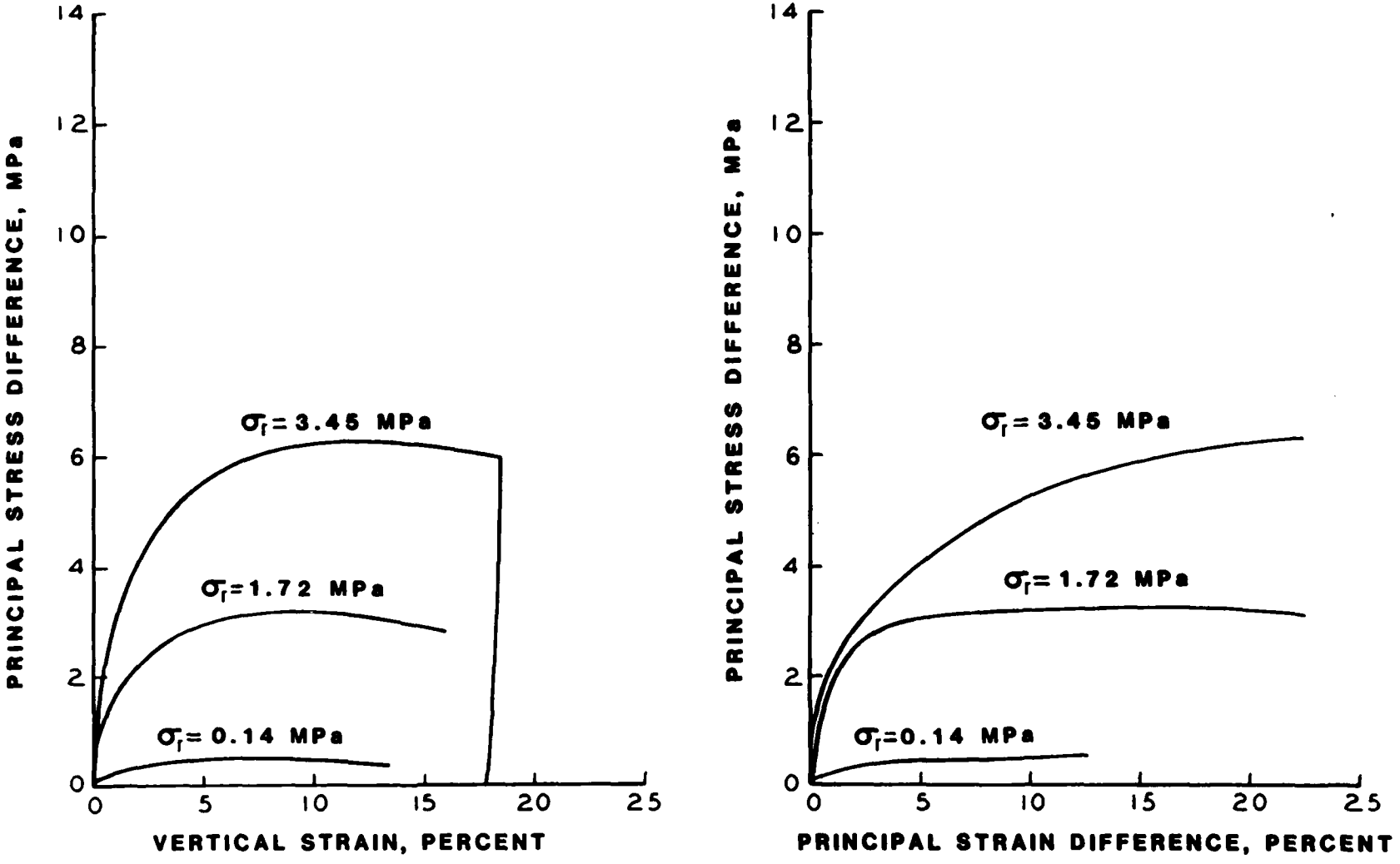

Figure 3.18 Representative TX stress-strain relations for dry RB sand at confining stresses of 0.14, 1.72, and 3.45 MPa.

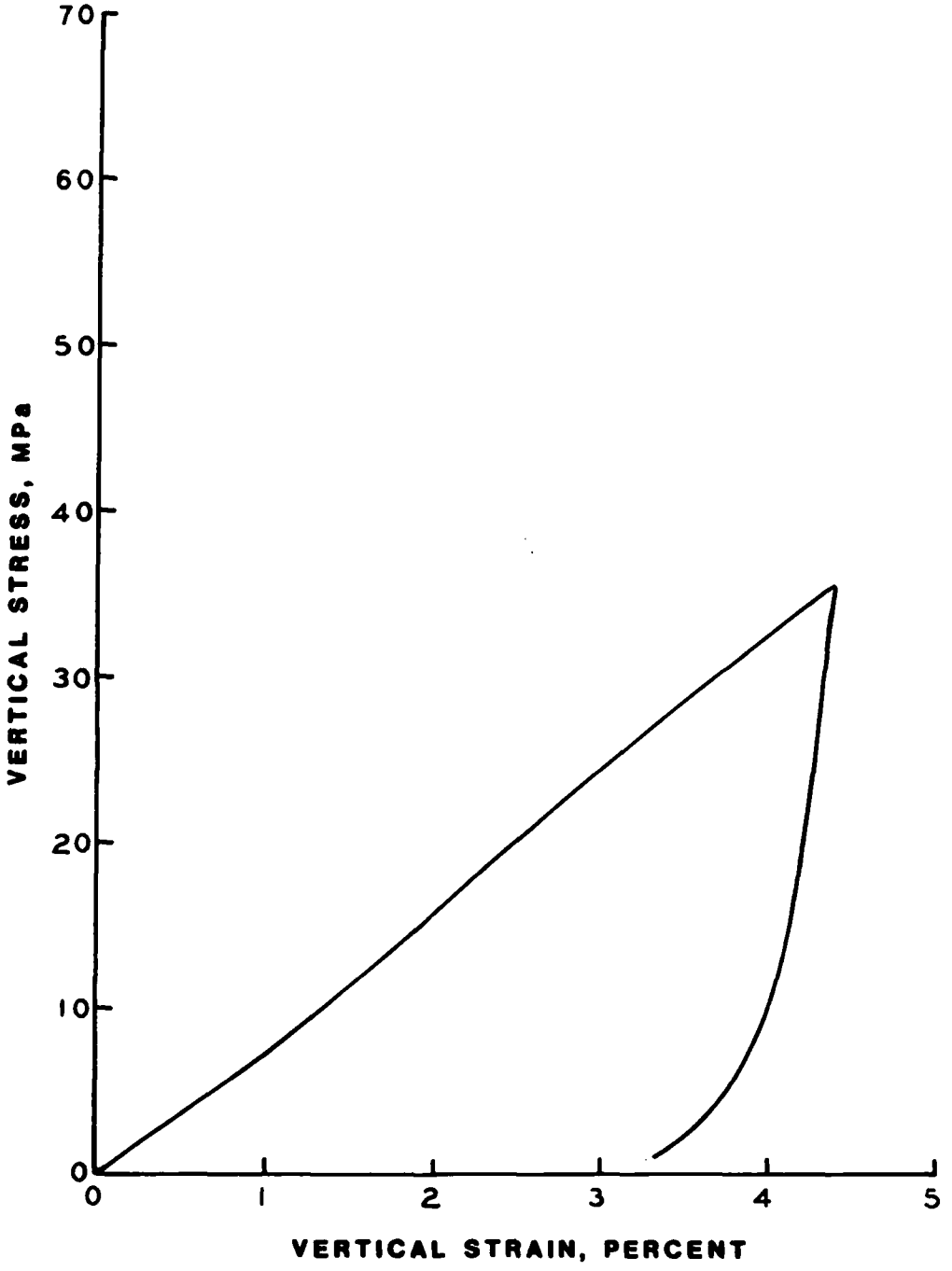

Figure 3.19 Representative drained UX compressibility for saturated RB sand.

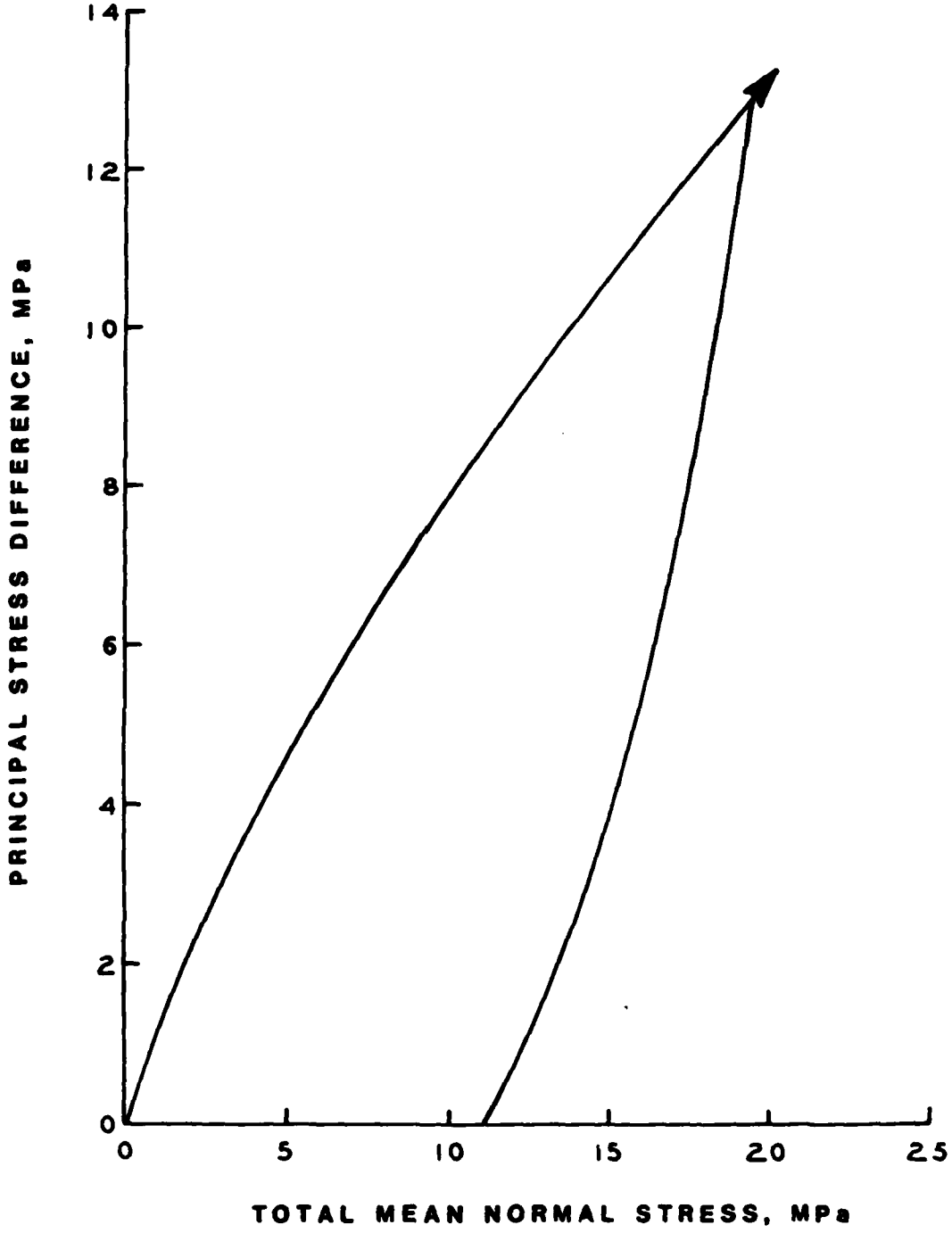

Figure 3.20 Representative drained UX stress path for saturated RB sand.

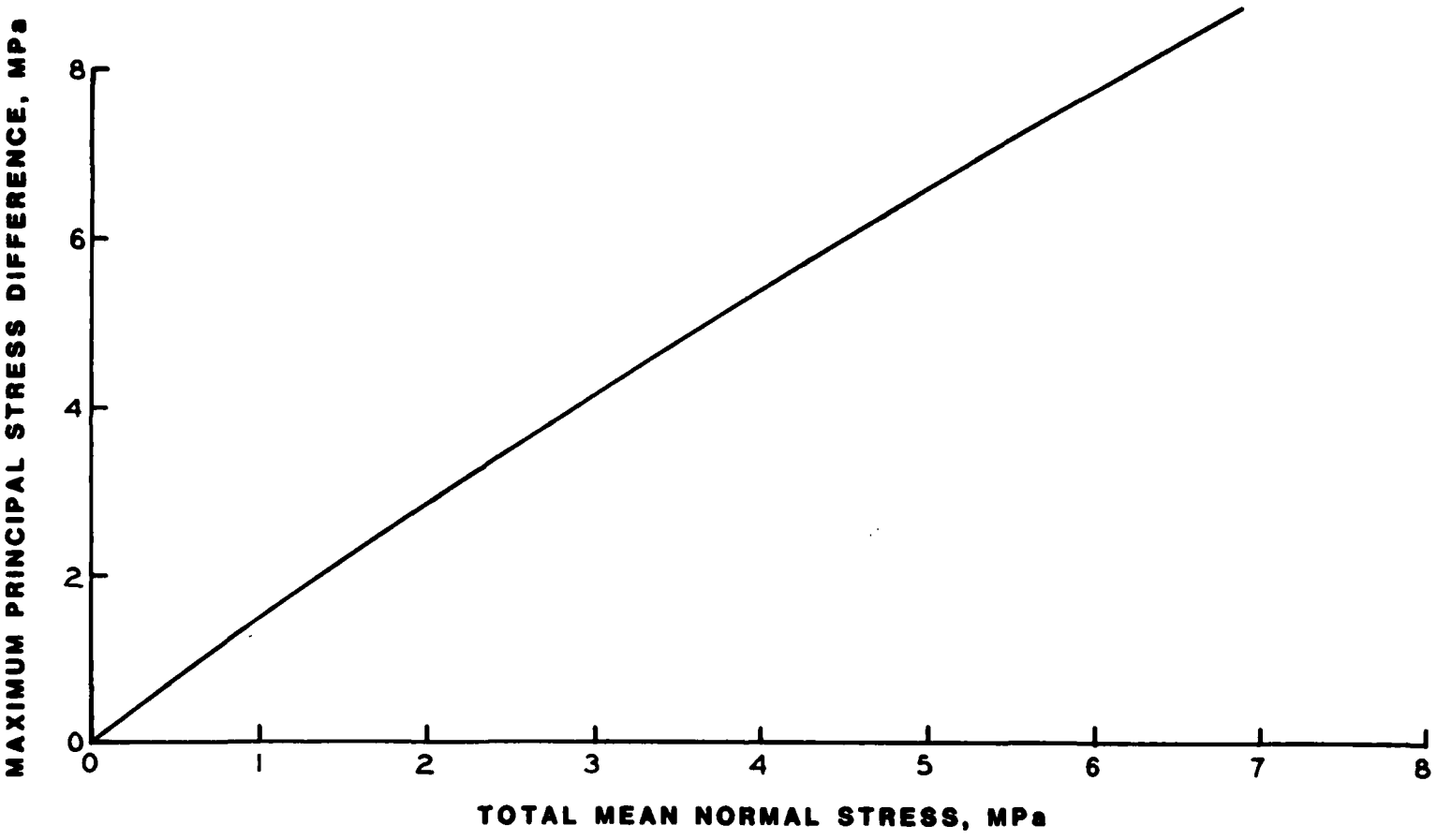

Figure 3.21 Representative drained TX failure relation for saturated RB sand.

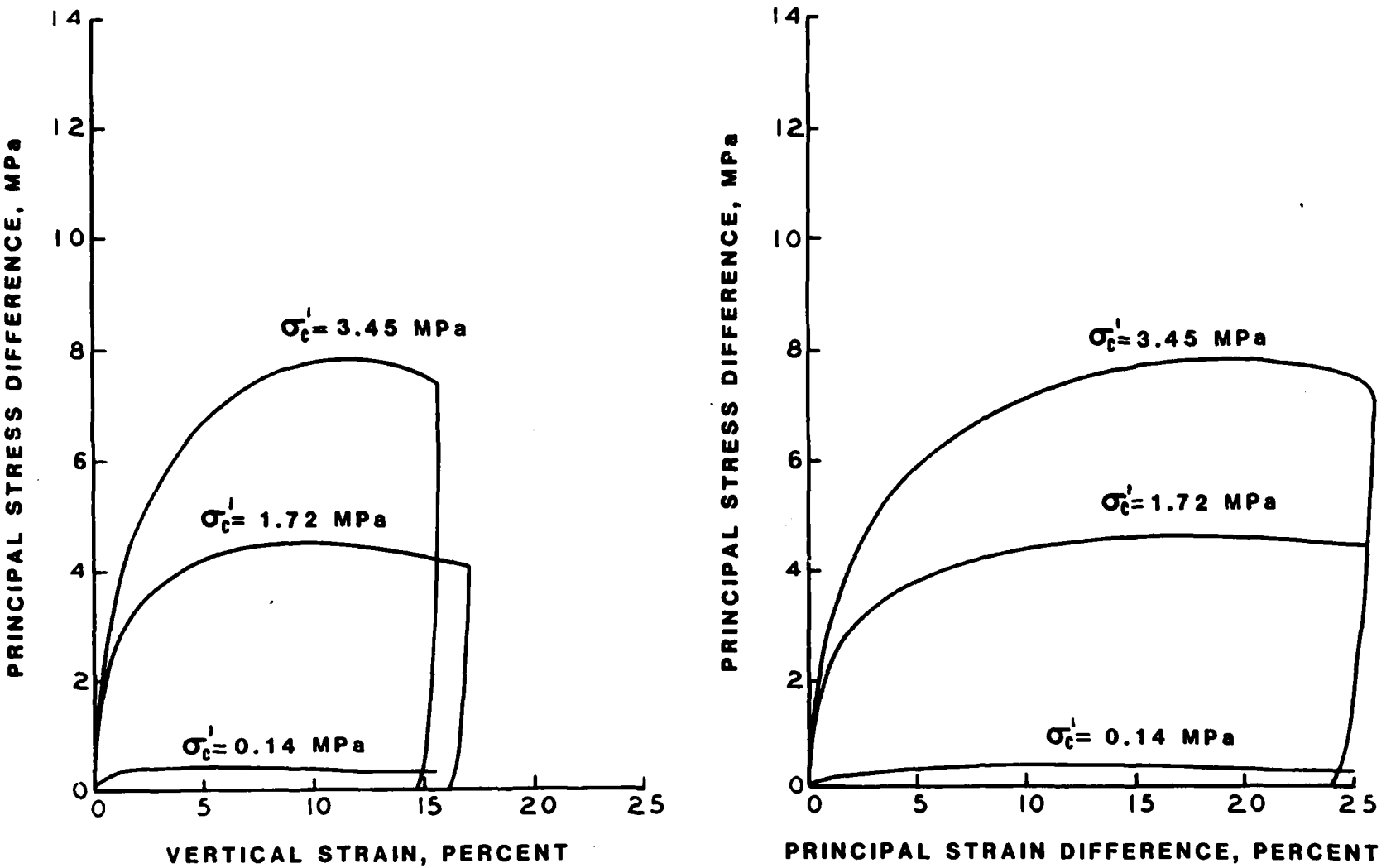

Figure 3.22 Representative drained TX stress-strain relations for saturated RB sand at effective stresses of 0.14, 1.72, and 3.45 MPa.

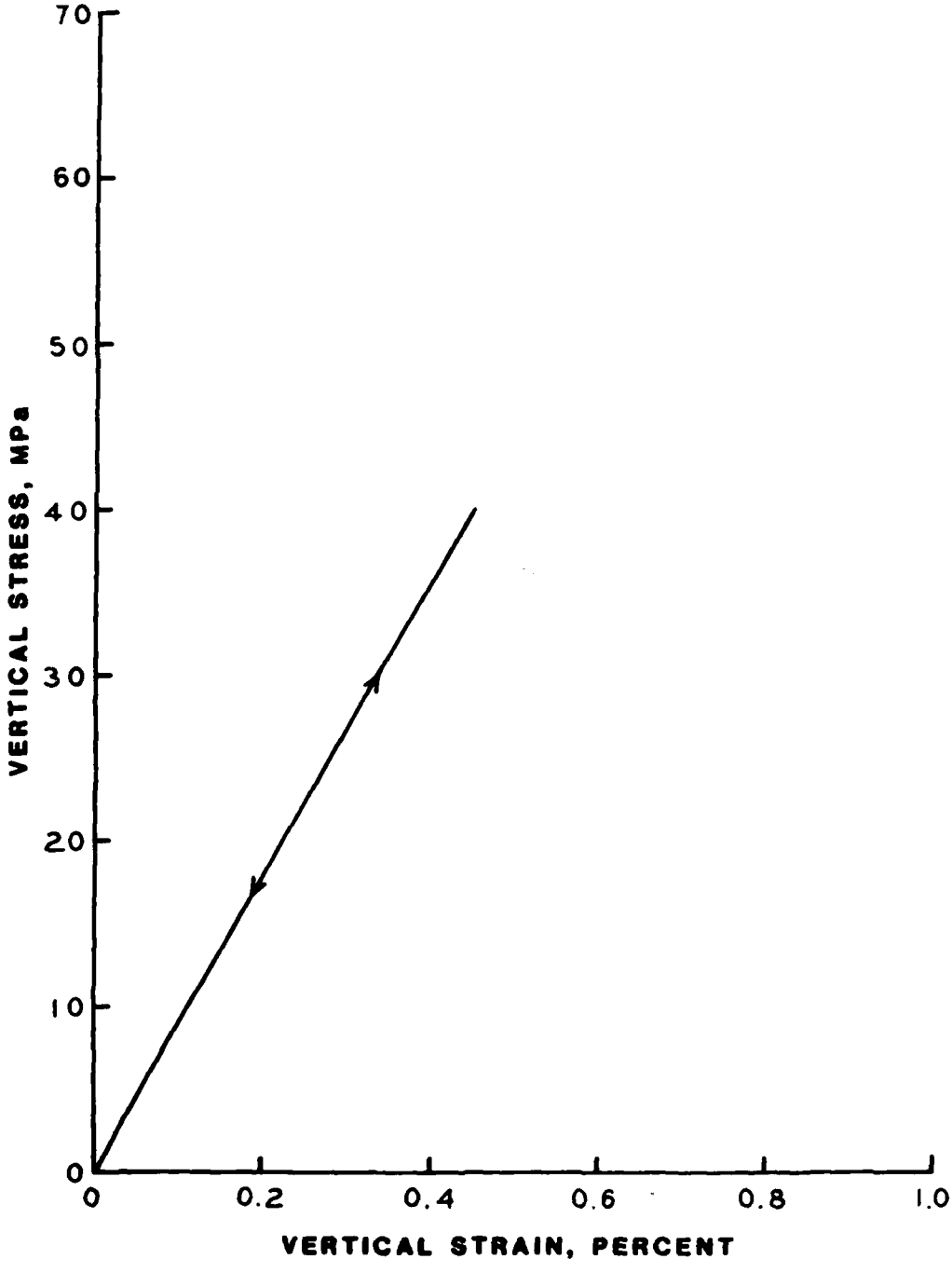

Figure 3.23 Representative undrained UX compressibility for RB sand.

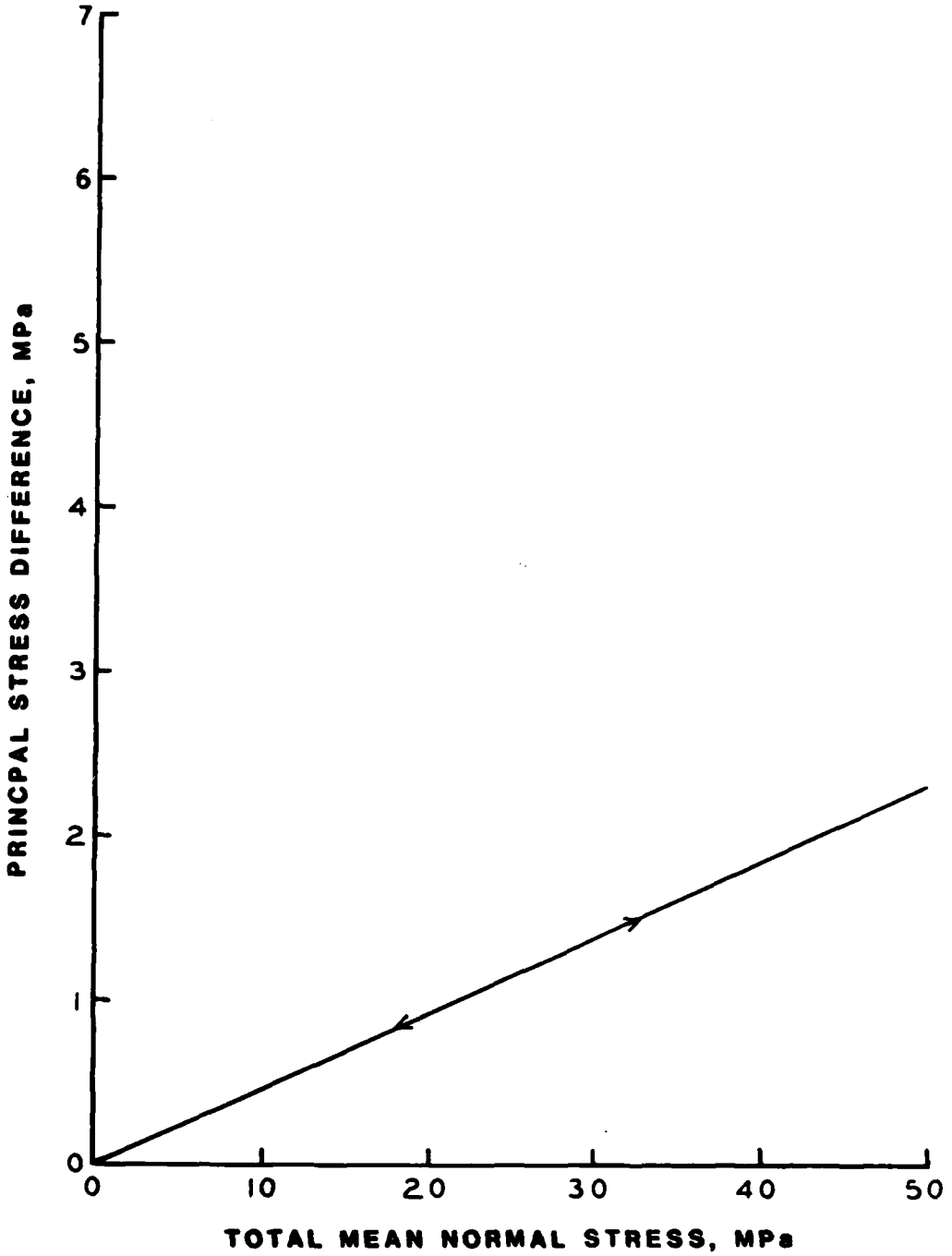

Figure 3.24 Representative undrained UX stress path for saturated RB sand.

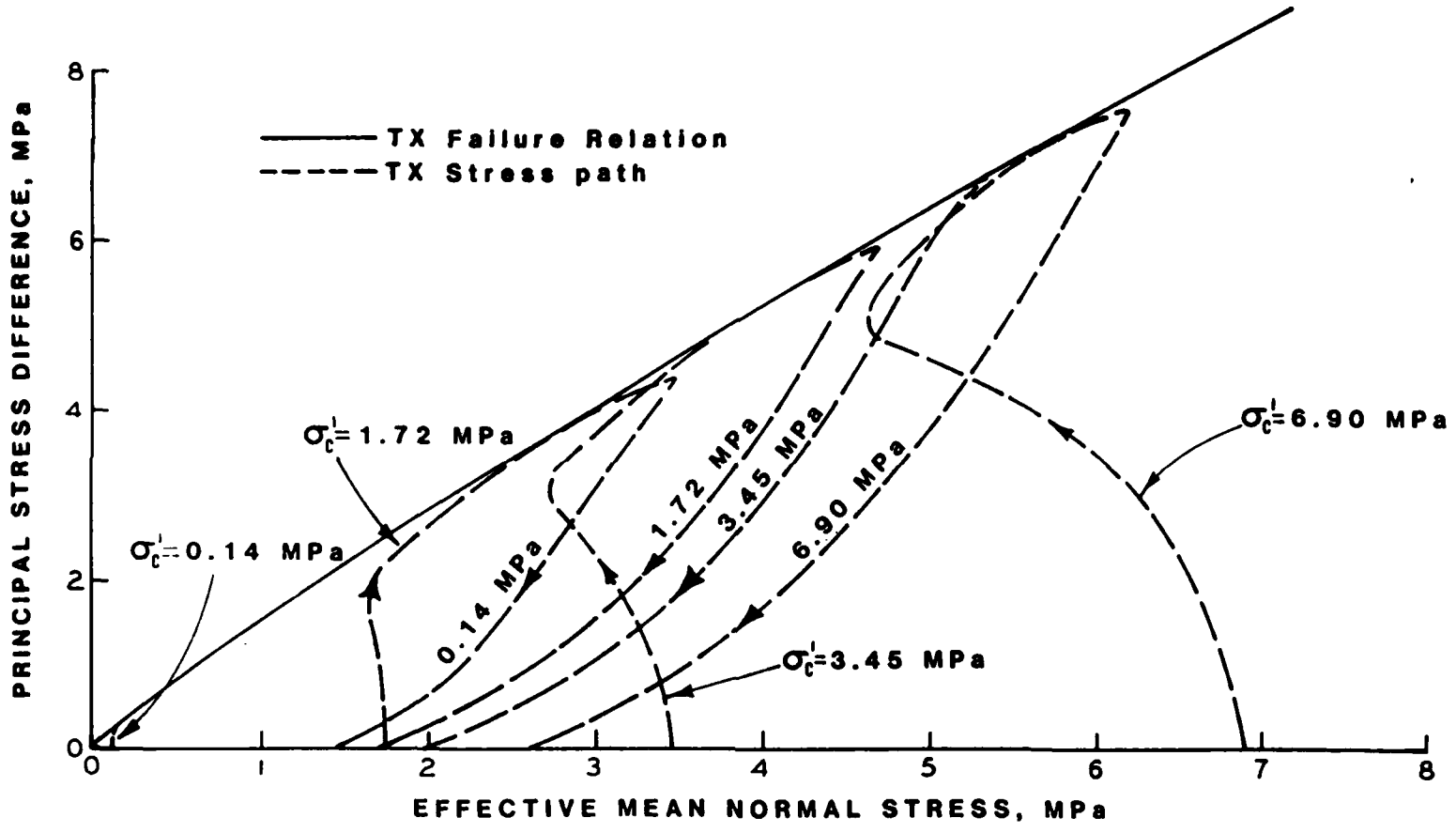

Figure 3.25 Representative undrained TX failure relation and TX effective stress paths for saturated RB sand at initial effective stresses of 0.14, 1.72, 3.45, and 6.90 MPa.

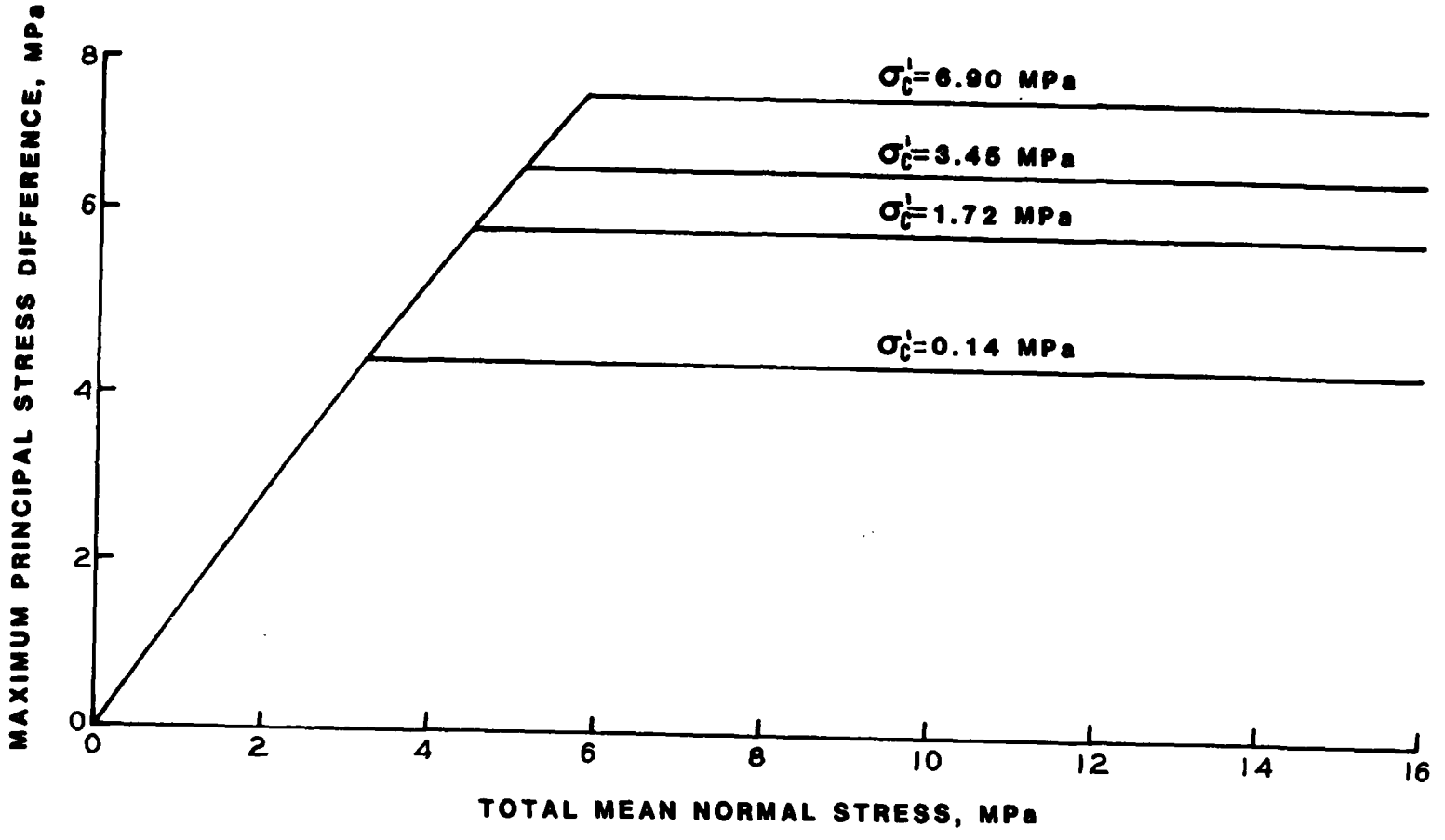

Figure 3.26 Representative undrained TX total stress failure relation for saturated RB sand at initial effective stresses of 0.14, 1.72, 3.45, and 6.90 MPa.

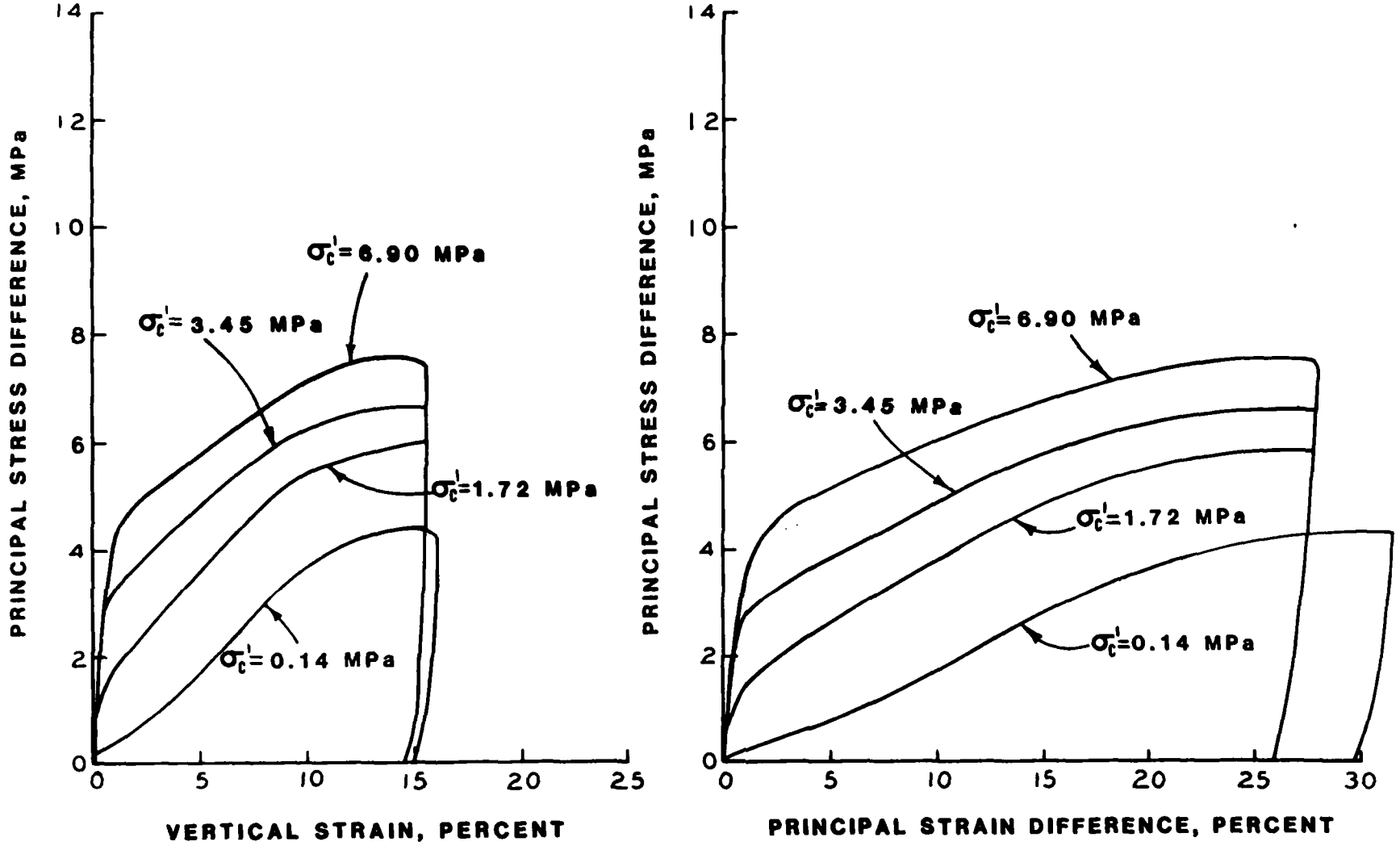

Figure 3.27 Representative undrained TX stress-strain relations for saturated RB sand at initial effective stresses of 0.14, 1.72, 3.45, and 6.90 MPa.

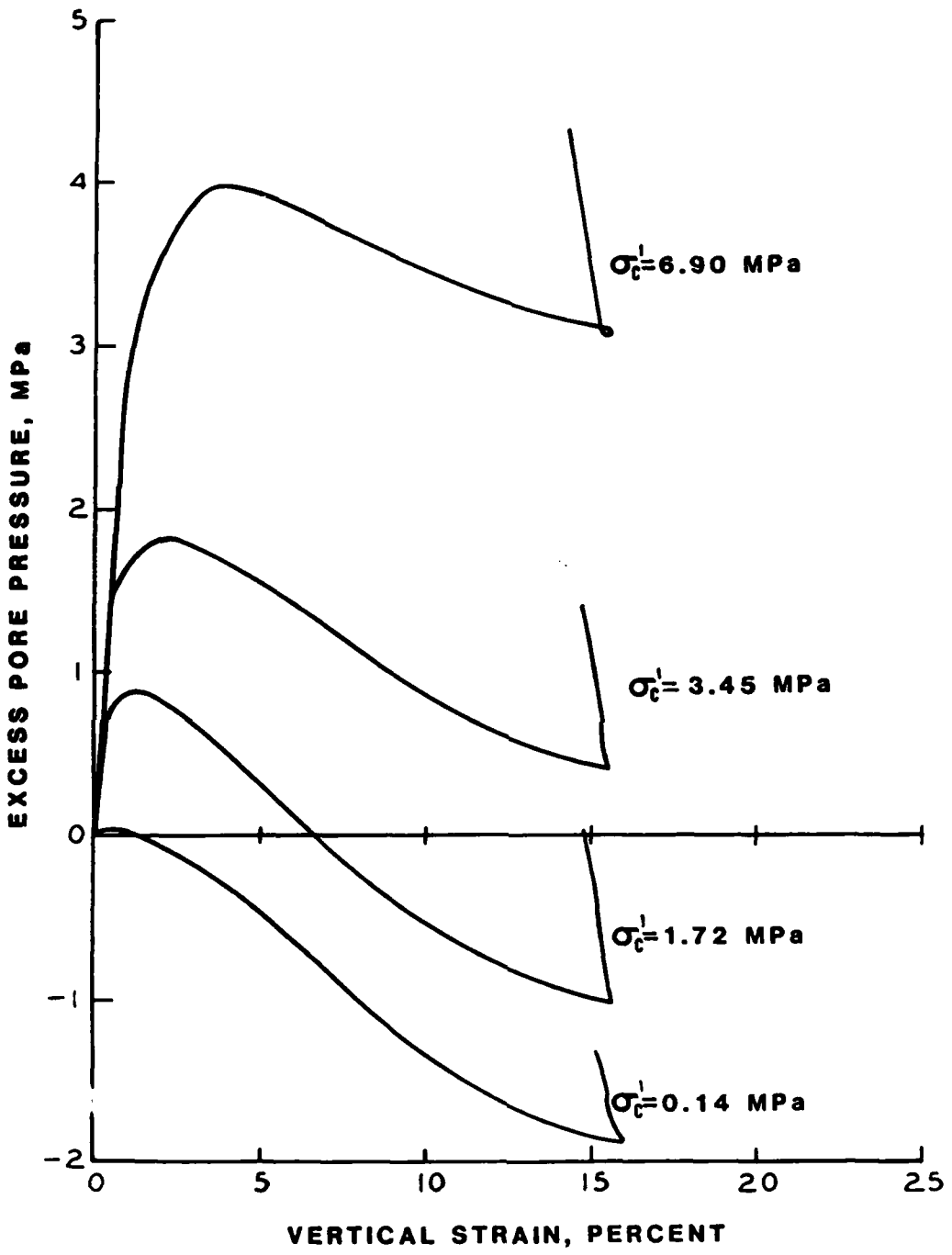

Figure 3.28 Representative undrained TX pore pressure versus vertical strain relations for RB sand at initial effective stresses of 0.14, 1.72, 3.45, and 6.90 MPa.

CHAPTER 4

COMPARISONS AND CONCLUSIONS

In the past, comparisons of the behavior of sands in a dry condition and the behavior of the same material in a saturated condition were based on laboratory tests conducted at relatively low stress levels, i.e., a few tenths of a megapascal. Reference 2, documented representative relations for MISERS BLUFF sand at effective stresses of 0.14, 1.72, and 3.45 MPa. In Chapter 3 of this report, these same representative relations were presented for RB sand under three different conditions, i.e., UU tests on dry sand (UD), CD tests on saturated sand (DS), and CU tests on saturated sand (US). These data offer an opportunity to examine the response of RB sand at higher stress levels than normally obtained in conventional testing laboratories.

4.1 UX RELATIONS

Figure 4.1 shows a comparison of the representative UX compressibility relations for each of the three test conditions. The UD and DS relations have similar shapes at stress levels above 10 MPa; however, the UD curve is more compressible primarily because of its softer response at low stress levels (<10 MPa). The US curve, as expected, is highly incompressible and corresponds to a constrained modulus of 8700 MPa. The representative UX stress paths for the three test conditions are shown in Figure 4.2. The UD and DS paths are almost identical. The slope of the US path is extremely small and has an implied value of Poission's ratio of 0.49.

4.2 TX RELATIONS

Figure 4.3 shows a plot of the representative TX principal stress difference versus vertical strain curves for the three initial effective and total confining stresses. The UD curves represent confining stresses of 0.14, 1.72, and 3.45. Representative curves for the DS and US tests are for initial effective stresses of 0.14, 1.72, and 3.45 MPa and 0.14, 1.72, 3.45, and 6.90 MPa respectively. A comparison of the DS and UD stress-strain relations at given stress levels of effective/total confining stress indicates that curve shapes and strains at failure are the same. However, DS failure strengths are higher than those for the UD condition except at

$\sigma_r = \sigma'_c = 0.14$ MPa where the DS and UD failure strengths are the same. The shapes and maximum principal stress differences of the US curves are related to the point at which the effective failure relation is encountered and the von Mises limiting strength for each level of effective stress, as discussed in Section 3.4.3.

A summary of the total-stress failure relations for the UD, DS, and US conditions are presented in Figure 4.4. The UD and DS relations diverge as principal stress difference increases. The Coulomb portion of the US relation is identical to that of the DS relation up to the point where the von Mises limit for each effective stress is reached.

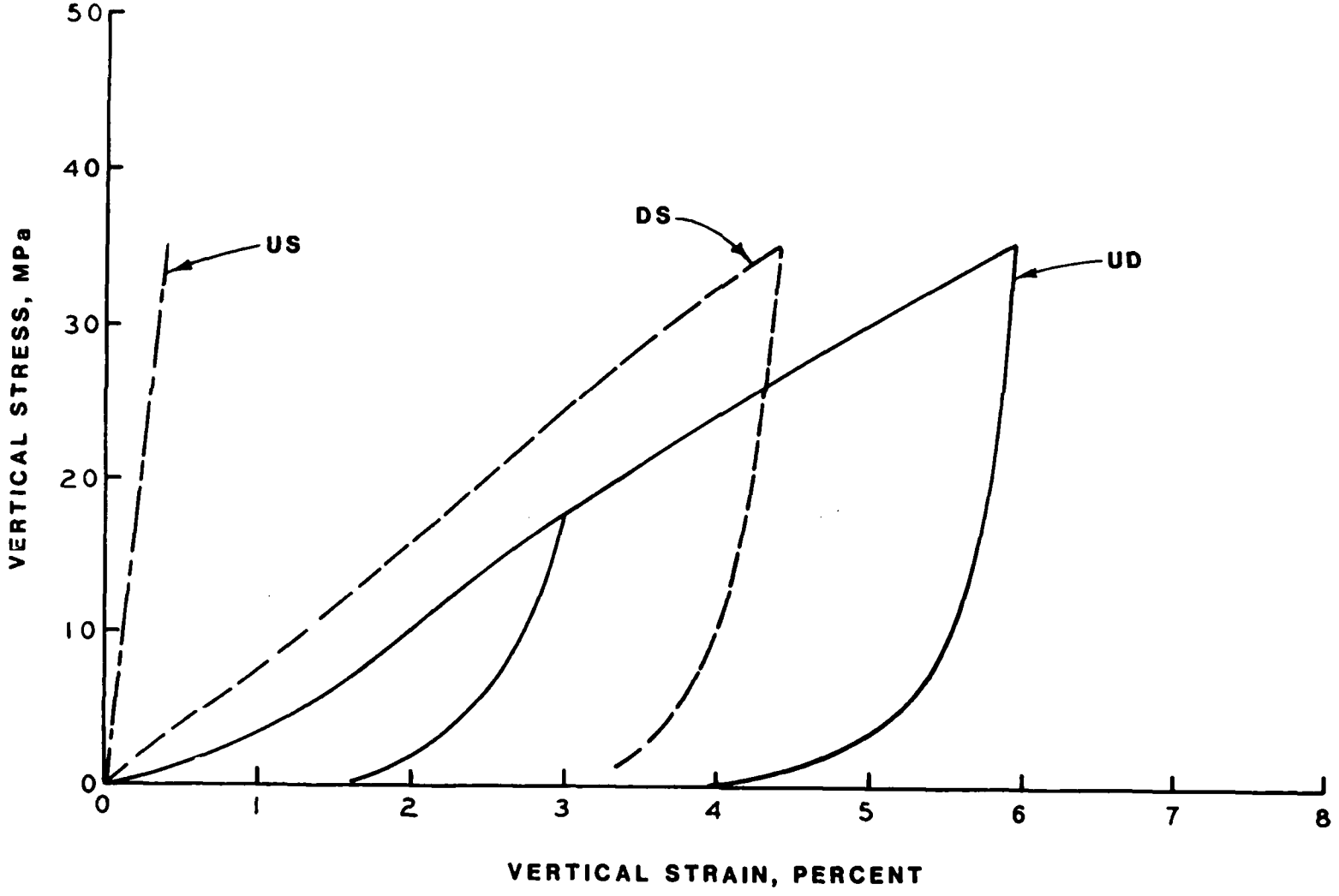

Figure 4.1 Comparison of the representative UX compressibility for dry RB sand with the representative drained and undrained UX compressibilities for saturated RB sand.

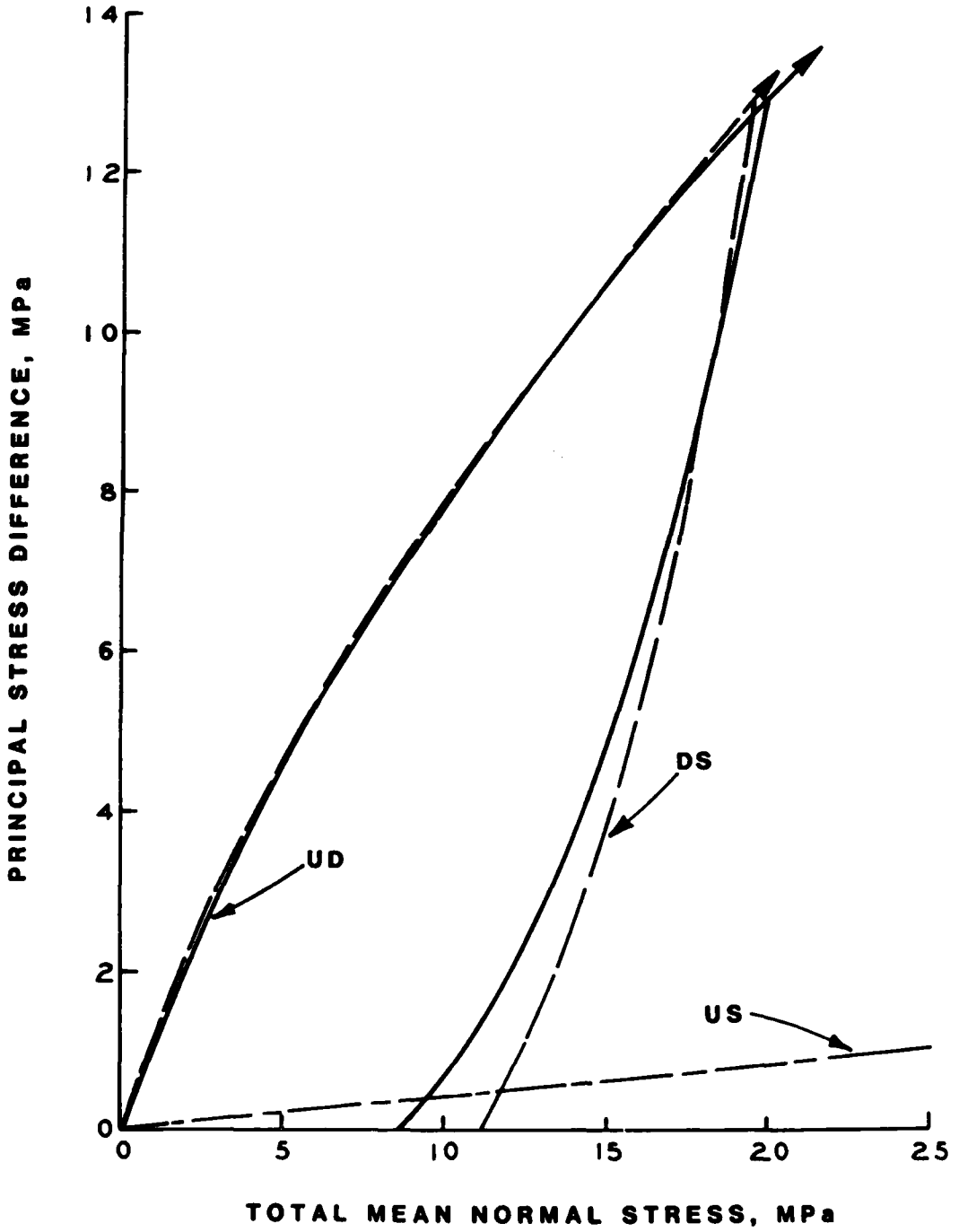

Figure 4.2 Comparison of the representative UX stress path for dry RB sand with the representative drained and undrained UX stress paths for saturated RB sand.

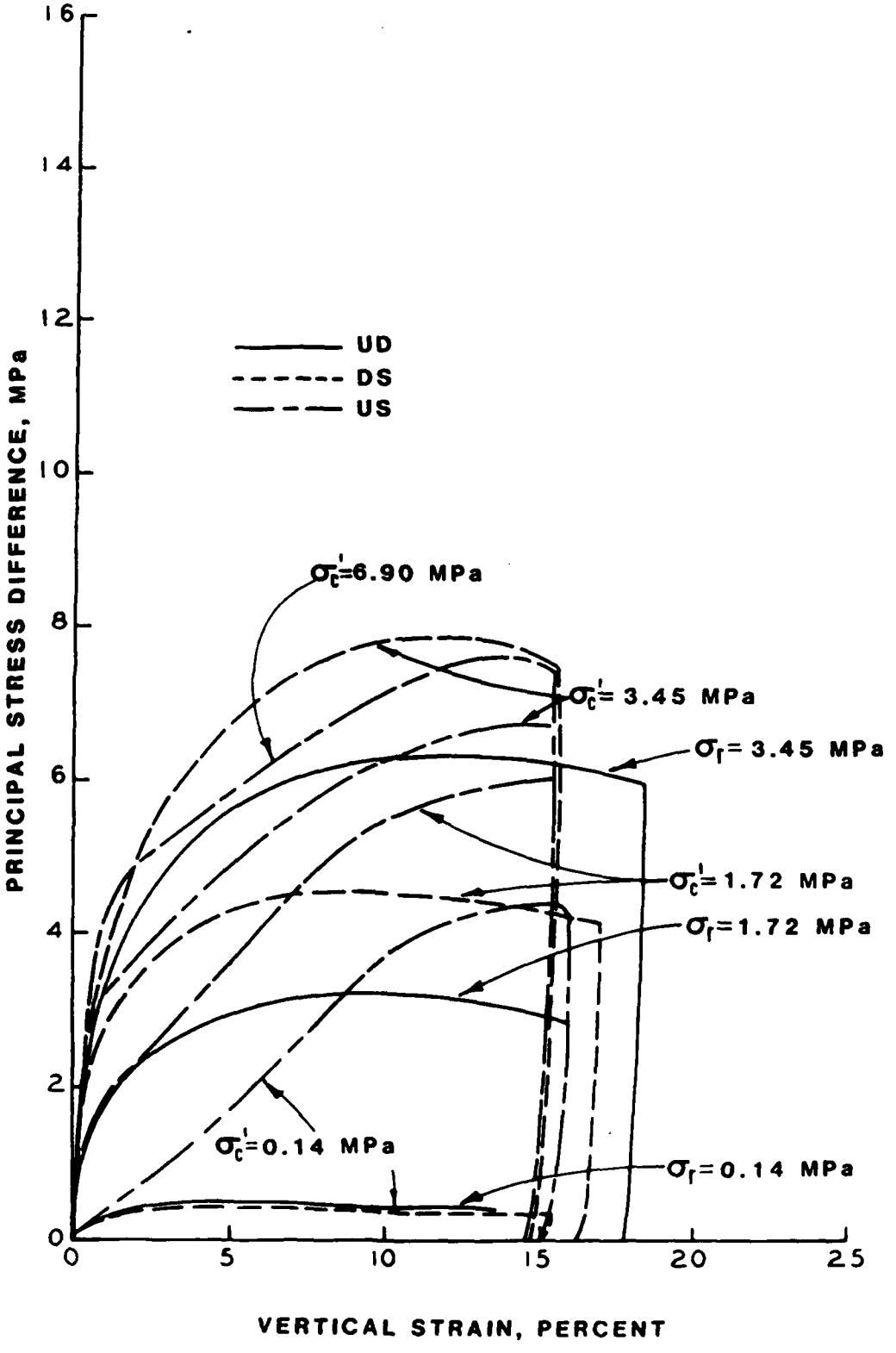

Figure 4.3 Comparison of the representative TX stress-strain relations for dry RB sand with the representative drained and undrained TX stress-strain relations for saturated MB sand.

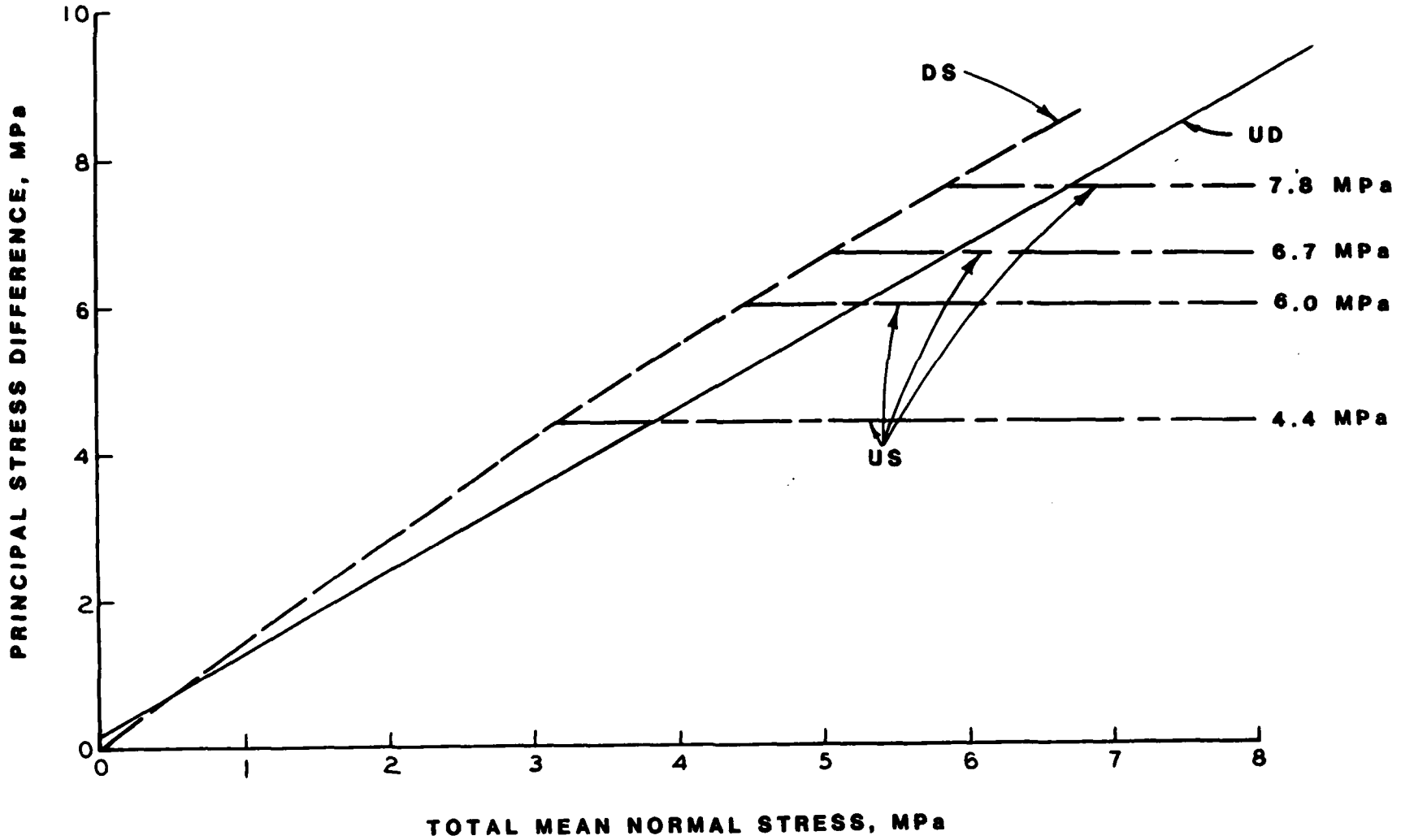

Figure 4.4 Comparison of the representative TX failure relation for dry RB sand with the representative drained and undrained total stress TX failure relations for saturated RB sand.

REFERENCES

1. B. R. Phillips; "Mechanical Response of Dry Reid-Bedford Model Sand and Saturated Misers Bluff Sand"; January 1982; U. S. Army Engineer Waterways Experiment Station, CE, Vicksburg, MS.

2. B. R. Phillips; "Mechanical Properties of Misers Bluff Sand"; September 1982; U. S. Army Engineer Waterways Experiment Station, CE, Vicksburg, MS.

3. Headquarters, Department of the Army, Office, Chief of Engineers; "Laboratory Soils Testing"; Engineering Manual No. EM-1110-2-1906, 30 November 1970; Washington, DC.

4. U. S. Army Engineer Waterways Experiment Station; "The Unified Soil Classification System"; Technical Memorandum No. 3-357, April 1960 (reprinted May 1967, Amended 1 May 1980); CE, Vicksburg, MS.

5. J. Q. Ehrgott; "Calculation of Stress and Strain from Triaxial Test Data on Undrained Soil Specimens"; Miscellaneous Paper S-71-9, May 1971; U. S. Army Engineer Waterways Experiment Station, CE, Vicksburg, MS.

6. R. O. Davis and J. J. Blake; "Synthesis of Soil Hugonoits Between 1 and 100 Kilobars"; AFWL-TR-72-83, September 1972; Air Force Weapons Laboratory, Air Force Systems Command, Kirtland Air Force Base, NM.

7. Alan W. Bishop and D. J. Henkel; The Measurement of Soil Properties in the Triaxial Tests; 1962; Edward Arnold LTD, London.

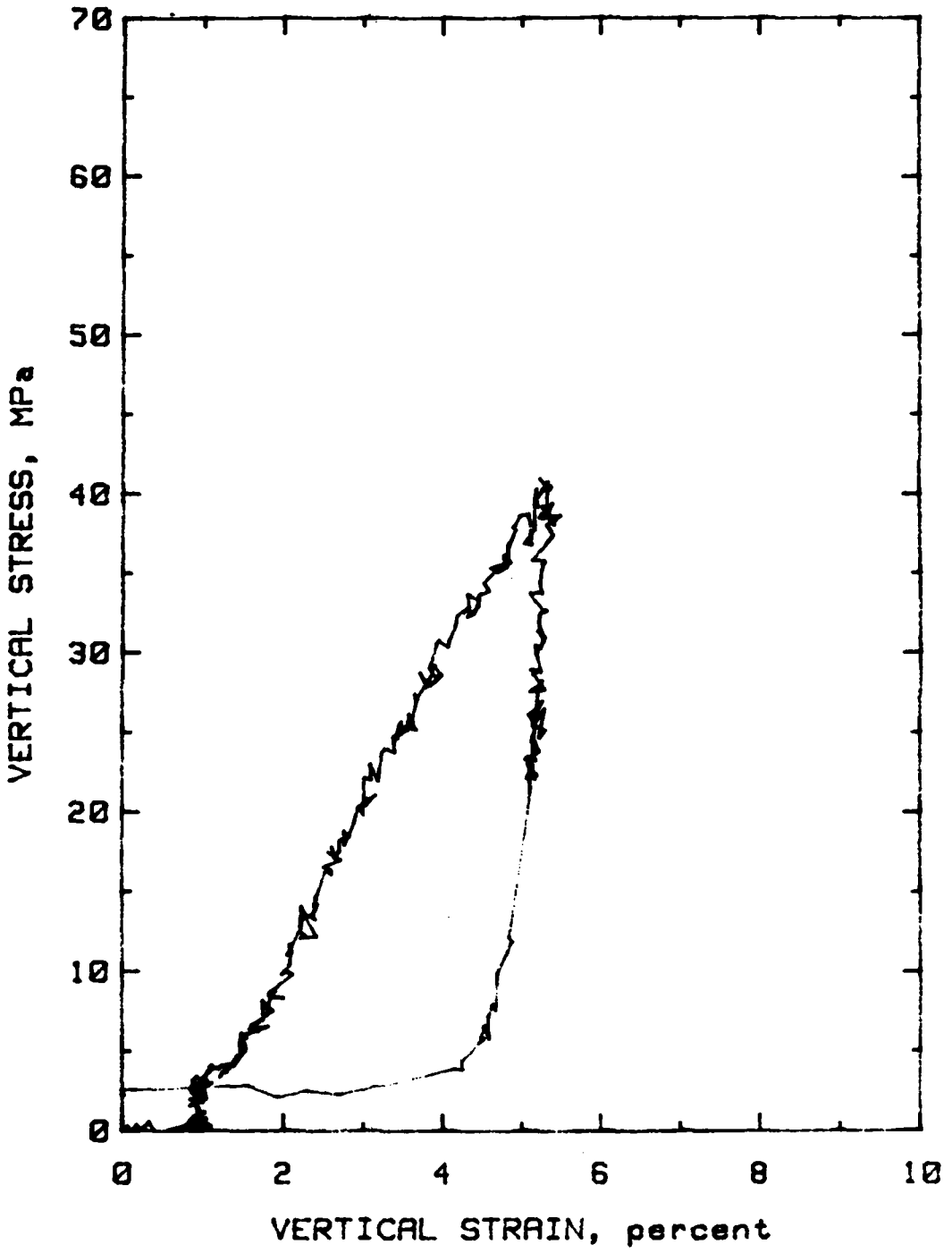

BACK PRESSURE SATURATED
STATIC UNDRAINED UNIAXIAL STRAIN
SPECIMEN RB.UX.1

PLATE 1

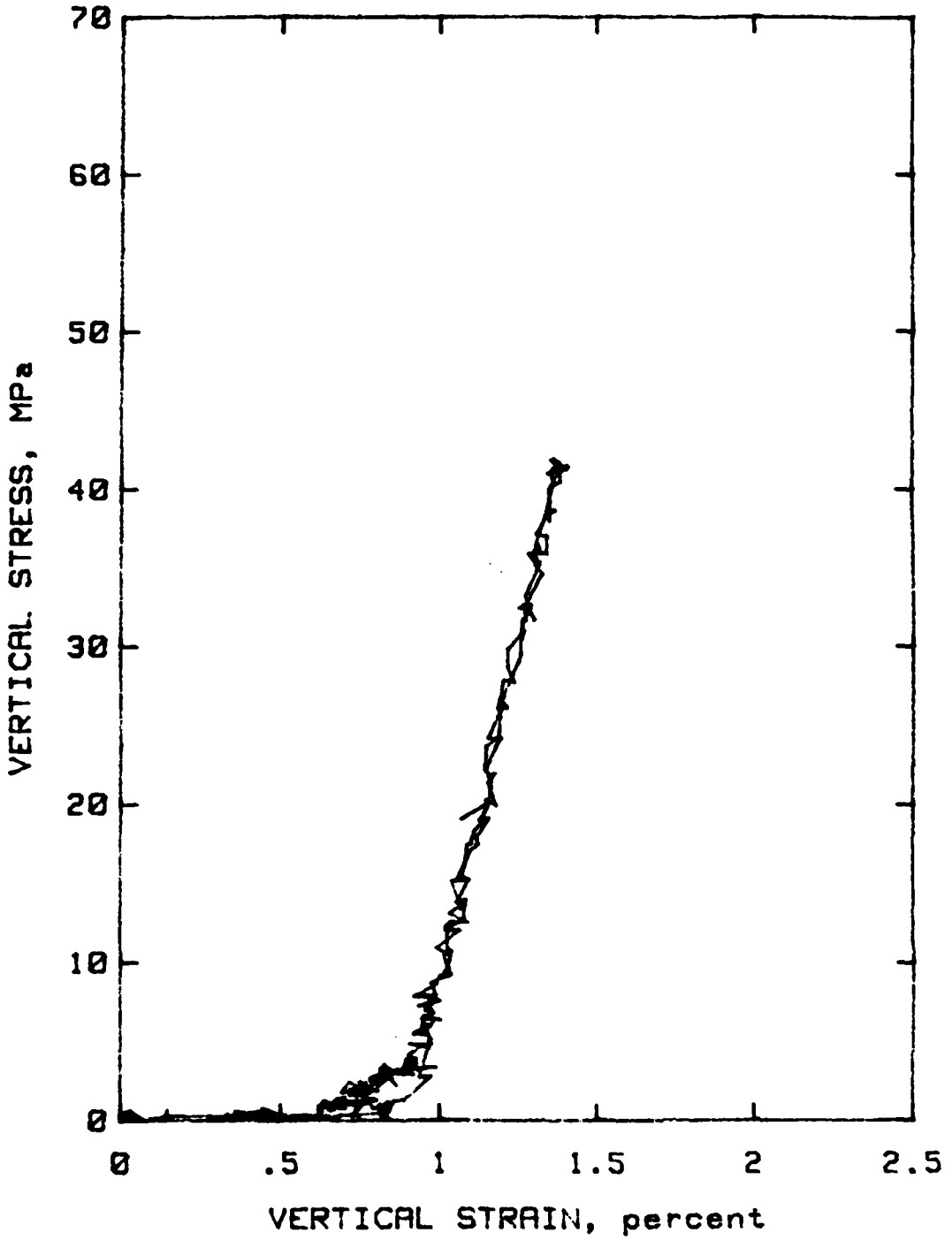

BACK PRESSURE SATURATED
STATIC UNDRAINED UNIAXIAL STRAIN
SPECIMEN RB.UX.2

PLATE 2

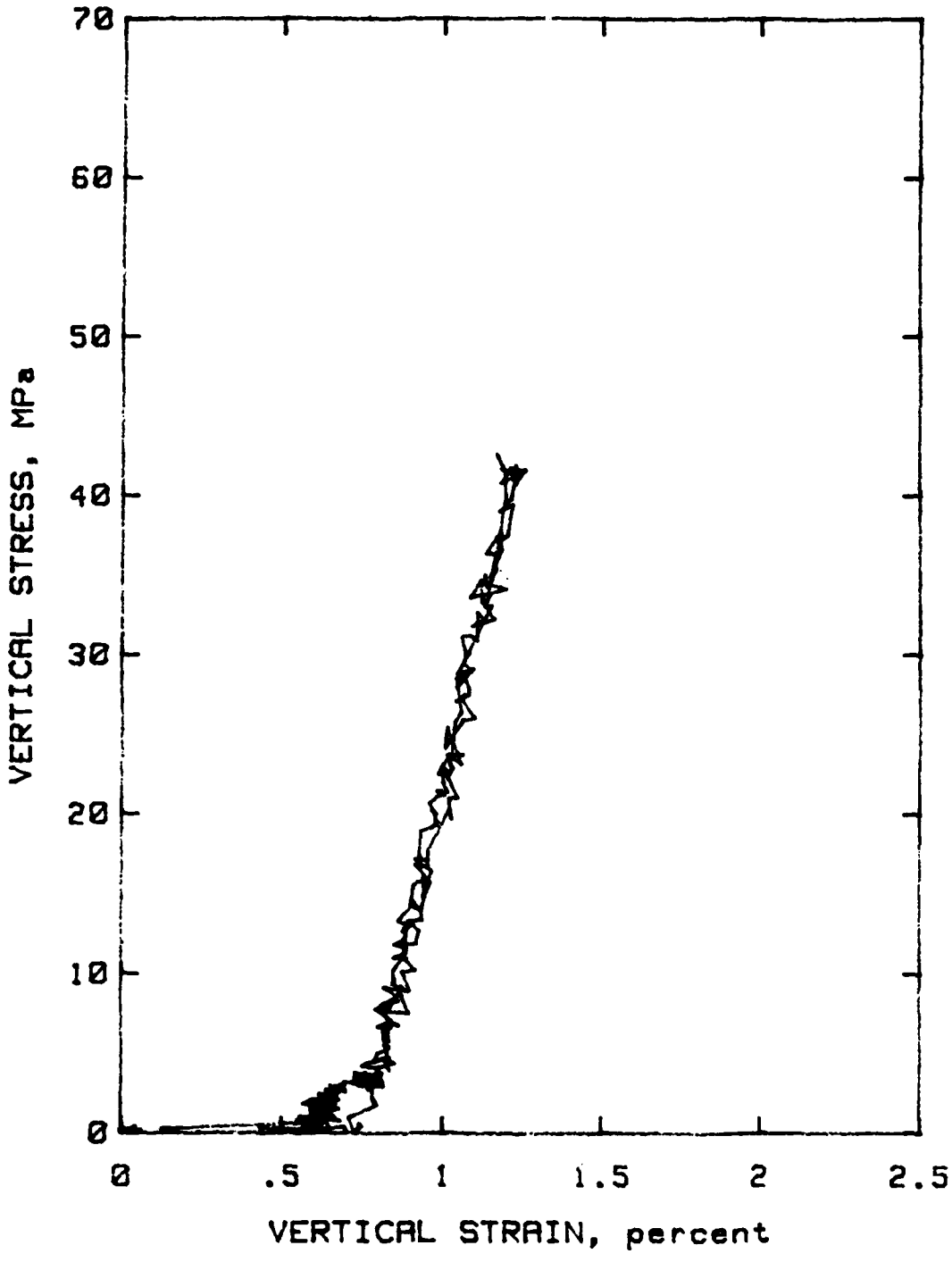

BACK PRESSURE SATURATED
STATIC UNDRAINED UNIAXIAL STRAIN
SPECIMEN RB.UX.2A

PLATE 3

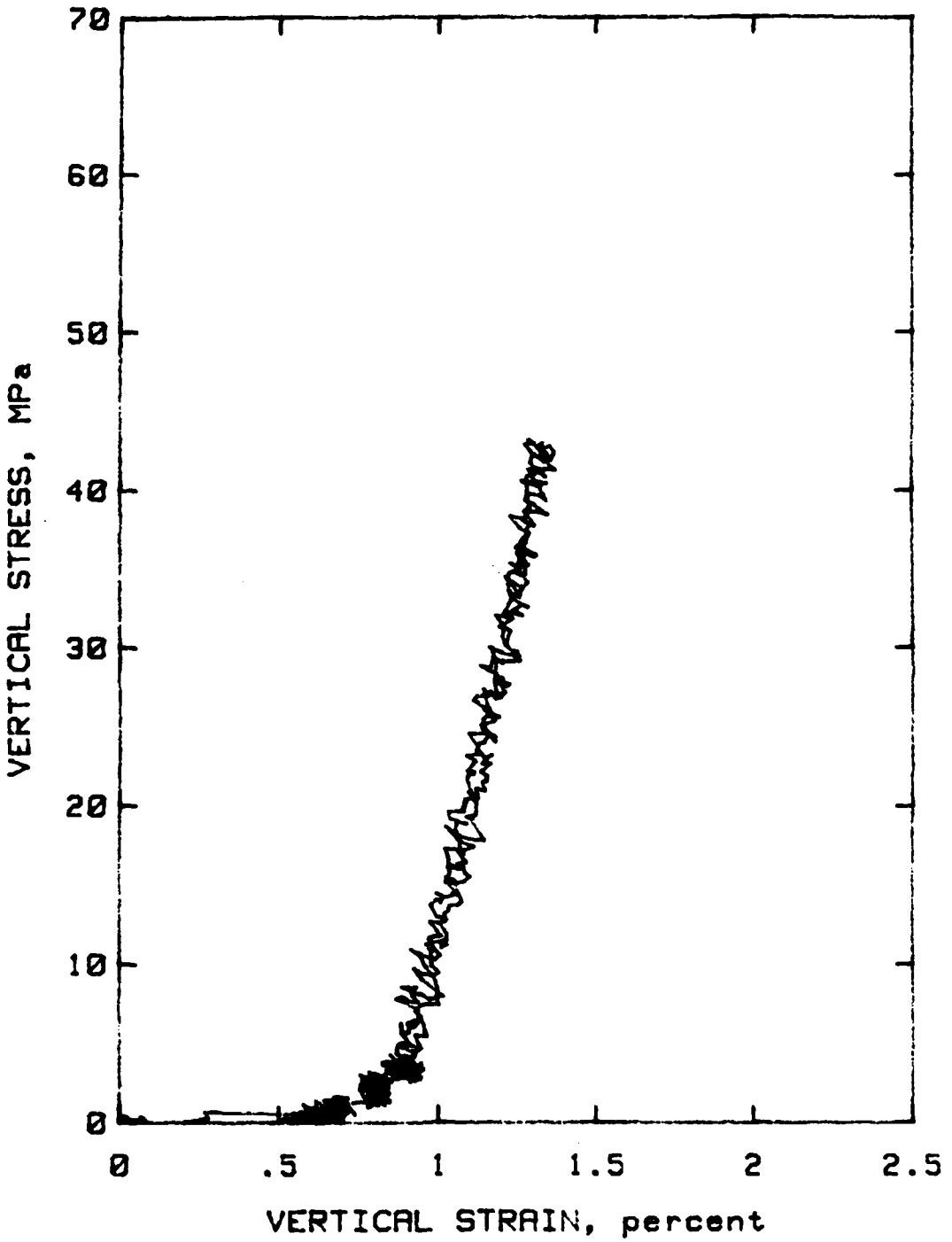

BACK PRESSURE SATURATED
DYNAMIC UNDRAINED UNIAXIAL STRAIN
SPECIMEN RB.UX.3

PLATE 4

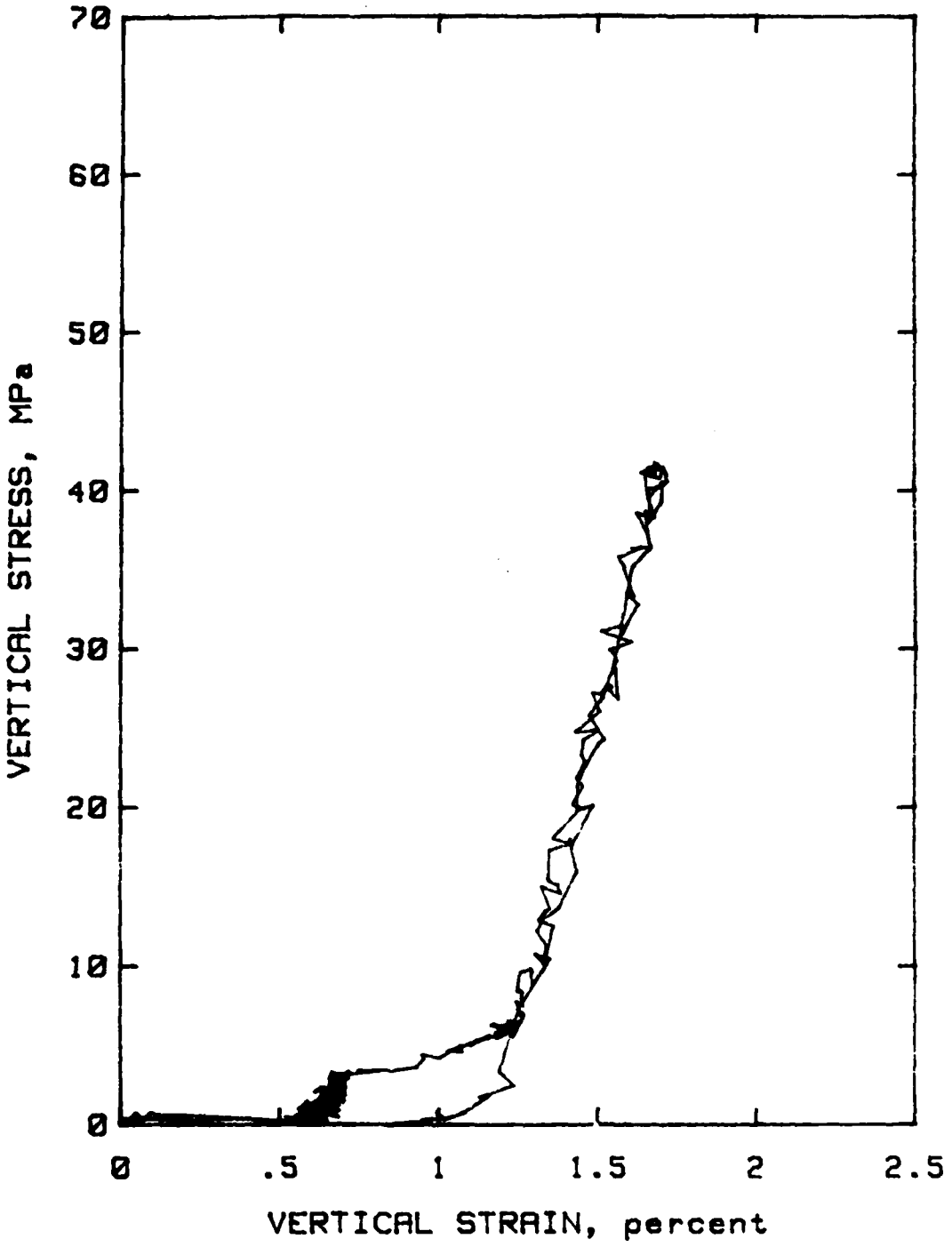

BACK PRESSURE SATURATED
STATIC UNDRAINED UNIAXIAL STRAIN
SPECIMEN RB.UX.4

PLATE 5

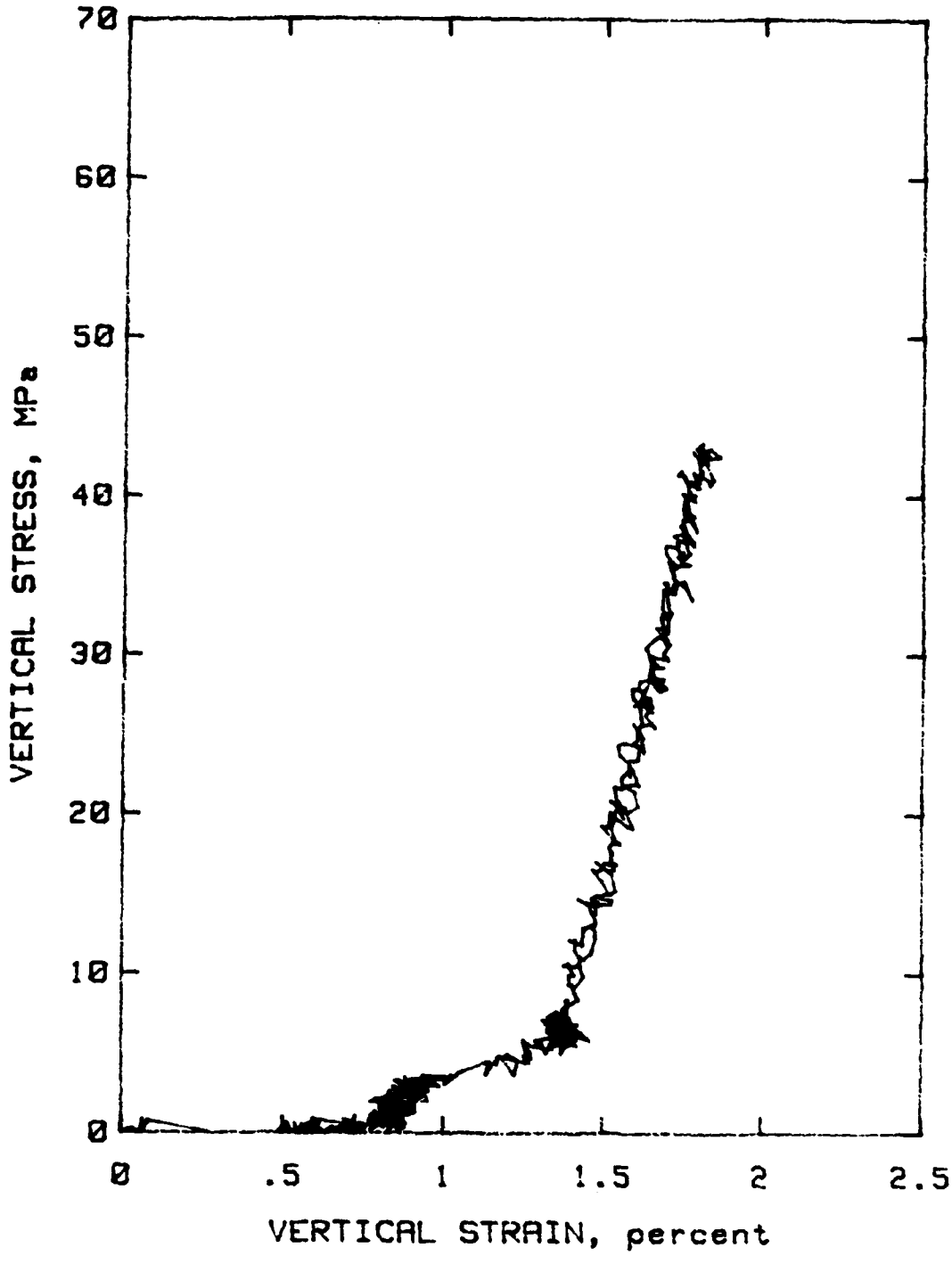

BACK PRESSURE SATURATED
DYNAMIC UNDRAINED UNIAXIAL STRAIN
SPECIMEN RB.UX.5

PLATE 6

STATIC UX/Ko TEST RESULTS

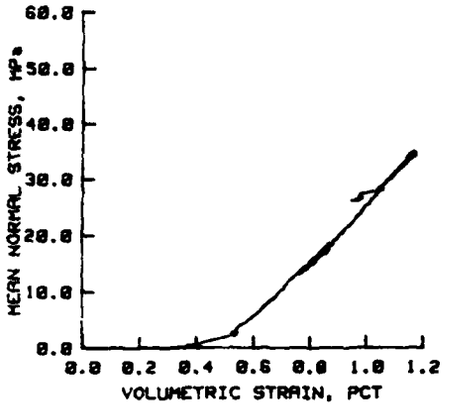

TEST RBDK.1

Density as remolded: 1.637 gm/cc

COMPOSITION PROPERTIES AT END OF BPS

Wet density:	2.025	gm/cc
Water content:	23.8	pct
Dry density:	1.646	gm/cc
Void ratio:	0.61	

PRESSURES AT END OF BPS, MPa

Confining pressure:	2.24
Pore pressure:	2.07

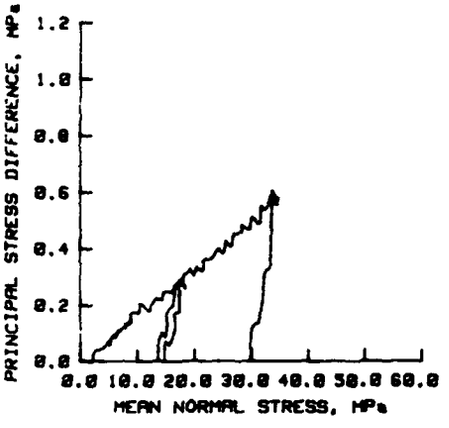

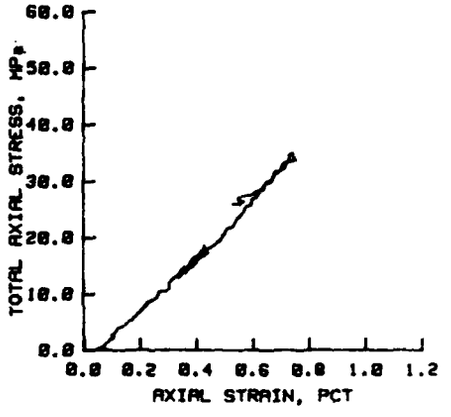

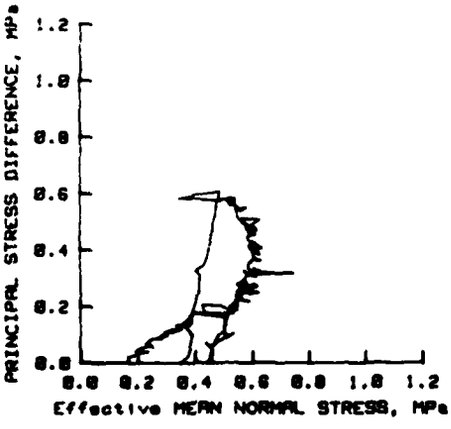

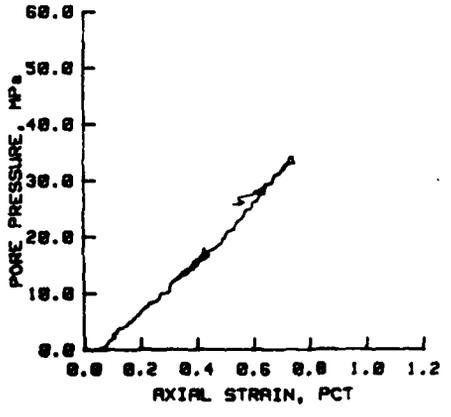

PLATE 7

STATIC UX/Ko TEST RESULTS

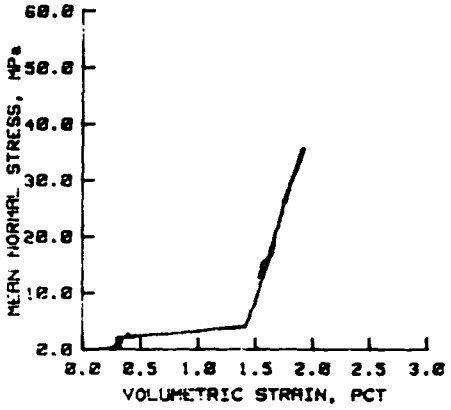

TEST RBDK.2

Density as remolded: 1.643 gm/cc

COMPOSITION PROPERTIES AT END OF BPS

Wet density:	2.027	gm/cc
Water content:	22.3	pct
Dry density:	1.643	gm/cc
Void ratio:	0.61	

PRESSURES AT END OF BPS, MPa

Confining pressure:	2.28
Pore pressure:	2.14

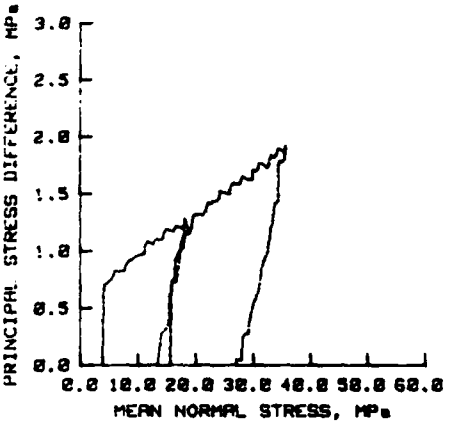

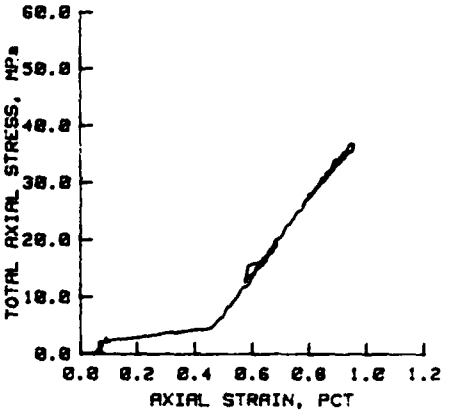

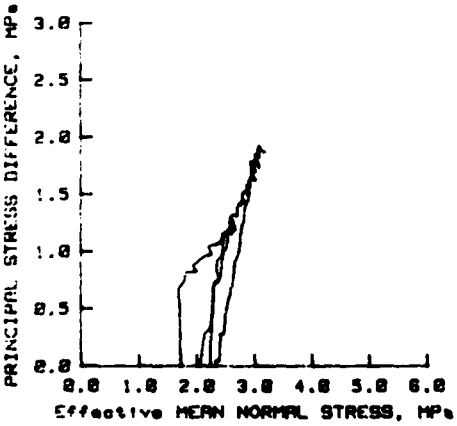

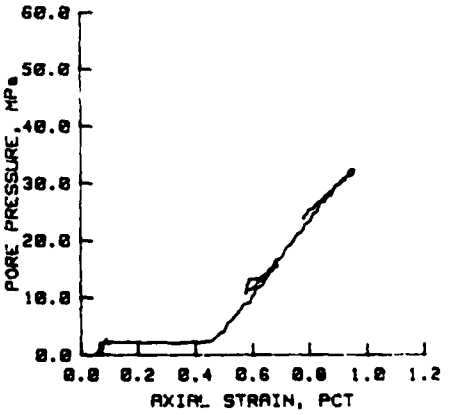

PLATE 8

STATIC UX/Ko TEST RESULTS

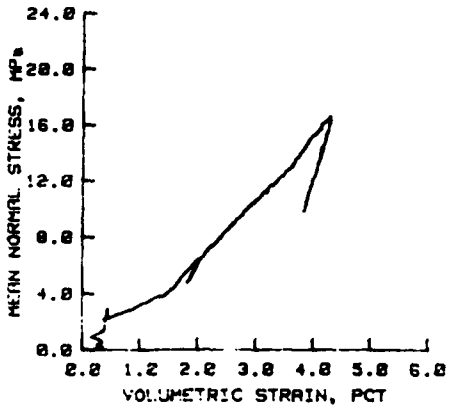

TEST RBDK.3

Density as remolded: 1.637 gm/cc

COMPOSITION PROPERTIES AT END OF BPS

Wet density:	2.019	gm/cc
Water content:	23.4	pct
Dry density:	1.637	gm/cc
Void ratio:	0.62	

PRESSURES AT END OF BPS, MPa

Confining pressure:	0.00
Pore pressure:	0.00

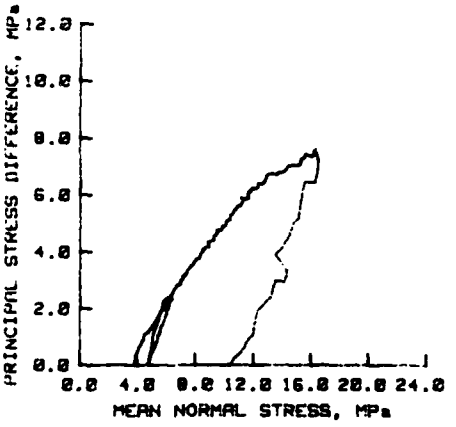

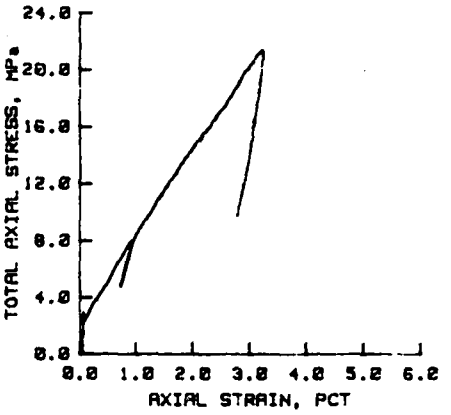

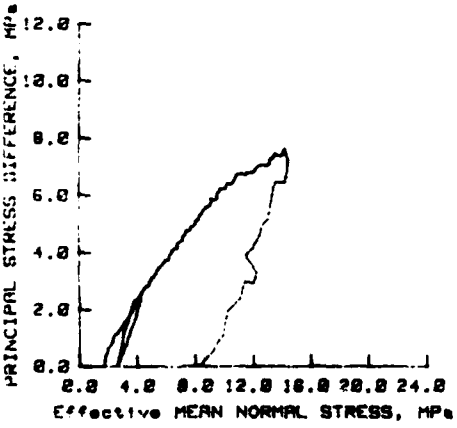

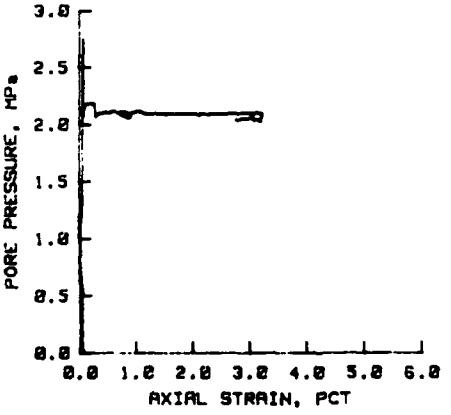

PLATE 9

STATIC UX/Ko TEST RESULTS

TEST RBDK.4

Density as remolded: 1.631 gm/cc

COMPOSITION PROPERTIES AT END OF BPS

Wet density:	2.828	gm/cc
Water content:	23.3	pct
Dry density:	1.638	gm/cc
Void ratio:	0.62	

PRESSURES AT END OF BPS, MPa

Confining pressure:	2.22
Pore pressure:	2.81

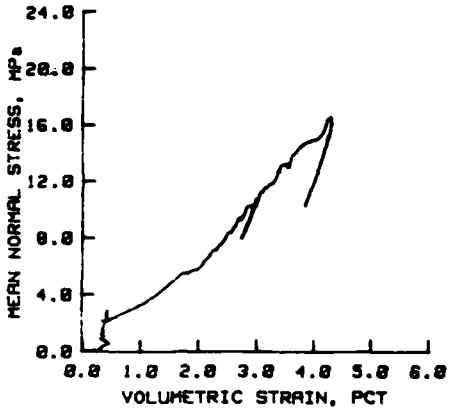

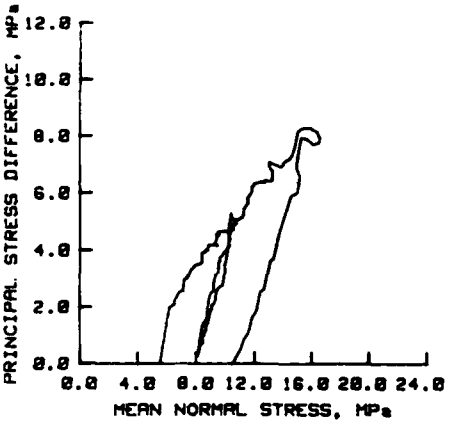

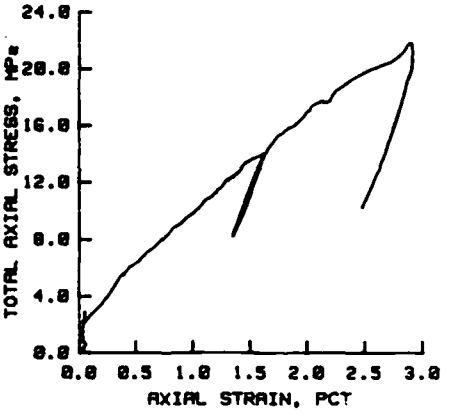

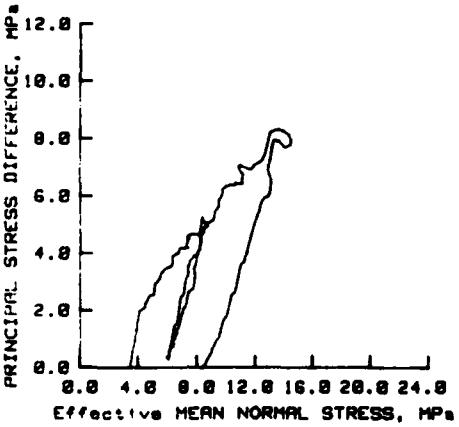

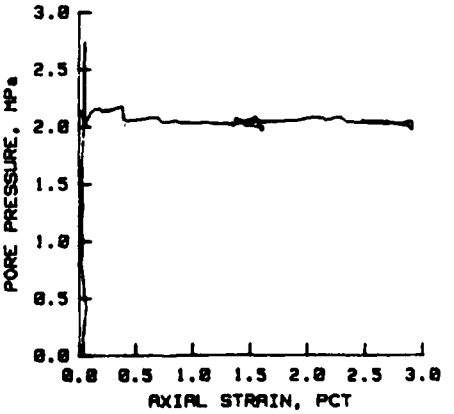

PLATE 10

STATIC UX/Ko TEST RESULTS

TEST RBDK.5

Density as remolded: 1.637 gm/cc

COMPOSITION PROPERTIES AT END OF BPS

Wet density:	2.025	gm/cc
Water content:	23.8	pct
Dry density:	1.646	gm/cc
Void ratio:	0.61	

PRESSURES AT END OF BPS, MPa

Confining pressure:	2.46
Pore pressure:	2.10

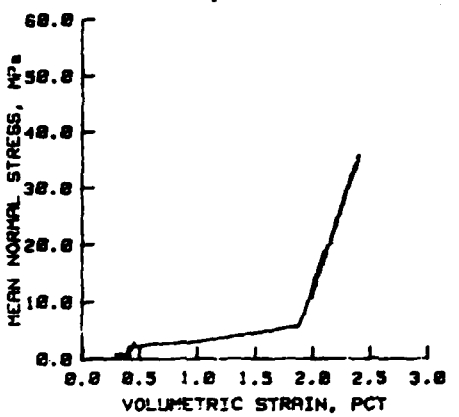

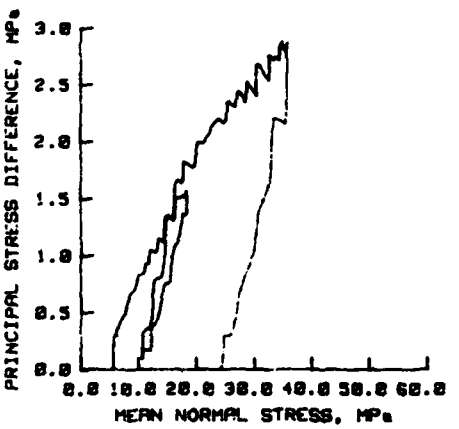

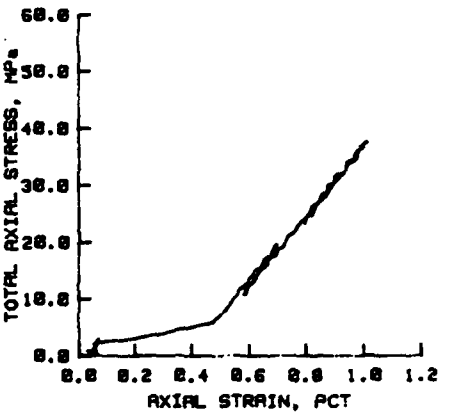

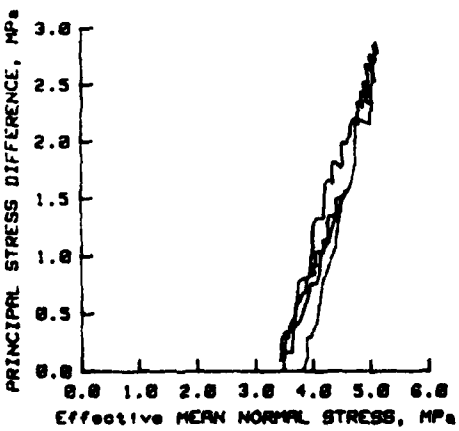

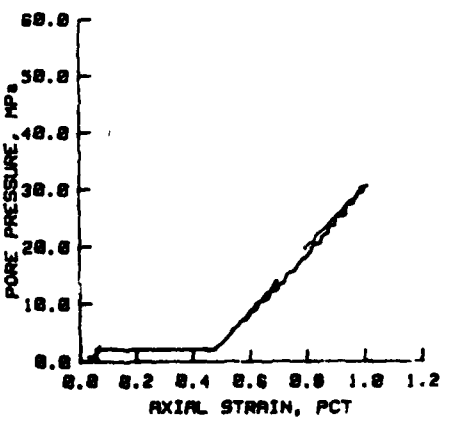

PLATE 11

STATIC IC TEST RESULTS

TEST RBIC.1

Density as remolded: 1.637 gm/cc

COMPOSITION PROPERTIES AT END OF BPS

Wet density:	2.022	gm/cc
Water content:	22.9	pct
Dry density:	1.645	gm/cc
Void ratio:	0.60	

PRESSURES AT END OF BPS, MPa

Confining pressure:	2.19
Pore pressure:	2.00

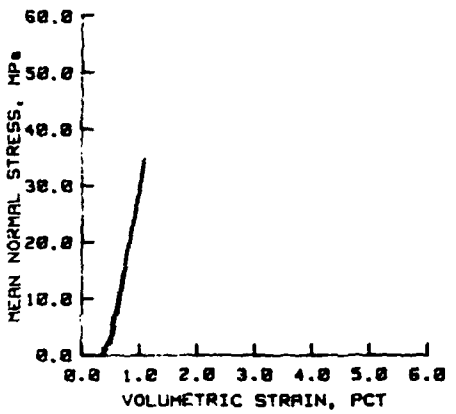

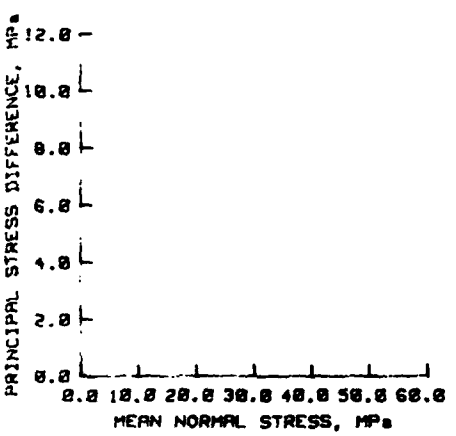

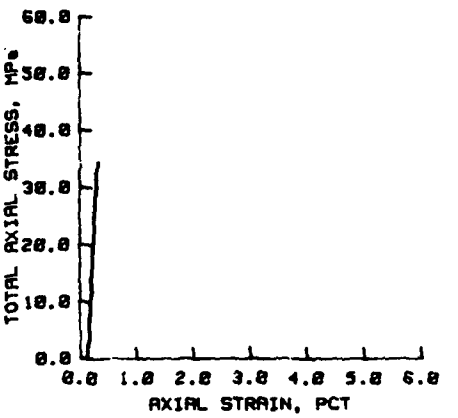

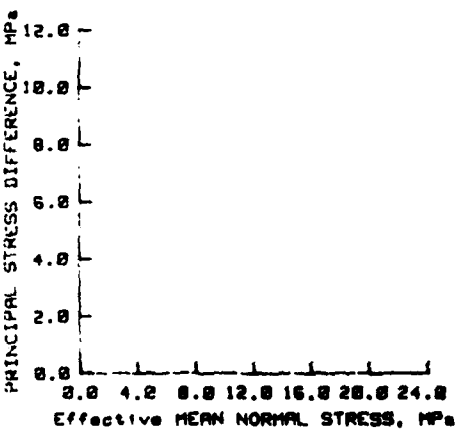

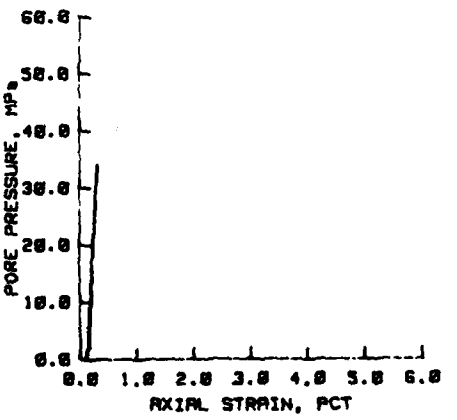

PLATE 12

STATIC IC TEST RESULTS

TEST RBIC.2

Density as remolded: 1.650 gm/cc

COMPOSITION PROPERTIES AT END OF BPS

Wet density:	2.034	gm/cc
Water content:	22.2	pct
Dry density:	1.665	gm/cc
Void ratio:	0.59	

PRESSURES AT END OF BPS, MPa

Confining pressure:	2.24
Pore pressure:	2.05

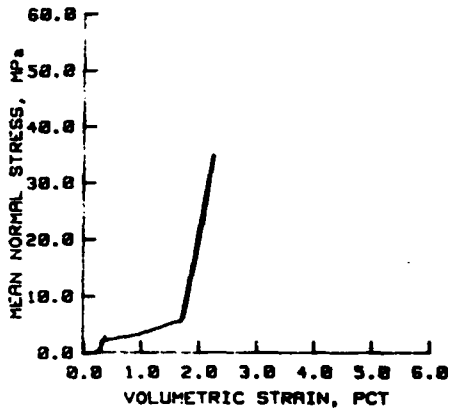

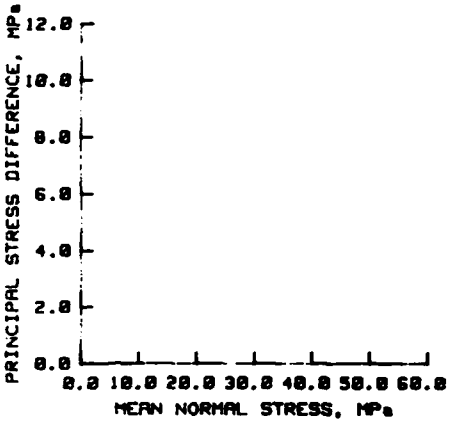

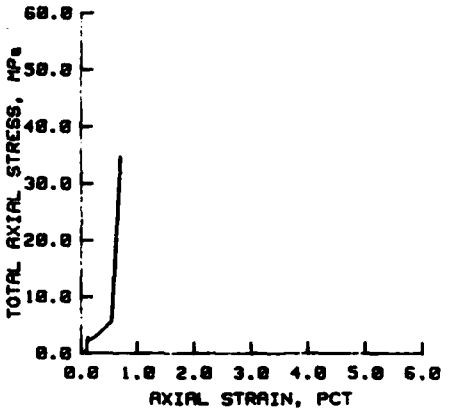

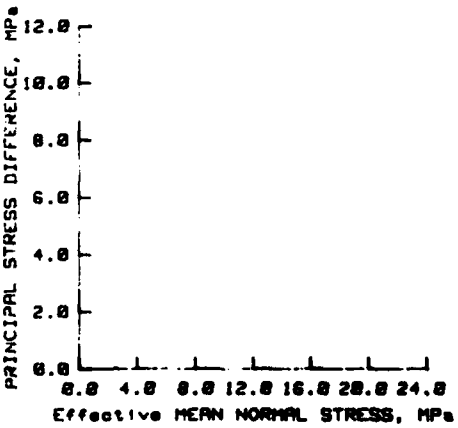

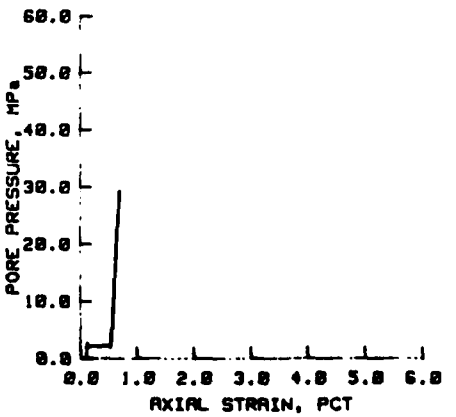

PLATE 13

STATIC IC TEST RESULTS

TEST RBIC.3

Density as remolded: 1.634 gm/cc

COMPOSITION PROPERTIES AT END OF BPS

Wet density:	2.028	gm/cc
Water content:	23.8	pct
Dry density:	1.643	gm/cc
Void ratio:	0.61	

PRESSURES AT END OF BPS, MPa

Confining pressure:	2.34
Pore pressure:	2.18

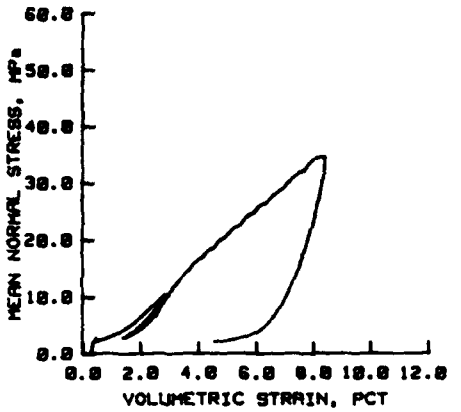

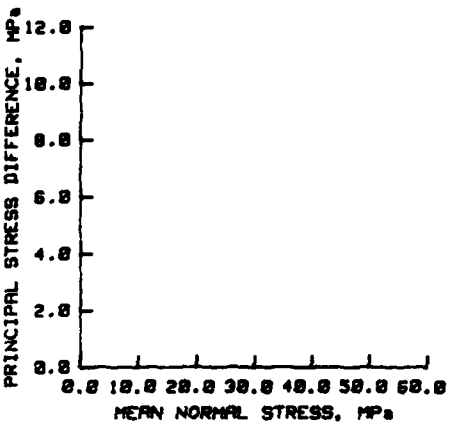

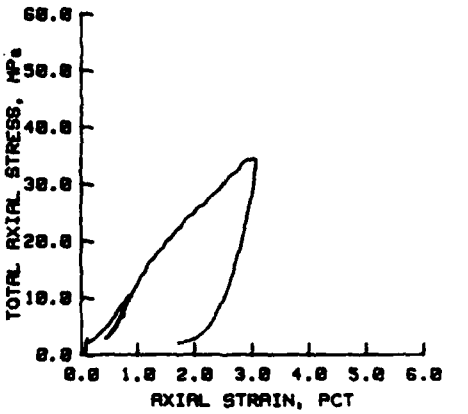

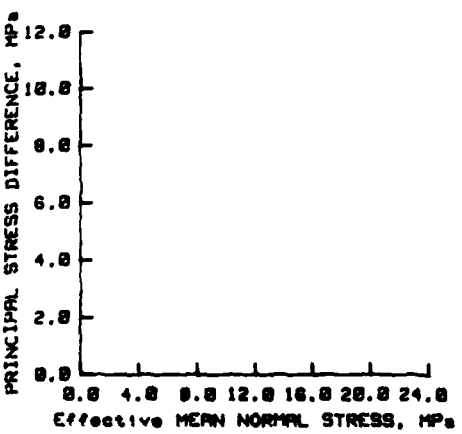

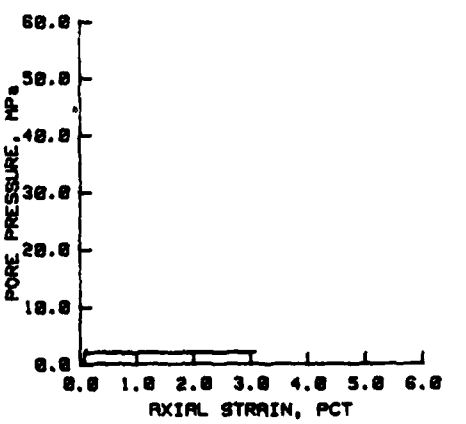

PLATE 14

STATIC IC-TX TEST RESULTS

TEST RBTX.1

Density as remolded: 1.647 gm/cc

COMPOSITION PROPERTIES AT END OF BPS

Wet density:	2.033	gm/cc
Water content:	22.3	pct
Dry density:	1.662	gm/cc
Void ratio:	0.59	

PRESSURES AT END OF BPS, MPa

Confining pressure:	2.56
Pore pressure:	2.19

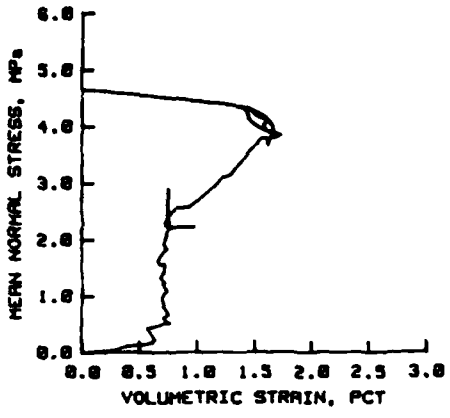

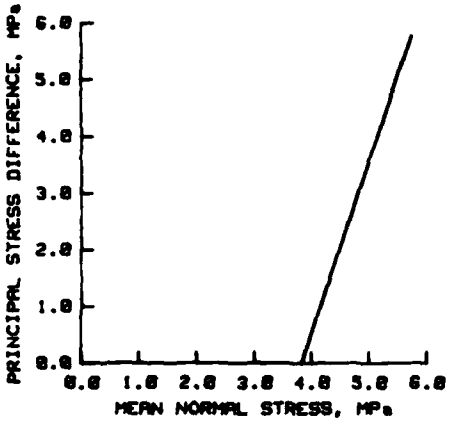

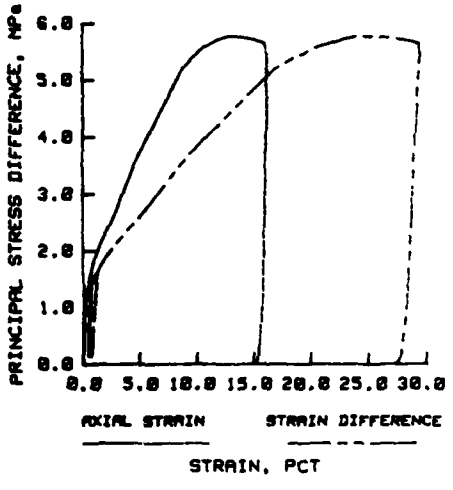

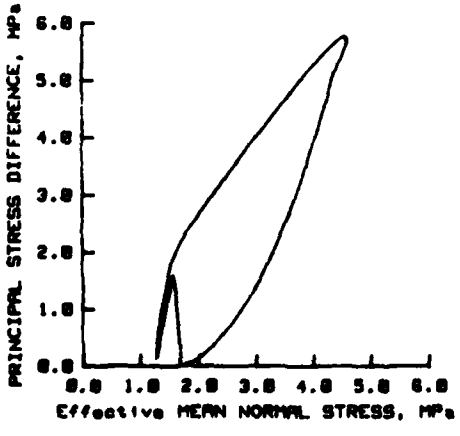

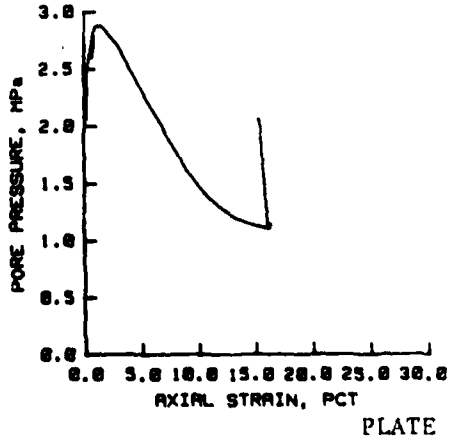

PLATE 15

STATIC IC-TX TEST RESULTS

TEST RBTX.2

Density as remolded: 1.634 gm/cc

COMPOSITION PROPERTIES AT END OF BPS

Wet density:	2.030	gm/cc
Water content:	22.7	pct
Dry density:	1.655	gm/cc
Void ratio:	0.60	

PRESSURES AT END OF BPS, MPa

Confining pressure:	2.27
Pore pressure:	2.07

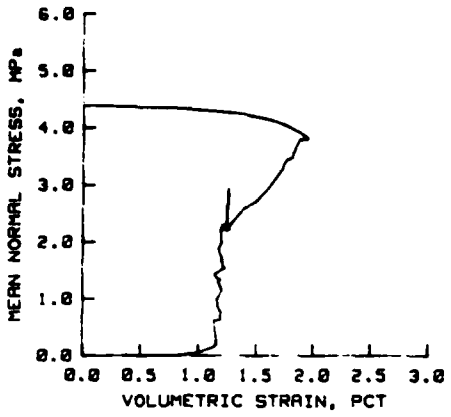

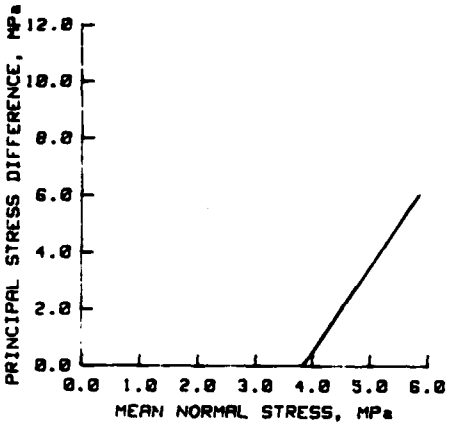

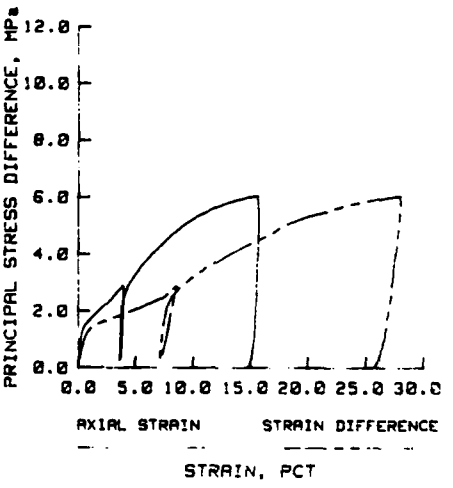

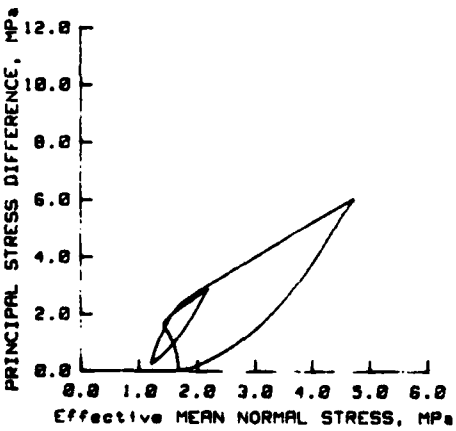

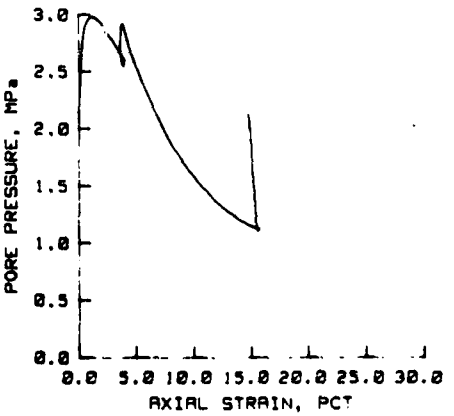

PLATE 16

STATIC IC-TX TEST RESULTS

TEST RBTX.3

Density as remolded: 1.632 gm/cc

COMPOSITION PROPERTIES AT END OF BPS

Wet density:	2.022	gm/cc
Water content:	23.2	pct
Dry density:	1.641	gm/cc
Void ratio:	0.62	

PRESSURES AT END OF BPS, MPa

Confining pressure:	2.22
Pore pressure:	2.16

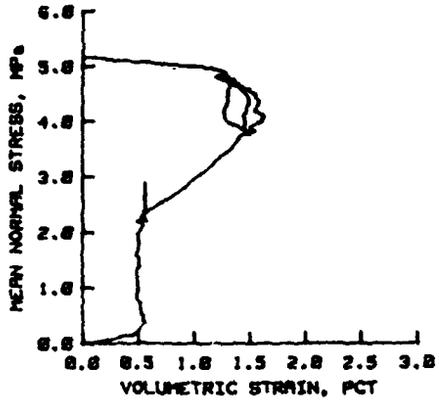

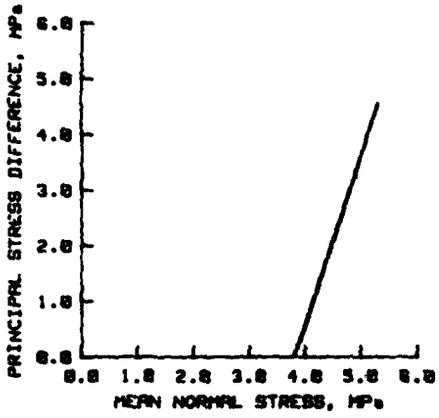

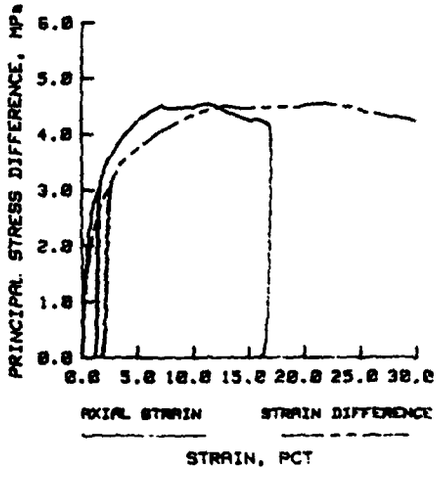

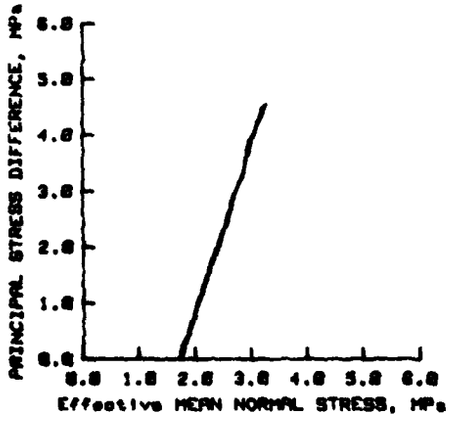

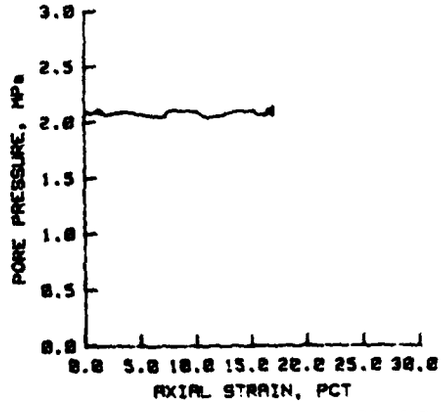

PLATE 17

STATIC IC-TX TEST RESULTS

TEST RBTX.4

Density as remolded: 1.655 gm/cc

COMPOSITION PROPERTIES AT END OF BPS

Wet density:	2.036	gm/cc
Water content:	22.1	pct
Dry density:	1.667	gm/cc
Void ratio:	0.58	

PRESSURES AT END OF BPS, MPa

Confining pressure:	2.20
Pore pressure:	2.29

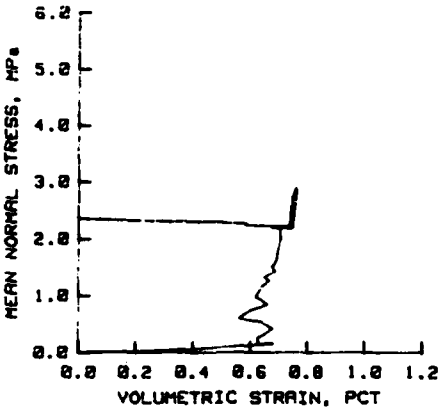

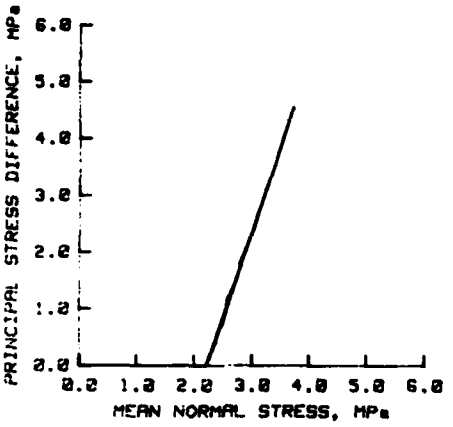

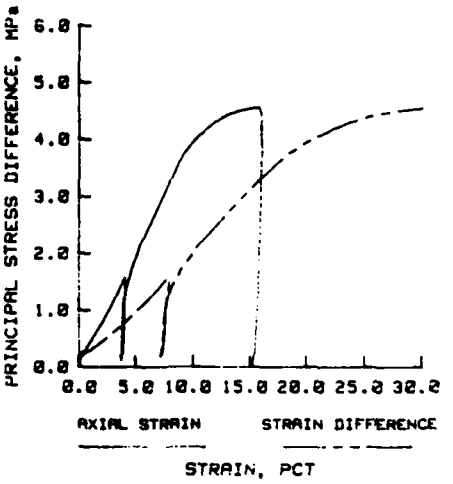

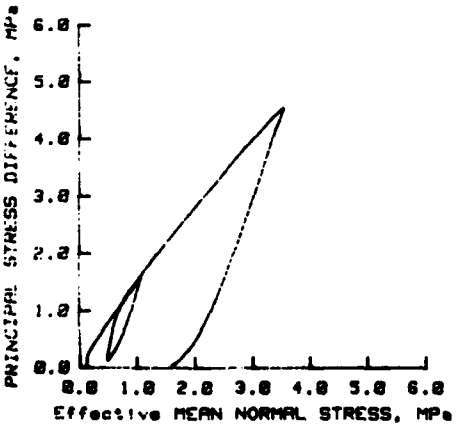

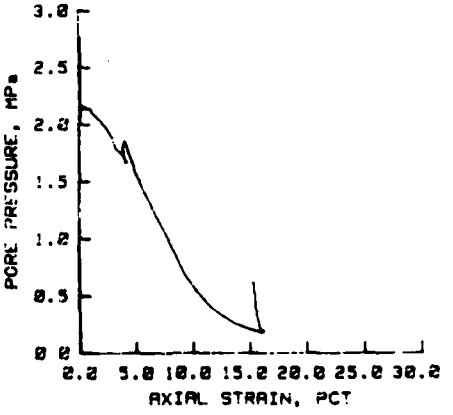

PLATE 18

STATIC IC-TX TEST RESULTS

TEST RBTX.5

Density as remolded: 1.628 gm/cc

COMPOSITION PROPERTIES AT END OF BPS

Wet density:	2.019	gm/cc
Water content:	23.4	pct
Dry density:	1.637	gm/cc
Void ratio:	0.62	

PRESSURES AT END OF BPS, MPa

Confining pressure:	2.22
Pore pressure:	2.11

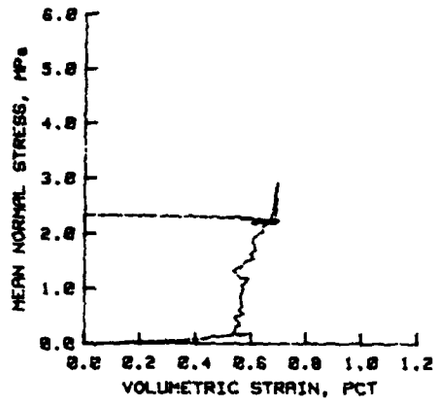

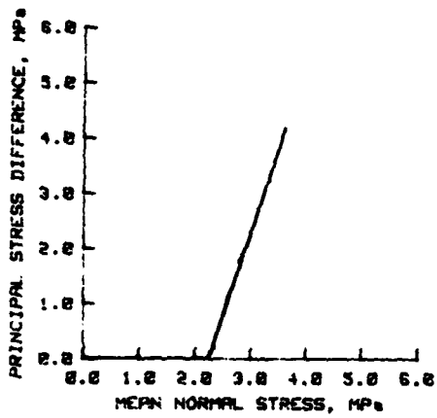

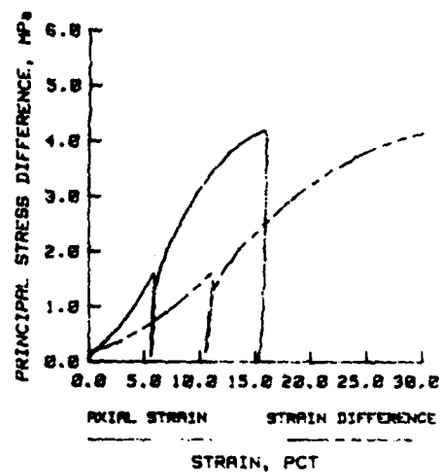

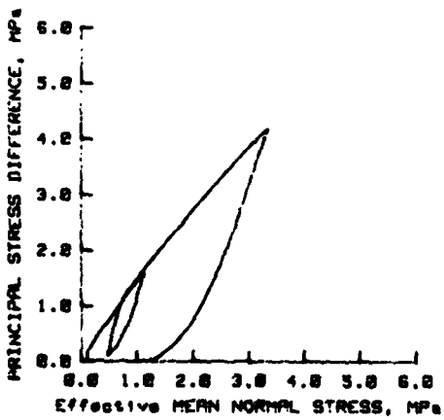

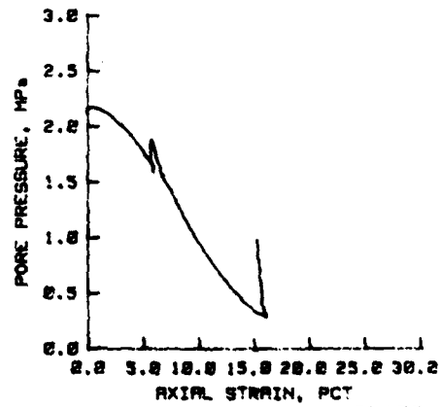

PLATE 19

STATIC IC-TX TEST RESULTS

TEST RBTX.6

Density as remolded: 1.645 gm/cc

COMPOSITION PROPERTIES AT END OF BPS

Wet density:	2.038	gm/cc
Water content:	22.7	pct
Dry density:	1.654	gm/cc
Void ratio:	0.60	

PRESSURES AT END OF BPS, MPa

Confining pressure:	2.23
Pore pressure:	2.00

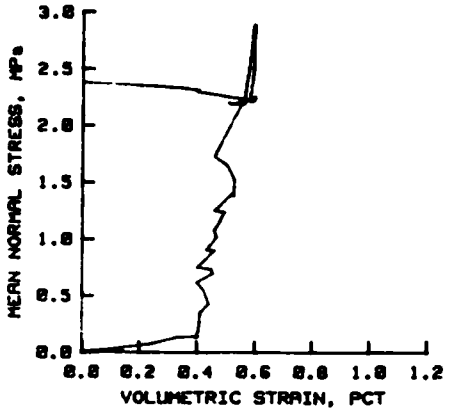

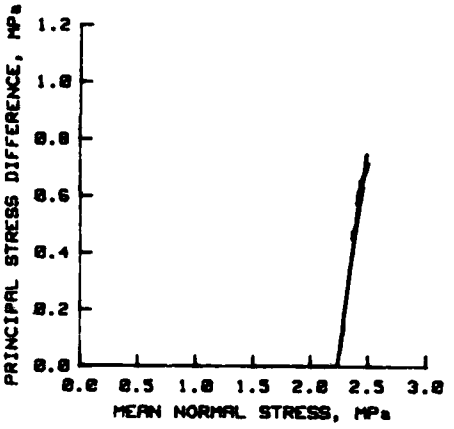

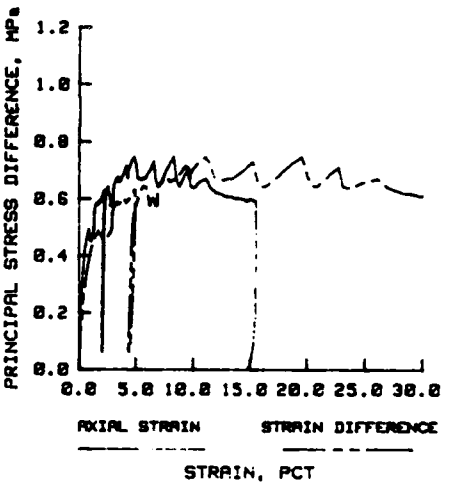

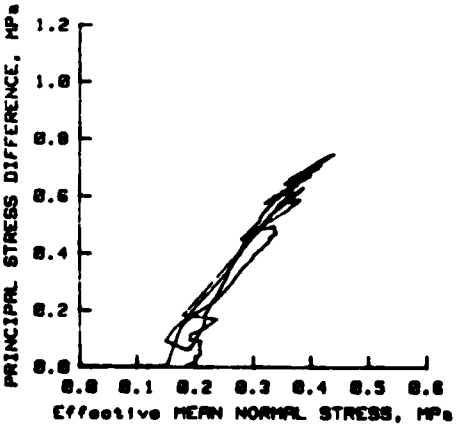

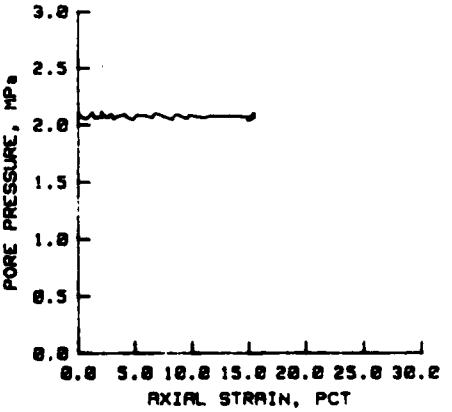

PLATE 20

STATIC IC-TX TEST RESULTS

TEST RBTX..7

Density as remolded: 1.634 gm/cc

COMPOSITION PROPERTIES AT END OF BPS

Wet density:	2.024	gm/cc
Water content:	23.1	pct
Dry density:	1.645	gm/cc
Void ratio:	0.61	

PRESSURES AT END OF BPS, MPa

Confining pressure:	2.45
Pore pressure:	2.19

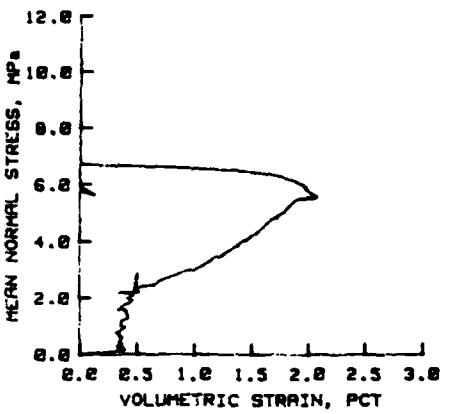

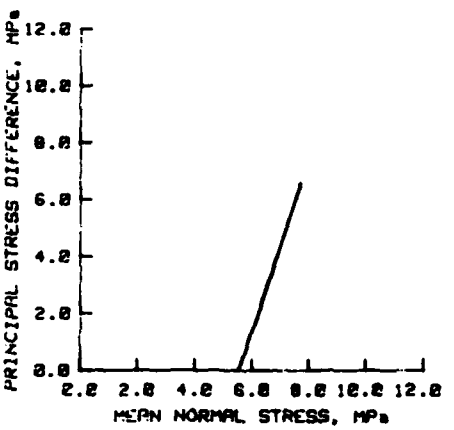

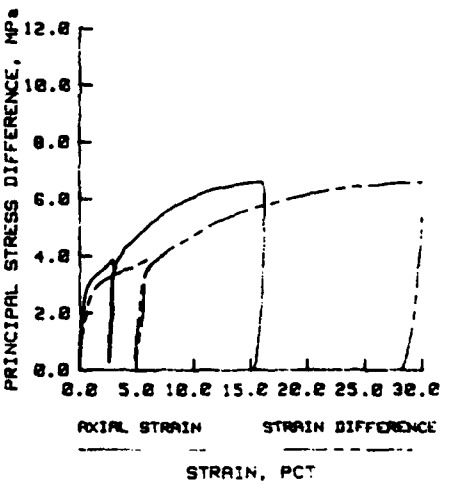

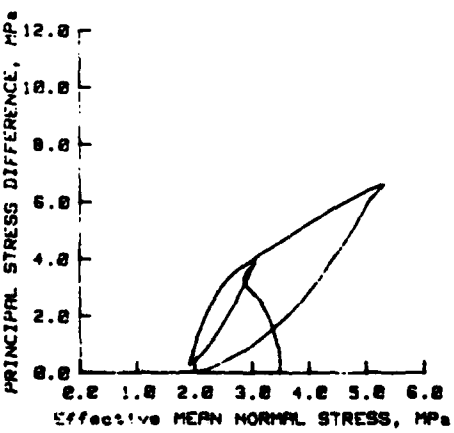

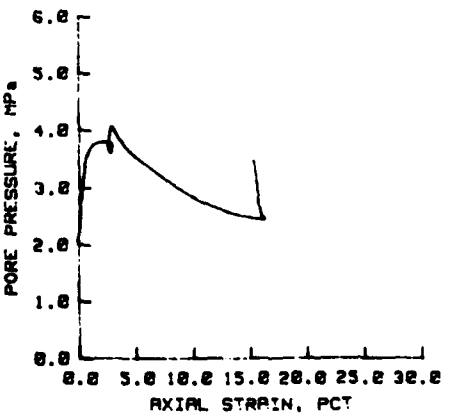

PLATE 21

STATIC IC-TX TEST RESULTS

TEST RBTX.8

Density as remolded: 1.626 gm/cc

COMPOSITION PROPERTIES AT END OF BPS

Wet density:	2.021	gm/cc
Water content:	23.2	pct
Dry density:	1.640	gm/cc
Void ratio:	0.62	

PRESSURES AT END OF BPS, MPa

Confining pressure:	2.41
Pore pressure:	2.17

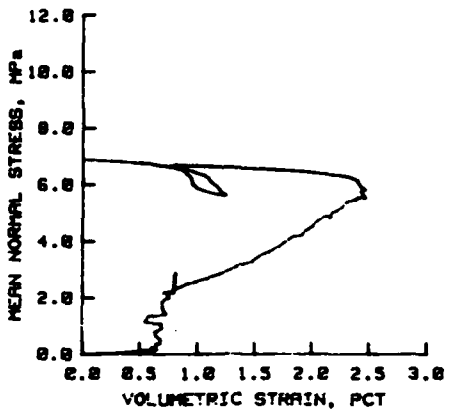

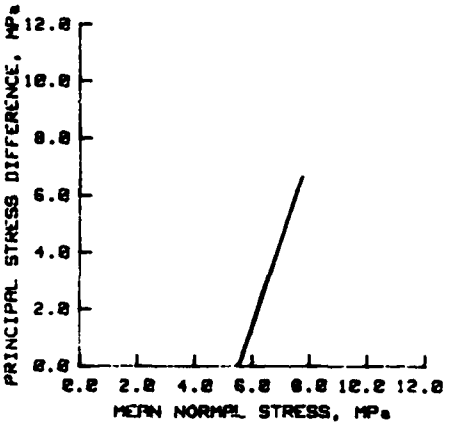

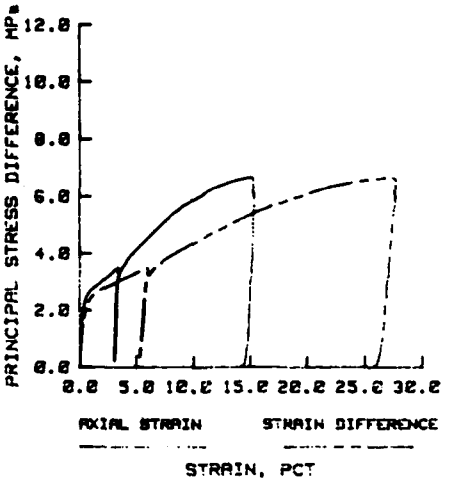

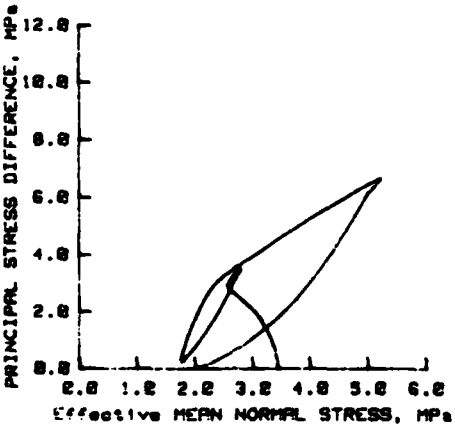

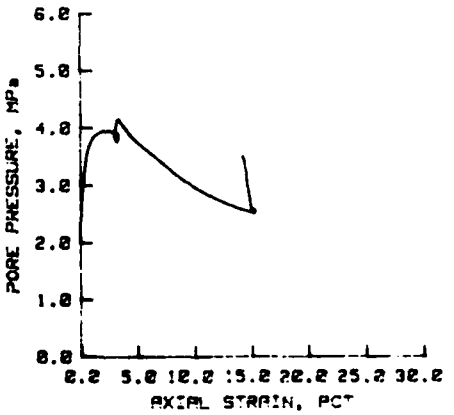

PLATE 22

STATIC IC-TX TEST RESULTS

TEST RBTX.9

Density as remolded: 1.637 gm/cc

COMPOSITION PROPERTIES AT END OF BPS

Wet density:	2.023	gm/cc
Water content:	22.9	pct
Dry density:	1.646	gm/cc
Void ratio:	0.60	

PRESSURES AT END OF BPS, MPa

Confining pressure:	2.22
Pore pressure:	2.12

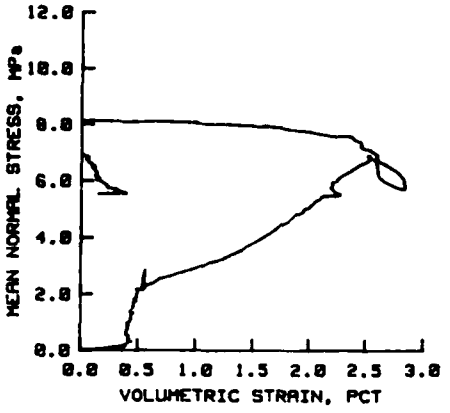

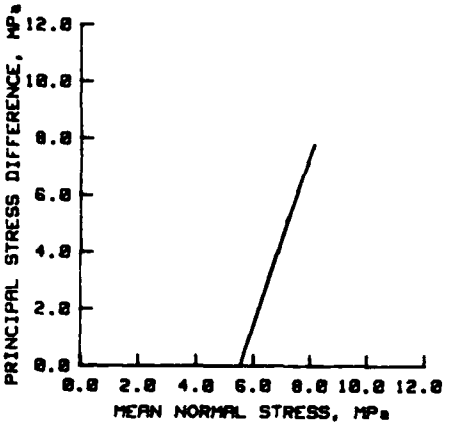

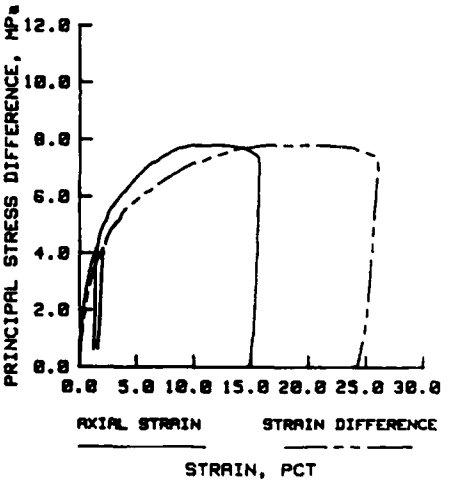

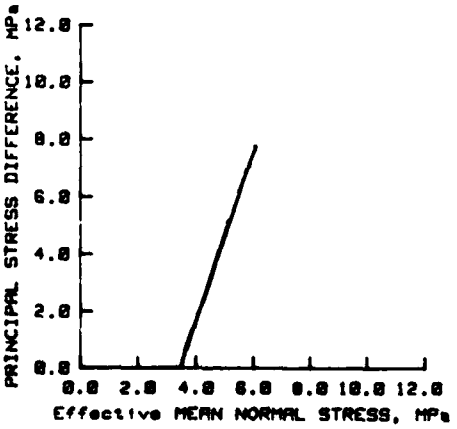

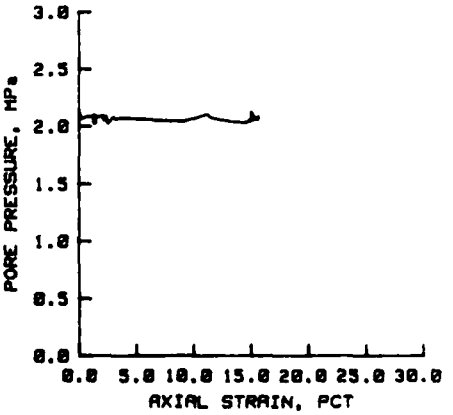

PLATE 23

STATIC IC-TX TEST RESULTS

TEST RBTX.10

Density as remolded: 1.666 gm/cc

COMPOSITION PROPERTIES AT END OF BPS

Wet density:	2.045	gm/cc
Water content:	21.8	pct
Dry density:	1.679	gm/cc
Void ratio:	0.58	

PRESSURES AT END OF BPS, MPa

Confining pressure:	2.68
Pore pressure:	2.18

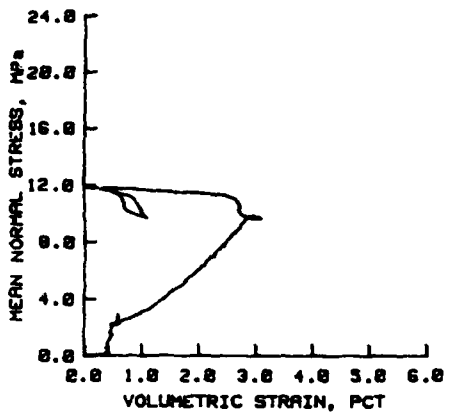

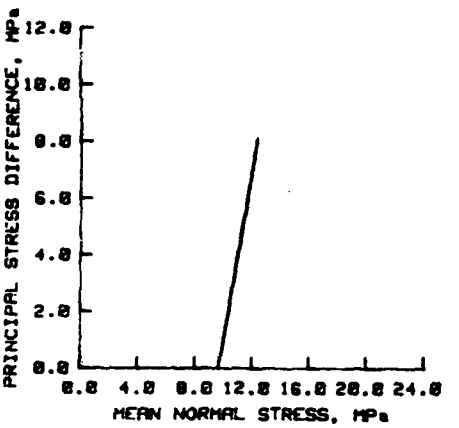

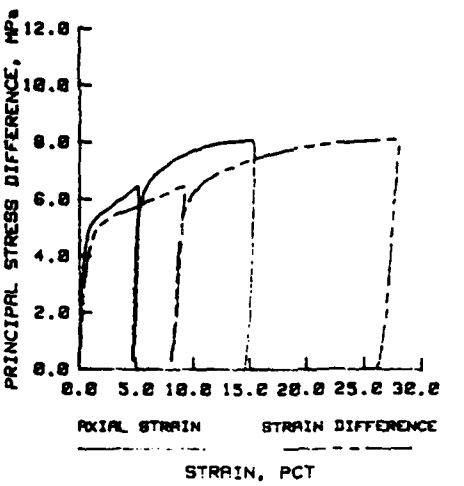

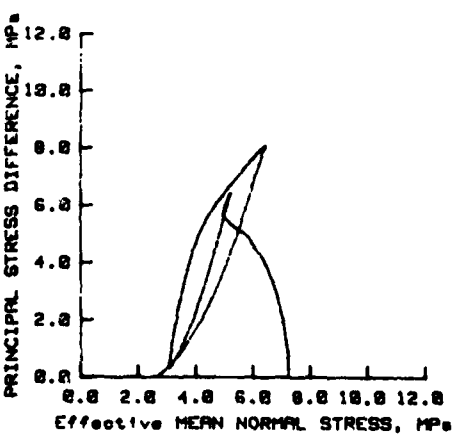

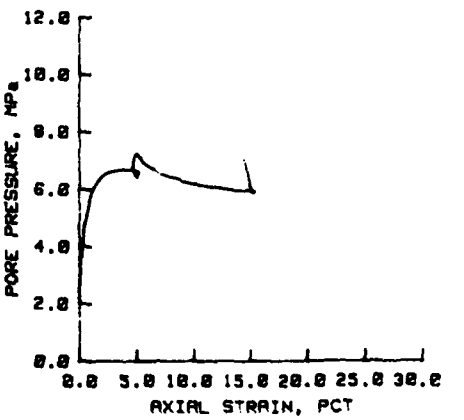

PLATE 24


DATE
FILMED
0-8